Temperature Variation Studies with *Candida Antarctica* Lipase B using Single Molecule Recognition Force Microscopy

Charlotte Nicolaou

Submitted for the Degree of PhD

Department of Physics and Astronomy

August 2014

Supervisor: Dr Ashley Cadby

Acknowledgements

I would like to thank the following people who supported me during the time spent producing this thesis. Without them the last three years would have been much harder and far less enjoyable.

First I would like to thank my supervisor Dr. Ashley Cadby for providing the opportunity to work on this research project and for giving assistance, guidance and support throughout. Also thanks goes to Procter & Gamble and EPSRC for providing the funding required to complete this research.

Next I would like to thank Dr Robert Turner and Dr Cvetelin Vasilev for spending time teaching me about the experiments and for helping me to get to grips with the basics of the project. Huge thanks also goes to Peter Tongeri from the University of Glasgow for both supplying the proteins I used and for answering a stream of very naive questions about biology. I also want to give thanks to Sam Barnett for taking over protein duties last minute.

Throughout my time as a postgraduate I have been a part of EPMM for which I am incredibly grateful as it is a group filled with very fun and incredibly helpful people. I've lost count at the number of times someone from this group has lent a hand when I've had a problem. The social aspect of this group has made these three years extremely good fun - where would I have spent my Tuesday and Friday evenings otherwise? Through my friends I have been introduced to AoE 2, seen a huge amount of terrible B movies, won multiple quiz leagues and learnt more about OPVs than I ever wanted to. In particular I would like to mention Nick, Chris, Theo, Jon, Darren and Ben who also gave me invaluable help with AFM.

Outside of academia Glenn, Georgia, Sam, Cathy, Hannah, Ellis, Catriona and John have provided welcome distractions from university and have been a fantastic group to hang out with.

Lastly I would like to thank my entire family to which I owe everything I am today. In particular my Mum for all kinds of support, many long phone calls when everything had gone wrong and for all that she has done for me over the twenty odd years and for Yaya and Papou for their never-ending love and belief in me.

Abstract

Atomic force microscopy (AFM) is an imaging technique that can provide high resolution images of a surface as well as information on a number of mechanical properties such as elasticity, deformation and adhesion. This final parameter can be exploited to measure the rupture force between two binding molecules in a procedure known as single molecule recognition force microscopy (SMRFM). One molecule is attached to the AFM tip and used to image the second molecule. This process has been applied to many areas including drug research, materials science and biochemistry.

The main purpose of this work was to use SMRFM to investigate the enzyme *Candida Antarctica* Lipase B (CAL B) as it shows potential for cool water washing detergents. By eliminating the need for heating, energy can be saved which is imperative in the world today.

A major challenge in SMRFM is the chemistry used to bind the molecules to the tip. Therefore the first step towards studying CAL B was to use the binding pair of avidin and biotin to recreate previous experiments and confirm that the selected chemistry was appropriate. These experiments reproduced similar forces for avidin and biotin as published results.

The system was then applied to measure the rupture force between CAL B and the carboxylic ester ±-2-acetoxypropionic acid at room temperature. It was found that unbinding events could be successfully observed and that leaving the AFM tip to dwell on the substrate for 100 ms produced significantly more specific events.

Next a cooling device that could reduce the temperature of the AFM environment was created. The temperature was varied between 29.3^{o}C and 7.4^{o}C. It was found that the binding probability of CAL B increases notably at the lowest temperatures to 0.1096 ± 0.002 which further strengthens the potential for CAL B as a component for cool water detergents.

Conference Presentations

Linz Winter Workshop. Linz 2012. **Poster.** *A Comparative Study of Polymer Adhesion Measurements Between PeakForce QNM and Force Volume AFM.*

Conference of Astronomy and Physics Students. Sheffield 2012. **Oral**. *Introduction to Single Molecule Recognition Force Microscopy with Enzymes.*

International Conference of Physics Students. Utrecht 2012. **Oral.** *Towards Cool Water Biological Detergents using Atomic Force Microscopy.*

Sheffield Soft Matter Physics. Sheffield 2012. **Poster.** *Using Atomic Force Microscopy to Probe Protein Binding Forces.* Recipient of best poster award.

Materials Research Society Spring Meet. San Francisco 2014. **Oral**. *Comparison of PeakForce QNM and Force Volume AFM for Single Molecule Recognition Force Microscopy.*

Table of Contents

List of Figures

List of Tables

List of Abbreviations

AFM - Atomic Force Microscopy

APA - ±-2-acetoxypropionic acid

APTES - 3-(aminopropyl)triethoxysilane

BSA - Bovine serum albumin

CAL B - *Candida Antarctica* Lipase B

DMSO - dimethyl sulfoxide

DMT - Derjaguin, Muller and Toporov

EDC - N-(3-dimethylaminopropyl)-N'-ethylcarbodiimide hydrochloride

HCL - hydrochloride

MAL - malemide

MUA - 11-mercaptoundecanoic acid

NHS - N-hydroxysuccinimide

PA3859 - *Pseudomonas Aeruginosa* 3859

PBS - Phosphate buffered saline

PDP - pyridyldithio propionate

PEG - poly(ethylene glycol)

QNM - PeakForce Quantitative Nanomechanical Property Mapping

SMRFM - Single Molecule Recognition Force Microscopy

SPIP - The Scanning Probe Image Processor

SPM - Scanning Probe Microscopy

TCEP.HCL - tris(2-carboxyethyl)phosphine hydrochloride

TEA - triethanolamine

TEC - Thermoelectric cooler

Chapter 1 - Introduction

Increasing global temperature caused by the emission of greenhouse gases is one of the greatest challenges that the human species has had to face [1]. The rising of temperatures is predicted to increase the frequency of catastrophic natural disasters, have huge negative effects on global health and cause sea levels to rise by up to 0.59 m by the end of the century [2, 3, 4]. The Intergovernmental Panel on Climate Change has predicted that temperatures will increase by a minimum of 1-3^{o}C even with a large curtailment of current emissions.

The largest contributor to the greenhouse effect is CO_2 released from the burning of fossil fuels which are the source of over 80% of our energy. Over a quarter of total greenhouses gas emissions come from energy production [4, 5]. Energy requirements worldwide are continuously rising as both developed and developing countries continue to demand more electricity [6]. This highlights the fact that we need to significantly change the way we produce and use energy. The main solution to this problem is to use renewable energy sources such as wind, photovoltaics, hydroelectric and biofuels to provide our electricity. Currently only 14% of Earth's energy is supplied with renewable sources which is not enough to curb the effects of climate change and whilst the adoption of these green technologies is on the rise they all have sizable issues that stop them being a true rival to fossil fuels [7, 8].

Until we have a sustainable power source that can handle the growing energy demands as technology advances and countries continue to consume more and

more it is imperative that we reduce that amount of energy required to complete everyday tasks. One ubiquitous process that expends a huge amount of energy is the washing of clothes. The average washing cycle in Europe consumes 60 litres of water, which due to the high specific heat capacity of water, requires approximately 1kWh of energy to heat to the average washing temperature of 40^{o}C [9]. A large amount of research is currently focused on lowering the operation temperature so that no heating is required which would save this 1kWh of energy. It is estimated that almost 24 million washing machines are used 3 times a week in the UK alone. This accounts for almost 5% of household energy consumption [9]. By removing the need for heating it would be possible to reduce the energy cost by a substantial proportion.

Another major benefit to ambient temperature washing cycles can be found in the developing world. 1.3 billion of the world's population do not have access to electricity and so must wash in cool water. They then have to spend many days washing their clothes to supply the energy to remove stains that would usually be provided by the heating of the water [10, 11]. If dirt and stains could be removed with little input and quickly in cold water it would have an obvious benefit to the consumer giving them more free time to focus on other areas of their lives.

Biological washing detergents rely on enzymes to remove the stains found on clothes. However enzymes usually work best at temperatures between 20-50^{o}C therefore they limit the temperature the washing cycle can be carried out at [12]. This thesis sets out to investigate an enzyme that has the potential to be able to break down stains at ambient temperatures called *Candida Antarctica*

Lipase B (CAL B). As the name suggests the enzyme is native to Antarctica and so has a high activity at temperatures near 0^{o}C due to it having a more flexible structure than other, similar enzymes. CAL B is a lipase enzyme meaning it breaks down lipids which are a substantial component of common stains in clothing.

The cool temperature exploration was accomplished by utilising the experimental procedure of single molecule recognition force microscopy (SMRFM). This process is an atomic force microscopy (AFM) technique that can measure the unbinding force between any binding pair of molecules. By performing this technique on *Candida Antarctica* Lipase B it was possible to see how variations in the temperature of the surrounding liquid affected the activity of the enzyme.

The work carried out was split into three fundamental aims which were as follows:

1. Set up a system for SMRFM using known molecules that have successfully been employed in previous studies.
2. Apply this working system to the enzyme *Candida Antarctica* Lipase B and witness unbinding events at room temperature.
3. Vary the temperature from as low as possible to room temperature to see how the activity of the target enzyme is affected by the environmental changes. Specifically looking at ambient water temperatures.

Other goals included finding a way to efficiently and effectively analyse the vast amounts of data that these experiments produce, to choose appropriate substrates for the enzyme and create a system that could cool the microscope sample area to the required temperatures.

This thesis consists of six main chapters. A brief description of each chapter will be given below

Chapter 2 - Catalysis and Enzymes

This section introduces enzymes, explains their structure and how they work and gives a detailed description of the low temperature enzyme *Candida Antarctica* Lipase B.

Chapter 3 - Experimental Techniques

Here the principles behind atomic force microscopy are given and the theory of SMRFM experiments is explained. This includes different imaging techniques, such as PeakForce QNM and Force Volume, the different types of chemistry used to attach molecules to the AFM tips and some of the alternative experiments used to measure unbinding forces such as optical tweezers. It also includes a description of other techniques used during this research.

Chapter 4 - Analysis Program

Over the course of the experiments it became apparent that the vast amount of data was not able to be analysed easily and quickly with commercial software. This chapter explains the method behind creating a tailored Matlab algorithm to increase the speed of analysis.

Chapter 5 - Single Molecule Force Spectroscopy Test System

In the experiments discussed in this section a test system for single molecule force measurements was set up using the molecules avidin and biotin. The chapter highlights the reasons behind the choice of molecules, binding chemistry and imaging parameters as well as presenting evidence that the experiments could successfully show unbinding between the two molecules.

Chapter 6 - *Candida Antarctica* Lipase B and *Pseudomonas Aeruginosa 3859*

The next step was to apply the avidin and biotin system developed in the previous chapter to the type of enzymes important for washing detergents. This included *Candida Antarctica* Lipase B which is the key enzyme for this work as well as a similar enzyme known as PA3859 which was used as a test molecule for the experimental method applied. A number of changes to the previous system were needed which are explained and justified here. Both enzymes were used in the AFM system and their unbinding forces were measured as well as the time taken for the enzymes to bind to their substrates.

Chapter 7 - *Candida Antarctica* Lipase B Temperature Variation

The last results chapter discusses the process of creating a cooling system for the AFM which could fit in the small area under the microscope and reach the likely ambient water temperatures of the UK to see how *Candida Antarctica* Lipase B responds in this environment. The cooling mechanism is then applied to single

molecule experiments allowing them to occur at a range of temperatures. The results found are presented at the end of this section.

Chapter 8 – Conclusion

In the final chapter of this thesis the findings discussed in Chapters 4, 5, 6 and 7 are summarised. Overall the work carried out suggests that SMRFM is a useful tool for investigating enzymes and that CAL B has good potential for low temperature detergents. Possible extensions to the experiments are also considered in this chapter.

1.1 References

[1] R. Garnaut, "The Garnaut climate change review," *Global Environmetal Change,* no. 13, pp. 1-5, 2008.

[2] F. de'Donato and P. Michelozzi, "Climate Change, Extreme Weather Events and Health Effects," *The Mediterranean Sea,* pp. 617-624, 2014.

[3] P. K. Thornton, P. J. Ericksen, M. Herrero and A. J. Challinor, "Climate variability and vulnerability to climate change: a review," *Global change biology,* 2014.

[4] S. Solomon, Climate change 2007-the physical science basis, vol. 4, Cambridge University Press, 2007.

[5] D. A. Lashof and D. R. Ahuja, "Relative contributions of greenhouse gas emissions to global warming," *Nature,* vol. 344, pp. 529-531, 1990.

[6] J. Conti, P. Holtberg, L. E. Doman, K. A. Smith, J. O. Sullivan and K. Vincent, International Energy Outlook 2011, US Energy Information Administration, 2011.

[7] N. L. Panwar, S. C. Kaushik and S. Kothari, "Role of renewable energy sources in environmental protection: a review," *Renewable and Sustainable Energy Reviews,* vol. 15, pp. 1513-1524, 2011.

[8] A. Evans, V. Strezov and T. J. Evans, "Assessment of sustainability indicators for renewable energy technologies," *Renewable and Sustainable Energy Reviews,* vol. 13, pp. 1082-1088, 2009.

[9] C. Pakula and R. Stamminger, "Electricity and water consumption for laundry washing by washing machine worldwide," *Energy Efficiency,* vol. 3, pp. 365-382, 2010.

[10] F. Birol, "World Energy Outlook 2010," International Energy Agency, 2010.

[11] L. Cozzi, World Energy Outlook 2011, International Energy Agency, 2011.

[12] K. Faber, Biotransformations in Organic Chemistry: a textbook, Springer, 2011.

Chapter 2 - Catalysis and Enzymes

In simple terms a catalyst is something that makes a chemical reaction 'go faster'. Catalysts open up new reaction pathways which have a lower energy barrier and therefore allow the reaction to proceed at a faster rate [1]. This not only means the product can be obtained in a shorter amount of time but that the reaction uses fewer resources and generates less waste. What makes a catalyst different from another reactant is that the catalyst is not consumed during the reaction. It is left unaltered to be used again in future cycles of the reaction. Catalysts have a huge variety of applications in the commercial sector including food, chemical, pharmaceutical and cosmetic manufacture. It is estimated that as of 2011 over 80% of all chemical processes involve a catalysed reaction which leads to the catalysts industry being valued at around 400 billion Euros worldwide [2, 3, 4].

Many substances can act as catalysts. In certain situations protons, polymers and proteins can all act as catalysts. In general there are three categories: homogenous, heterogeneous and biological catalysts. Homogenous catalysis reactions are ones where the catalyst and the reactant or reactants are in the same phase. Heterogeneous catalysis occurs when the reactants are in a different state to the catalyst. For example a number of industrial reactions use a sheet metal catalyst on gas reactants. Biocatalysis usually refers to enzymes which will be discussed in more detail in section 2.2. It is enzymatic biocatalysts that are of importance in this project so this chapter will outline catalysis,

enzyme properties, structure and mechanism and talk about the specific enzyme of interest – *Candida Antarctica* Lipase B

2.1 Catalysis

As mentioned above catalysts open up a new pathway for a reaction. This path is not necessarily less complicated and it can have a number of intermediate steps but the highest activation barrier for one of these steps is always lower than the barrier of the uncatalysed reaction [5, 6].

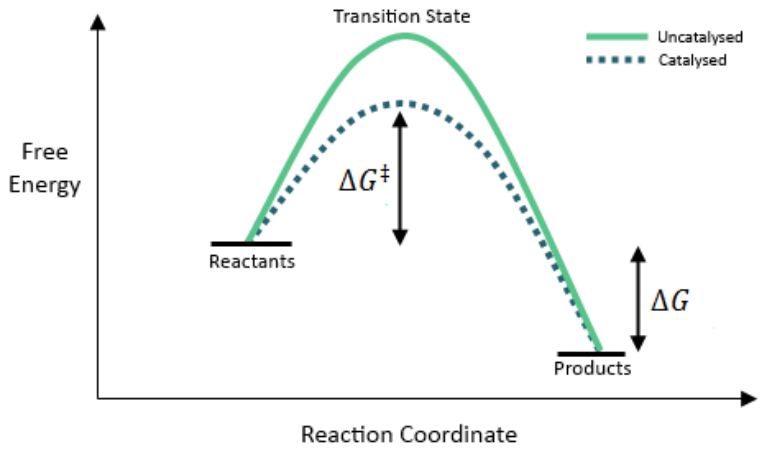

Figure 2.1: Reaction coordinate diagram for a simple reaction. The dashed curve represents how the energy barrier is effectively lowered in a catalysed reaction.

Catalyst kinetics can be described by transition state theory which looks at the energy levels during the reaction. A reaction coordinate diagram (figure 2.1) shows an example reaction pathway. The vertical axis shows the free energy and the horizontal axis is an arbitrary quantity known as the reaction coordinate. This parameter can represent any variable that changes over the course of the reaction for example the length of a bond in a bond breaking reaction. The peak

of this diagram is the transition state where bonds can be broken or created. This state is very short lived, surviving for a time of the order of ~10^{-12}s [6]. Reaching the transition state does not mean that the product is definitely formed. Sometimes the transition state will return to the reactants due chemical equilibrium.

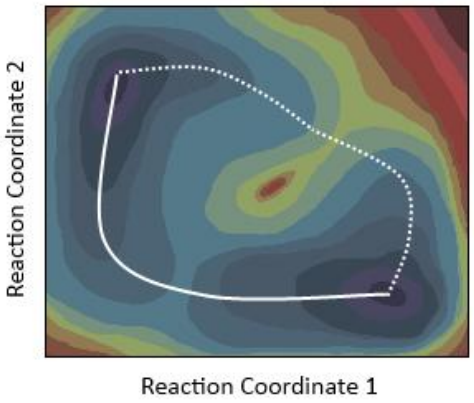

Figure 2.2: Reaction coordinate diagram with an extra dimension. Blue represents the lowest energy and therefore the favourable route (solid line). The dashed line shows another possible reaction pathway.

This is a very simplified look at the reaction mechanism. It only looks at what happens with one change in the system but the energy required to break a bond for instance can depend on multiple parameters such as angle of the bond or the presence of a neighbouring bond. Figure 2.2 shows a diagram with two reaction coordinates and examples of multiple reaction pathways. A better representation of a reaction coordinate diagram will have many dimensions giving a huge number of potential pathways than those shown in figure 2.2. However many of these pathways have activation energies so high that they are effectively impossible.

2.1.1 Reaction Mechanism

The population of the transition state can be found by assuming that the transition and reactant states are in thermal equilibrium [5, 7]. The transition state and the product states are not always in equilibrium. Sometimes the reaction is irreversible as the energy barrier to overcome is too high.

Substrate + Catalyst ⇌ Transition State → Product + Catalyst

A real life example could be a reaction such as the enzyme sucrase breaking down sucrose in the body:

Sucrose + Sucrase ⇌ Sucrose-Sucrase Transition State → Glucose + Fructose + Sucrase

This can be generalised in the following equation where A is the substrate, B is the enzyme and P is the product.

$A + B \rightleftharpoons AB^{\ddagger} \rightarrow P + B$

$$K^{\ddagger} = \frac{[AB^{\ddagger}]}{[A][B]} \quad (1)$$

Where $K^{\ddagger}$ is the equilibrium constant. The rate is equal to the population of the transition state multiplied by the frequency of vibration of the bond that is being broken denoted by ν.

$$rate = \frac{d[P]}{dt} = \nu[AB^{\ddagger}] = \nu K^{\ddagger}[A][B] \quad (2)$$

The rate constant k is defined as:

$$k = \nu K^{\ddagger} \tag{3}$$

The frequency of the vibration of the bond is given by:

$$\nu = \frac{k_B T}{h} \tag{4}$$

Where k_B is the Boltzmann constant, T is the temperature and h is Planck's constant.

From thermodynamics it is known that the activation energy, which is related to the Gibbs free energy $\Delta G^{\ddagger}$, is linked to the equilibrium constant by the following equation:

$$\Delta G^{\ddagger} = -RT \ln K^{\ddagger} \tag{5}$$

Where R is the molar gas constant and T is temperature. Substituting equation (4) and (5) into (3) we get:

$$k = \frac{k_B T}{h} e^{-\frac{\Delta G^{\ddagger}}{RT}} \tag{6}$$

It is known that the Gibbs free energy can be described by the following:

$$\Delta G^{\ddagger} = \Delta \mathrm{H}^{\ddagger} - T\Delta \mathrm{S}^{\ddagger} \tag{7}$$

Where H is the enthalpy and S is the entropy. Equation (6) now becomes:

$$k = \frac{k_B T}{h} e^{-\frac{\Delta H^{\ddagger}}{RT}} e^{+\frac{\Delta S^{\ddagger}}{R}} \tag{8}$$

This equation is the Eyring equation which comes from transition state theory. It shows that to produce the product faster the activation energy must be reduced or the temperature increased. The latter is not always possible as it can be expensive or, in the case of cells for instance, it can damage the reactants.

A catalyst lowers the free energy needed to overcome the energy barrier. To do this the energy of the initial reagent needs to increase or the transition state energy needs to decrease. In the case of catalysed reactions, the enthalpy in the system, usually refers to the bond strength so weaker bond strength means less enthalpy needed. The entropy of the system, can relate to the structure of the molecule. By reducing the bond strength and adding entropy to the system catalysis can lower the activation energy for the reaction and so increase the probability of the reaction occurring.

2.1.2 Restriction of Catalytic Activity

There are many factors that can dictate the efficiency with which a catalyst works. All types of catalysts can be affected by changes in pH, temperature, salinity and pressure. There are usually specific groups in the molecular structure of the catalyst on which the activity depends. These groups can be altered or removed by changes to the environment. If this occurs the catalyst will be deactivated. For example metal catalysts can sinter at high temperatures which cause their structures to collapse reducing the surface area and therefore reducing the activity.

Enzyme activity is particularly influenced by high temperature which is explained in greater detail in section 2.2 but they are also seriously affected by inhibition,

as are other catalysts [8]. There are two types of inhibitor: competitive and non-competitive. The former occurs when two molecules compete for the binding site of the catalyst. This competitor is usually a molecule that is similar to the transition state of the reaction. A non-competitive inhibitor is one that binds to another part of the catalyst which results in a change in the structure and shape of the binding site [8]. Sometimes an inhibitor binds to a catalyst irreversibly. When this occurs the catalyst is said to have been poisoned. If enough 'poison' is present then the reaction will stop completely. Some catalysts can have temporary poisoning. For example the affected area on a metal catalyst can be burnt off to reveal the unaltered surface underneath.

2.1.3 Significance of Catalysis

There are a huge number of industrial uses for catalysts, a few of which have been highlighted below to give an indication of how important they are to everyday life and to show where current areas of research are focused.

All types of catalyst have found applications in the pharmaceutical industry. Metal catalysts have been used to increase the efficiency of drug research processes [9]. Enzymes, due to their high specificity for substrates, have been used as actual drugs. Activase is an enzyme drug that reduces the risk of heart attacks from blood clots by thinning blood. Others have been used to treat auto immune diseases, leukaemia and other forms of cancer by either directly destroying the offending molecules or by synthesising products that can [10, 11]. Inhabitation of catalysts is important for drug research too, for instance in Alzheimer's disease treatment and restriction of cancerous cell growth [12].

Enzymes are also being purposely inhibited to reduce the side effects of many anti-cancer drugs [13].

Another area of catalytic research is in green technologies which is the focus of the work carried out in this thesis. With current concern about diminishing resources, energy production and the pollution of our planet there is a large push for new technologies which reduce energy costs and environmental impact [2].

Many commercial processes require large amounts of resources, generate lots of waste and can also use dangerous chemicals. Catalysts are being used to try and counter these negative consequences of our industrial society. For example the creation of chemicals and petrochemicals use catalytic oxidisation reactions. Research has begun to focus on removing the toxic reactants and recycling by-products in these catalysed reactions [2, 14]. Much of this research involves looking at potential new catalysts.

Biological catalysts are being used in green technology research too. For example many biocatalysts are used to form polymers which then go on to be used in organic photovoltaics and LEDs research [15, 16]. Another area of interest is to reduce the temperature needed for everyday reactions to take place to save energy. As catalysts, especially enzymes, have an optimum working temperature looking for new catalysts that can work at low temperatures is of great interest. The focus of this project it to look at low temperature enzymes for use in detergents which is explained in detail in section 2.3.

2.2 Enzymes

Enzymes have been used for millennia in food processing including the production of beer, wine, cheeses, meat tenderisation and citrus peeling but the term enzyme was first used relatively recently. Scientists started to recognise enzymes and their reactions during the early 1800s but it was not until 1877 that the term enzyme was used by German scientist Wilhelm Kühne [8]. Originally the name enzyme was given to the unknown reaction caused by yeast in the fermentation process but as research continued into biological catalysis the term evolved to mean proteins that catalyse reactions and the naming convention to add the suffix '-ase' was adopted [17]. It is now known that enzymes also play a vital role in life as fundamental processes such as respiration, DNA transcription and digestion are only possible due to enzymes.

Despite giant leaps in the understanding of enzymes, which produced a number of Nobel Prize Laureates, it was not until the early 21st century that enzymes started to be widely used in commercial processes such as those in the pharmaceutical and fine chemical industries. This was due to enzymes being very expensive and hard to isolate. Any industrial application involving enzymes usually did so with the 'wild type' enzyme which is how the enzyme is found in the organism it is created from. With the development of genetic engineering enzymes are not only cheap and readily available but can be genetically altered and adapted to be more efficient and, more importantly, stable at unfavourable conditions so they are now found in a huge host of new industrial processes

including cosmetics, biodiesels, laundry detergents, fine chemicals and bioremediation [1, 4, 8, 18, 19, 20].

This section will give a background to enzyme structure and mechanism and explain their advantages and disadvantages over traditional catalysts.

2.2.1 Structure

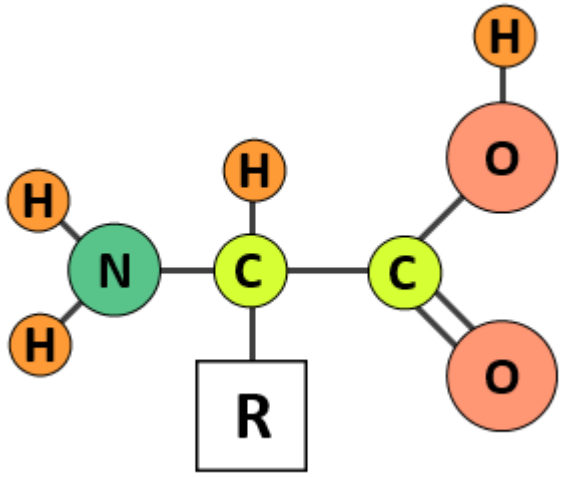

Figure 2.3: Generalised form of an amino acid. The R group represents the residue of the amino acid.

Enzymes are proteins that can catalyse reactions. Proteins are the building blocks of life and play a integral role in cell structure, cell division, the transport of oxygen and more. They are formed of chains of covalently linked amino acids known as polypeptides. Amino acids are small compounds that are composed of amine and carboxylic acid groups each with their own specific side chain that determines the particular amino acid, known as the residue, as seen in figure 2.3. These side chains are known as residues. There are over 500 known amino

acids but living organisms only use 20 to form over 100,000 proteins that are needed to survive.

The order of the amino acids in the polypeptide chain is known as the primary structure of the protein and it is responsible for the overall shape of the protein. One end of the polypeptide chain is known as the carboxyl terminus and the other the amino terminus, known as the C-terminus and N-terminus respectively. The primary structure is unique to each type of protein and is coded into the host genome.

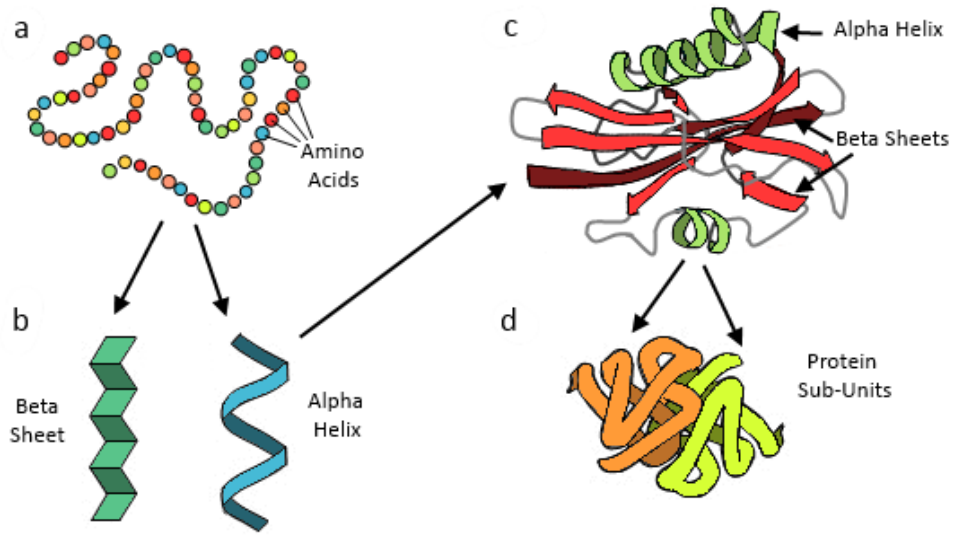

Figure 2.4: Schematic of protein structure. a) Primary structure – determined by the order of amino acids in the polypeptide chain. b) Secondary structure – primary structure folds into specific shapes caused by hydrogen bonds between amino acids. c) Tertiary structure – the three dimensional shape of the polypeptide chain containing multiple secondary structures. d) Quaternary structure – multiple tertiary sub-units can join together to form a larger protein.

Amino acids contain hydrophilic and hydrophobic sections which determine the way the amino acid chain folds as the hydrophobic parts move to be hidden from the surrounding solvent. Small sections of amino acids will form basic substructures bound together by hydrogen bonds known as α-helices, β-sheets and β-turns [8]. These substructures are known as the secondary structure of the protein. The final three-dimensional shape of the protein is its tertiary structure. In practice many proteins are actually a combination of these tertiary structures which join together to form the protein's quaternary structure [6, 21, 22]. This is summarised in figure 2.4.

Within the tertiary or quaternary structure of an enzyme, depending if it is a multi-subunit protein, is an 'active site' which can be simply be thought of as a dent in the side of the protein which has a number of amino acid residues in it. An enzyme's substrate is just a molecule that is involved in the reaction taking place. A substrate will bind to the enzyme's active site during catalysis and this act of binding is what facilitates the increase in reaction rate.

2.2.2 Reaction Kinetics and Mechanism

The most common model of enzyme kinetics is the Michaelis-Menton model [1]. This looks at the binding between the substrate, S and the enzyme, E in the following reaction. The product is denoted P.

$$E + S \underset{k_{-1}}{\overset{k_1}{\rightleftharpoons}} ES \xrightarrow{k_2} E + P$$

The first step is reversible whereas the second is irreversible. k represents a rate constant. The rate of product formation can be given by:

$$\frac{dP}{dt} = \frac{k_2[E]_0[S]}{K_m + [S]} \quad (9)$$

Where K_m is the Michaelis constant and represents the substrate concentration at which the reaction is going at half its maximum rate. This equation shows that when the substrate concentration is much greater than the Michaelis constant the rate becomes $v=k_2[E]_0$. This occurs when all the enzyme active sites are full and is known as saturation kinetics. This produces the maximum rate of the reaction.

The most popular model for enzyme interactions is the induced fit model. It was previously thought that an enzyme's active site was perfectly shaped to fit the substrate but in this 'lock and key' model there is no explanation as to how the enzyme lowers the transition state energy. Instead the induced fit model implies that enzymes are flexible and the active site bends to accommodate the substrate. Residues, the side chain specific to a particular amino acid, in the active site help bind the substrate to the active site. Enzymes use four types of binding to attach their substrates: van der Waals, electrostatic, hydrogen bonds and hydrophobic binding [6]. The reaction now becomes:

$$E + S \longrightarrow ES \longrightarrow ES^{\ddagger} \longrightarrow E + P$$

Here ES → $ES^{\ddagger}$ represents the enzyme substrate complex going from an inactive to active form.

There are a number of different mechanisms that can effectively lower the energy barrier of the transition state with the induced fit model. One mechanism is mediated by the physical binding as this will impose stresses and strains onto

both the enzyme and the substrate. This can expose target bonds or make the substrate more unstable and so there is a smaller jump in energy to the transition state. Proximity and orientation can also have an effect on reaction rate. Enzymes, by binding to multiple substrates, turn the reaction from an intermolecular reaction to an intramolecular one. Intramolecular reactions tend to be faster as all the reactants are in close proximity to one another [23].

Amino acid residues can also play an important role in enzyme catalysis as they can act as proton donors or acceptors which help neutralise any charges that are created in the transition state or they can form ionic bonds with the substrate both of which increase stability. Residues can also covalently bond with the substrate. This forms another intermediated state of higher energy and so it takes less energy to reach the transition state. As mentioned the process of the enzyme binding to its substrate can alter the enzyme's shape which in turn can expose more residues which help the catalysis further [8].

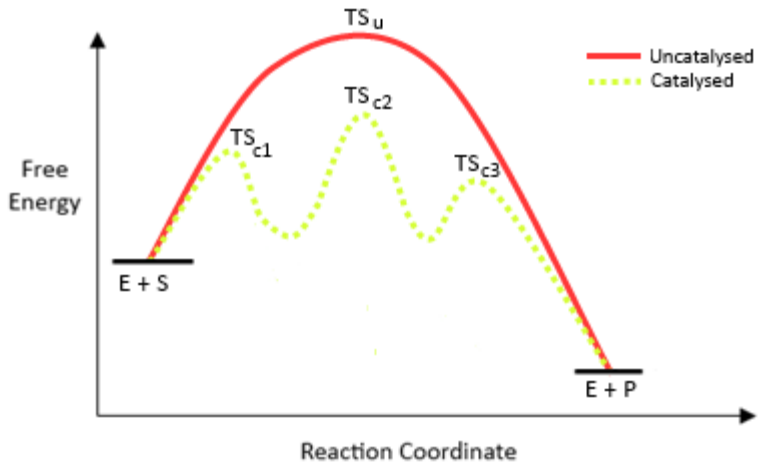

Figure 2.5: Reaction coordinate diagram showing a catalysed reaction with three transition states and two intermediate states between them.

In reality, as with all catalysts, the true reaction pathway includes a number of transition states which are separated by intermediate states. At the intermediate states the bonds being created or destroyed during the transition states are fully formed or broken. Intermediate states are significantly longer lived than the transitions states which can live for as little as tens of picoseconds. Figure 2.5 shows a truer representation of a catalysed representation than that shown in figure 2.1 as there are a number of stages in the process [5].

2.2.3 Cofactors

As a significant proportion of proteins are formed from the same 20 amino acids the functional groups that proteins contain are rather limited. Because of this many enzymes need cofactors before they can carry out certain functions. These are non-protein molecules which bind to the original enzyme now known as the apoenzyme. There are three types of cofactor: coenzymes – organic molecules which attach weakly to the apoenzyme, prosthetic group cofactors – similar to coenzymes but with a large binding force, and metal ions such as iron and copper.

Chlorophyll is a well known example of a cofactor which enables the photosystem II protein complex found in plants to be able to catalyse the harvesting of light [6]. Vitamin A, B_1, C and E and folic acid are all examples of cofactors for a number of enzymes that help with biological processes such as protein synthesis and digestion which is why a healthy diet contains sources of these compounds [8].

2.2.4 Advantages

As mentioned in section 2.1 enzymes are just one type of catalyst available so why should industry focus on enzymes over non-biocatalysts? Enzymes have a considerable number of advantages which, along with their drawbacks, will be discussed below.

First and foremost enzymes are significantly more efficient than chemical catalysts. An enzyme can complete 1000 reaction cycles per second whilst other catalysts usually cycle through 2-165 per second [8]. Enzymes can increase the reaction rates of the uncatalysed reaction by a factor of 10^{8}-10^{10} which is higher than heterogeneous or homogenous catalysts [24, 25, 26]. The concentration of enzymes in a typical reaction can be 10^{-3}-10^{-4} % by molar concentration as opposed to 0.1-1% for conventional catalysts [4].

Enzymes work under much milder conditions, usually at neutral pH with temperatures typically between 20^{o}C – 50^{o}C, due to their biological requirements. This means less energy is needed to heat the environment and can reduce the unwanted effects introduced when reactions take place in harsh conditions such as decomposition, the breakdown of the molecule, and isomerisation, the rearrangement of the molecule. They are also biodegradable which means they are environmentally friendly giving them a huge advantage over heavy metal catalysts which are pollutants [4].

Another benefit of enzymes comes from the fact that they are usually compatible with each other due to their narrow range of working conditions. This means multi-step enzyme systems can be created where many enzymes

catalyse sequential reactions in the same environment. By having multiple enzymes in the same space reversible reactions can be made irreversible by immediately transforming the first product into another product that is more stable. It also leads to less energy and resources being used and also produces less waste than having each step of the overall reaction carried out in separate stages [27]. Cells would be unable to function correctly without multi-step enzyme processes and many processes in the pharmaceutical and chemical manufacture industries utilise the principle to produce products such as amino acids [28]

An enormous advantage of enzymes is their diversity and their specificity. There is a huge range of enzymes and with genetic modification this catalogue will continue to grow. For virtually all organic reactions there is an enzyme catalysed version [29]. The specificity of an enzyme relates to which substrates the enzyme can work on. Enzymes have unique and complex active sites which usually gives them a high specificity. The amino acid residues present at the active site as well as the shape are responsible for the specificity. Enzymes can be specific to a particular functional group on the substrate. They can also be specific to the layout of various functional groups relative to each other despite them being chemically identical [30, 31]. Finally enzymes are chiral molecules as amino acids are chiral. This means enzymes can be chirally specific and so will catalyse a reaction of one enantiomer but not the other. This is very important for the pharmaceutical industry as different enantiomers can have drastically different effects as most processes in the body depend on enzymes which need a particular enantiomer.

2.2.5 Disadvantages

Despite the numerous benefits to enzyme catalysis there are a few shortcomings some of which are caused by their properties that give the advantages highlighted above. Firstly their high chiral specificity comes from the fact that the enzyme itself is chiral. There is no way of creating the other enatiometric form of an enzyme to catalyse the other enatiometric form of the substrate. To get the opposite enatiometric product the enzyme with opposite sterochemical selectivity has to be found which is not always possible [4].

As enzymes come from nature which predominantly uses water as a solvent most enzymes are at their most efficient in water. Unfortunately many organic compounds are not very soluble in water and switching to an organic solvent may cause a loss of enzyme activity [32].

Another disadvantage is an enzyme's dependence on its cofactors. Despite being able to bind to many unnatural substrates enzymes can only use their natural cofactors. Some of these cofactors can be expensive, environmentally damaging and hard to recycle which generates waste [4].

Finally the limited and mild operating conditions enzymes require which makes them a cost efficient and environmentally friendlier option restricts the control over the reaction environment as the parameters cannot be altered too drastically without affecting the enzyme's activity. This means the efficiency of a reaction cannot be fully optimised as parameters that suit the substrate will destroy the enzyme.

The rate of enzyme reactions is heavily dependent on temperature. At too low temperatures there is not enough energy for the substrate to move enough to bind to the enzyme so no reaction takes place. Increasing the temperature will increase the rate. A change of 10^{o}C can increase the activity of the enzyme by over 50% but too large an increase in temperature will lead to the enzyme being denatured. Most enzymes will denature at temperatures above 40^{o}C. When this happens bonds involved in the quaternary and tertiary structures can break and cause the enzyme to lose its structure. Consequently the active site is not the correct morphology to bind to the substrate anymore and the reaction stops [21, 22].

Denaturisation is usually a reversible process but if the temperature increase is too great hydrogen bonds between sections of the polypeptide chain will be broken and the secondary structure can be lost. As this happens molecules can be exposed to water which creates new hydrogen bonds in different places. These bonds are at a greater energy level than the initial bonds meaning a lot more energy is required to break them. This larger energy barrier leads to the denaturisation being irreversible and the native structure is lost. The pH level and salt concentration can also cause unfolding of the enzyme structure. This issue is being overcome with the use of enzymes from extremophiles.

2.2.6 Enzymes From Extremophiles

Extremophile is the name given to a microorganism that thrives in a harsh environment such as arctic tundra, arid deserts or the depths of the ocean. Enzymes from these extremophiles unlock the potential for use as biocatalysts in

reactions that were previously impossible as they are adapted to work in traditionally unfriendly conditions. As mentioned in section 2.2.5 biocatalysts have a number of great advantages over traditional catalysts but one of their largest downside is their inability to cope with inhospitable environments. Many of these 'extremozymes' can catalyse the same reactions as standard enzymes but at much higher or lower temperatures, pHs, pressures and salinities without inhabitation or denaturisation [33].

An example of an industrial extremozyme is an enzyme from thermus brokianus which is found in the geysers in Yellowstone National Park. This enzyme can break down hydrogen peroxide which is a harmful waste product from many commercial bleaching processes in the paper and fabric industries. Those reactions occur at high pH and temperature which would render most enzymes useless. But as thermus brokianus's enzymes have adapted to these conditions naturally the enzyme is able to handle the commercial reaction and reduce waste. There are many other industrial applications for extremozymes including improved food and cosmetic production, starch processing and animal feed creation but the one of importance for this research is in the detergent sector [34].

2.3 Lipases

A huge potential for extremozymes is the use of psychrophilic enzymes for laundry detergents. Psychrophilic enzymes are a subcategory of extremophile enzymes that have an optimum working temperature that is below 15^{o}C.

Detergents can come in two forms: biological and non-biological. Biological washing powders use enzymes to break down the stains in fabrics whilst non-biological use chemicals. These chemicals can be damaging to the environment and can actually leave permanent stains on fabrics when they are used to remove protein stains due to bleaching and the denaturing of the proteins [35]. High temperatures are also needed to remove fatty stains from clothes using non-biological washing powders. In contrast biological detergents are environmentally friendly and due to extremozymes there is the possibility of them being able to operate at much cooler temperatures.

There are three main constituents of biological detergents: surfactants to solubilise stains, enzymes to digest them and bleaches to break down and loosen coloured stains. It is the enzyme step that is limited by temperature [36]. By using psychrophilic enzymes the operating temperature can be lowered and with little or no heating required energy can be saved.

Enzyme	**Function in detergents**
Proteases	Removing protein stains e.g. egg, blood, grass and sweat
Amylases	Removing starch stains e.g. potatoes, pasta, chocolate and custard
Lipases	Removing fatty materials e.g. butter, oils, fats and sauces
Cellulases	Modifying the fabric e.g. colour brightening, softening

Table 2.1: The common enzyme types used in bio-detergents and their particular functions.

Four types of enzyme are regularly used in detergents which are summarised in table 2.1. Many studies have shown that lipases are very effective at removing dirt from fabric [36, 37, 38]. Lipases decompose fatty stains into a more hydrophilic form which makes them easier to remove [37]. Natural substrates for

lipases are triglycerides. These long molecules are the main constituent of many food stains such as frying oil, salad dressings and other fatty substances. Skin also secretes oils to make it waterproof which can get on clothes. These oils are one third triglycerides so can be broken down by lipases too.

There are a large number of psychrophilic lipases which make them an ideal candidate for low temperature detergents. These cold active lipases are biodegradable, pose no threat to aquatic life and do not have an impact on sewage treatment which gives them a big advantage over chemical detergents [39].

2.3.1 Function and Structure of Lipases

Lipases are arguably one of the most important groups of biocatalysts. They have found use in the synthesis of biopolymers, biofuels, pharmaceuticals and flavourings and so are of great interest to scientists and industry [39].

Lipases' substrates are lipids. Lipids are either completely hydrophobic molecules or consist of a hydrophilic head and a hydrophobic tail making them usually insoluble in water. In biology they are used for energy storage, signalling and cell structure. Lipids have very diverse structures; fatty acids for instance are long chains whereas steroids contain four central rings and tend to be more compact. Lipids can be organised into eight different categories based on their function. Common molecules such as fats, waxes and certain vitamins such as A and D are all examples of lipids.

Lipases catalyse the hydrolysis of lipids or the synthesis of long chain glycerol molecules [40, 41]. They usually have broad substrate specificity and have good chemoselectivity, enantioselectivity and regioselectivity due to their active site shape meaning they prefer certain functional groups, chirality and reaction sites respectively [42]. Lipases are important for digestion, transport and the processing of lipids in all living organisms and find their largest commercial use in the detergent industry [43]. Lipases, unlike lipids, are usually water soluble [40].

Most lipolytic enzymes contain an alpha/beta hydrolase fold which makes up the core structure for many other enzymes including protases, esterases and peroxisdases [44]. The active sites of lipases have lids which can open or close the active site from the surroundings. As the enzyme binds to its substrate the lid opens and lets the solvent access the active site. This also exposes a hydrophobic surface which helps bind the lipase to the substrate interface [40].

2.3.2 Psychrophilic Lipases

As mentioned psychrophilic lipases are those that have an optimum temperature below 15^{o}C and still have a high activity at very low temperatures. They have been found in a wide range of sources including sea sediments, frozen and refrigerated food, glaciers and in Antarctica. The microorganisms that provide the lipases are bacteria and fungi. The majority of psychrophilic enzymes are isolated from microorganisms found in the Polar Regions which stay at a fairly constant temperature between -2^{o}C – 2^{o}C.

Standard lipases do not work at low temperatures due to the reduction of collisions between it and the substrate as under these conditions the diffusion is

slowed. If the enzyme's affinity for its substrate could be increased without a temperature rise the enzyme would have a greater activity at lower temperatures as a collision would be more likely to result in the substrate binding to the enzyme. Currently the mechanism by which psychrophilic lipases work is not fully understood. Studies into these enzymes have been scattered and mainly focus on isolation, purification and characterisation [42].

Those studies that do investigate why they have increased activity at low temperatures suggest that it is a higher flexibility that increases this affinity for the substrate [39, 45, 46, 47]. The lipases are structurally changed by having more flexible polypeptide chains. This lets the active site change shape so it can be more accommodating of the substrate and increase the chances of binding during a collision. This increase in flexibility comes from a reduction in the bonds between various points in the chains. However there is a balancing act between increased flexibility and decreased stability. Too much flexibility will mean the active site no longer fits the substrate [48].

2.4 *Candida Antarctica* Lipase B

The enzyme that is investigated in this work is *Candida Antarctica* Lipase B or CAL B shown in figure 2.6. Candida is a genus of yeast which is responsible for many infections of the blood and organs in humans. The species *Antarctica* is named after its place of origin which makes it very well adapted to cold temperatures meaning it is potentially a great source of psychrophilic lipases [42]. Lipase B is one of two lipolytic enzymes from *Candida Antarctica*. Lipase B is a carboxylesterase which means it allows the catalysis of the splitting of a

carboxylic ester into an acid and an alcohol with the addition of water. It is composed of 317 amino acids, has a molecular weight of 33 kDa and is 3 x 4 x 5 nm in size [49, 50]. It is a highly stereoselective enzyme due to a small pocket on its active site. This pocket binds to alcohols on the substrate but as it is on one side of the active site it binds to one enantiomer only [51].

It has been used commercially and in research for a number of processes including polymerisation and polyester synthesis and has a number of patents in the food, chemical and pharmaceutical industries [52, 53]. Mutated variations of CAL B have also been created to try and improve the activity and raise the temperature that it irreversibly denatures at [54, 55].

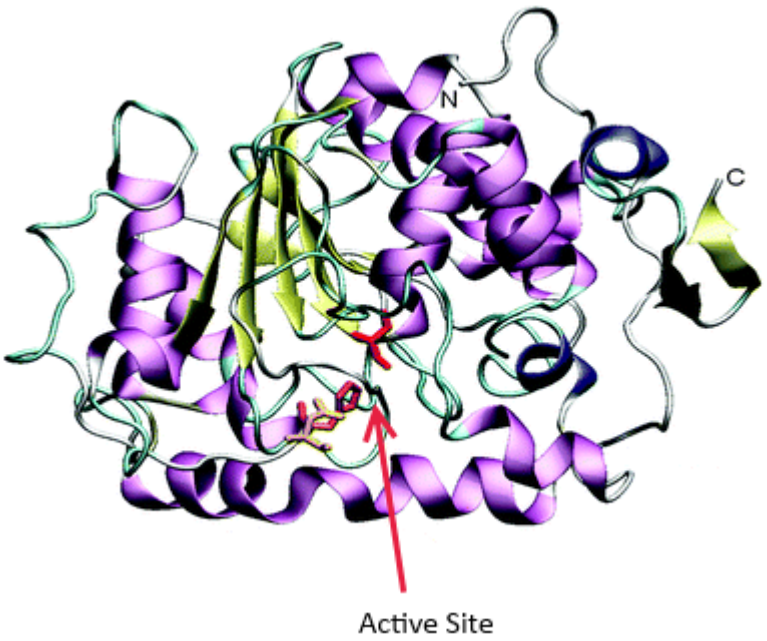

Figure 2.6: Ribbon structure diagram of CAL B showing its secondary structures and active site [56]**.**

As of writing no comprehensive study into how temperature variation effects CAL B has been carried out and its optimum temperature is unknown. It is known that it denatures at 40°C in aqueous solutions and a bit higher in organic solvents [54]. Other studies have shown that it is active at 0°C and simulations have shown that at 5°C the lid is flipping between open and closed formations and at 35°C and 50°C the lid is closed and the enzyme activity stops [50].

This project's main aim is to carry out a thorough study of how CAL B's activity changes over a range of temperatures and to try and gain more information about its optimum working temperature. This is predominately carried out with Atomic Force Microscopy which will be discussed in detail in the next chapter.

2.5 References

[1] K. Buchholz, V. Kasche and U. T. Bornscheuer, Biotcatalysis and enzyme technology, John Wiley & Sons, 2012.

[2] K. Wilson and A. F. Lee, Heterogeneous Catalysts for Clean Technology: Spectroscopy, Design, and Monitoring, John Wiley & Sons, 2013.

[3] U.S. Climate Change Technology, "Technology Optins for the Near and Long Term," 2005.

[4] K. Faber, Biotransformations in Organic Chemistry: a textbook, Springer, 2011.

[5] A. Fersht, Structure and Mechanism in Protein Science: A Guide to Enzyme Catalysis and Protein Folding, W. H. Freeman, 1999.

[6] M. Williamson, How Proteins Work, Garland Science, 2012.

[7] R. Chang, Physical chemistry for the biosciences, University Science Books, 2005.

[8] G. Rothenberg, Catalysis: Concepts and Green Applications, Wiley-VCH,

2008.

[9] J. F. Sonnenberg, N. Coombs, P. A. Dube and R. H. Morris, "Iron Nanoparticles Catalyzing the Asymmetric Transfer Hydrogenation of Ketones," *Journal of the American Chemical Society,* vol. 134, no. 13, pp. 5893-5899, 2012.

[10] M. Vellard, "The enzyme as drug: application of enzymes as pharmaceuticals," *Current opinion in biotechnology,* vol. 14, no. 4, pp. 444-450, 2003.

[11] K. D. Courtney, R. B. Corcoran and J. A. Engelman, "The PI3K pathway as drug target in human cancer," *Journal of Clinical Oncology,* vol. 28, no. 6, pp. 1075-1083, 2010.

[12] A. M. Lilja, Y. Luo, Q. S. Yu, J. L. Y. M. A. M. Röjdner and A. G. N. H. Nordberg, "Neurotrophic and Neuroprotective Actions of (-) and (+)-Phenserine, Candidate Drugs for Alzheimer's Disease," *PloS one,* vol. 8, no. 1, p. 54887, 2013.

[13] B. D. Wallace, H. Wang, K. T. Lane, J. E. Scott, J. Orans, J. S. Koo, M. Venkatesh, C. Jobin, L. M. S. Yeh and M. R. Redinbo, "Alleviating Cancer Drug Toxicity by Inhibiting a Bacterial Enzyme," *Sciencce,* vol. 330, pp. 831-835, 2010.

[14] F. Cavani, "Catalytic selective oxidation faces the sustainability challenge: turning points, objectives reached, old approaches revisited and solutions still requiring further investigation," *Journal of chemical technology and biotechnology,* vol. 85, no. 9, pp. 1175-1183, 2010.

[15] A. Suzuki, "Organoborates in new synthetic reactions," *Accounts of Chemical Research,* vol. 15, no. 6, pp. 178-184, 1982.

[16] D. Milstein and J. K. Stille, "A general, selective and facile method for ketone synthesis from acid chlorides and organotin compounds catalyzed by palladium," *Journal of the American Chemical Society,* vol. 100, no. 11, pp. 3636-3638, 1978.

[17] D. Blow, "So do we understand how enzymes work?," *Structure,* vol. 8, no. 4, pp. R77-R81, 2000.

[18] C. Wandrey, A. Liese and D. Kihumbu, "Industrial biocatalysis: past, present and future," *Organic Process Research & Development,* vol. 4, no. 4, pp. 286-

290, 2000.

[19] D. Muñoz Solano, P. Hoyos, M. J. Hernáiz, A. R. Alcántara and J. M. Sánchez-Montero, "Industrial biotransformations in the synthesis of building blocks leading to enantiopure drugs," *Bioresource technology,* vol. 115, pp. 196-207, 2012.

[20] K. R. Jegannathan and P. H. Nielsen, "Environmental assessment of enzyme use in industrial production – a literature review," *Journal of Cleaner Production,* vol. 42, pp. 228-240, 2013.

[21] T. P. Bennett and E. Frieden, "Modern Topics in Biochemistry," Macmillan, 1969, pp. 43-45.

[22] J. Holum, Elements of General and Biological Chemistry, Wiley, 1968.

[23] A. Warshel, P. K. Sharma, M. Kato, Y. Xiang, H. Liu and M. H. Olsson, "Electrostatic basis for enzyme catalysis," *Chemical reviews,* vol. 106, no. 8, pp. 3210-3235, 2006.

[24] R. S. M. J. Wolfenden, "The depth of chemical time and the power of enzymes as catalysts," *Accounts of chemical research,* vol. 34, no. 12, pp. 938-945, 2001.

[25] F. M. Menger, "Enzyme reactivity from an organic perspective," *Accounts of chemical research,* vol. 26, no. 4, pp. 206-212, 1993.

[26] D. L. Zechel and S. G. Withers, "Glycosidase mechanisms: anatomy of a finely tuned catalyst," *Accounts of chemical research,* vol. 33, no. 1, pp. 11-18, 200.

[27] E. Garcia-Junceda, Multi-step enzyme catalysis, Wiley, 2008.

[28] Z. Findrik and Đ. Vasiæ-Raèk, "Overview on Reactions with Multi-enzyme Systems," *Chem. Biochem. Eng.,* vol. 23, no. 4, pp. 545-553, 2009.

[29] C. J. Sih, E. Abushanab and J. B. Jones, "Biochemical Procedures in Organic Synthesis," *Annual Reports in Medicinal Chemistry,* vol. 12, pp. 298-308, 1977.

[30] H. M. Sweers and C. H. Wong, "Enzyme-catalyzed regioselective deacylation of protected sugars in carbohydrate synthesis," *Journal of the American Chemical Society,* vol. 108, no. 20, pp. 6421-6422, 1986.

[31] N. B. Bashir, S. J. Phythian, A. J. Reason and S. M. Robers, "Enzymatic esterification and de-esterification of carbohydrates: synthesis of a naturally occurring rhamnopyranoside of p-hydroxybenzaldehyde and a systematic investigation of lipase-catalysed acylation of selected arylpyranosides," *Journal of the Chemical Society, Perkin Transactions,* vol. 1, no. 18, pp. 2203-2222, 1995.

[32] A. M. Kilbanov, "Asymmetric transformations catalyzed by enzymes in organic solvents," *Accounts of Chemical Research,* vol. 23, no. 4, pp. 114-120, 1990.

[33] R. Karan, M. D. Capes and S. DasSarma, "Function and biotechnology of extremophilic enzymes in low water activity," *Aquatic Biosystems,* vol. 8, no. 4, 2012.

[34] B. Ven den Burg, "Extremophiles as a source for novel enzymes," *Current opinion in microbiology,* vol. 6, no. 3, pp. 213-218, 2003.

[35] F. Hasan, A. A. Shah and S. H. A. Javed, "Enzymes used in detergents: lipases," *African Journal of Biotechnology,* vol. 9, no. 31, pp. 4836-4844, 2013.

[36] E. Jurado, V. Bravo, G. Luzon, M. Fernández-Serrano, M. García-Román, D. Altmajer-Vaz and V. J. M., "Hard-surface cleaning using lipases: enzyme-surfactant interactions and washing tests," *Journal of surfactants and detergents,* vol. 10, no. 1, pp. 61-70, 2007.

[37] T. Fujii, T. Tatara and M. Minagawa, "Studies on applications of lipolytic enzyme in detergency I. Effect of lipase from Candida cylindracea on removal of olive oil from cotton fabric," *Journal of the American Oil Chemists' Society,* vol. 63, no. 6, pp. 796-799, 1986.

[38] D. Aaslying, E. Gormsen and H. Malmos, "Mechanistic studies of proteases and lipases for the detergent industry," *Journal of Chemical Technology and Biotechnology,* vol. 50, no. 3, pp. 321-330, 1991.

[39] B. Joseph, P. W. Ramteke, G. Thomas and N. Shrivastava, "Standard Review Cold-active microbial Lipases: a versatile tool for industrial applications," *Biotechnology and Molecular Biology Review,* vol. 2, no. 2, pp. 39-48, 2007.

[40] K. E. Jaeger and M. T. Reetz, "Microbial lipases from versatile tools for biotechnology," *Trends in biotechnology,* vol. 16, no. 9, pp. 396-403, 1998.

[41] R. K. Saxena, A. Sheoran, B. Giri and W. Davidson, "Purification strategies for microbial lipases," *Journal of Microbiological Methods,* vol. 52, no. 1, pp. 1-18, 2003.

[42] B. Joseph, P. W. Ramteke and G. Thomas, "Cold active microbial lipases: some hot issues and recent developments," *Biotechnology advances,* vol. 26, no. 5, pp. 457-470, 2008.

[43] X. L. Li, Y. Shi, W. H. Zhang, Y. J. Dai, H. T. Zhang, Y. Wang, H. K. Wang and F. P. Lu, "A high-detergent-performance, cold-adapted lipase from Pseudomonas stutzeri PS59 suitable for detergent formulation," *Journal of Molecular Catalysis B: Enzymatic,* vol. 102, pp. 16-24, 2014.

[44] M. Nardini and B. W. Dijkstra, "α/β hydrolase fold enzymes: the family keeps growing," *Current opinion in structual biology,* vol. 9, no. 6, pp. 732-737, 1999.

[45] N. More, R. M. Daniel and H. H. Petach, "The effect of low temperatures on enzyme activity," *Biochem,* vol. 305, pp. 17-20, 1995.

[46] E. E. Di Lorio, U. R. Hiltpold, D. Filipovic, K. H. Winterhalter, E. Gratton, E. Vitrano, A. Cupane, M. Leone and L. Cordone, "Protein dynamics. Comparative investigation on heme-proteins with different physiological roles," *Biophysical journal,* vol. 59, no. 3, pp. 742-754, 1991.

[47] J. W. Deming, "Psychrophiles and polar regions," *Current opinion in microbiology,* vol. 5, no. 3, pp. 301-309, 2002.

[48] S. D'Amico, P. Claverie, T. G. D. Collins, E. Gratia, A. Hoyoux, M. Meuwis, G. Feller and C. Gerday, "Molecular basis of cold adaptation," *Philosophical Transactions of the Royal Society of London. Sereis B: Biological Sciences,* vol. 357, no. 1423, pp. 917-925, 2002.

[49] J. Uppenberg, M. T. Hansen, S. Patkard and T. A. Jones, "The sequence, crystal structure determination and refinement of two crystal forms of lipase B from Candida Antarctica," *Structure,* vol. 2, no. 4, pp. 293-308, 1994.

[50] M. R. Ganjalikhany, B. Ranjbar, A. H. Taghavi and T. T. Moghadam, "Functional Motions of Candida Antarctica Lipase B: A Survey Through Open-Close Conformations," *PloS one,* vol. 7, no. 7, p. e40327, 2012.

[51] J. Uppenberg, N. Oehrner, M. Norin, K. Hult, G. J. Kleywegt, S. Patkar and T. A. Jones, "Crystallographic and molecular-modeling studies of lipase B from

Candida Antarctica reveal a stereospecificity pocket for secondary alcohols," *Biochemistry,* vol. 34, no. 51, pp. 16838-16851, 1995.

[52] A. Kumar, B. Kalra, A. Dekhterman and R. A. Gross, "Efficient Ring-Opening Polymerization and Copolymerization of ε-Caprolactone and ω-Pentadecalactone Catalyzed by Candida antartica Lipase B," *Macromolecules,* vol. 33, no. 17, pp. 6303-6309, 2000.

[53] A. Idris and A. Bukhari, "Immobilized Candida antarctica lipase B: Hydration, stripping off and application in ring opening polyester synthesis," *Biotechnology advances,* vol. 30, no. 3, pp. 550-563, 2012.

[54] N. Zhang, W. C. Suen, W. Windsor, L. Xiao, V. Madison and A. Zaks, "Improving tolerance of Candida Antarctica lipase B towards irreversible thermal inactivation through directed evolution," *Protein Engineering,* vol. 16, no. 8, pp. 599-605, 2003.

[55] Z. Qian and S. Lutz, "Improving the Catalytic Activity of Candida antarctica Lipase B by circular permutation," *Journal of the American Chemical Society,* vol. 127, no. 39, pp. 13466-13467, 2005.

[56] M. Klähn, G. S. Lim, A. Seduraman and P. Wu, "On the different roles of anions and cations in the solvation of enzymes in ionic liquids," *Physical Chemistry Chemical Physics,* vol. 13, no. 4, pp. 1649-1662, 2011.

[57] W. R. Cannon, S. F. Singleton and S. J. Benkovic, "A perspective on biological catalyst," *Nature Structural Biology,* vol. 3, pp. 821-833, 2006.

Chapter 3 - Experimental Techniques

3.1 Atomic Force Microscopy

Developed in the 1980s by researchers at IBM, atomic force microscopy (AFM) has become one of the most widely used scanning probe microscopy (SPM) techniques today with applications in electronics, pharmaceuticals, materials physics, biophysics and biology. The basic principle of all SPM systems is a probe that is scanned across a surface to extract properties such as topography, conductivity, mechanical properties and forces [1, 2, 3, 4].

AFM, like other SPM processes, has the major benefit that the resolution is not reliant on the diffraction limit. Instead the lateral resolution is dependent on the sharpness of the AFM scanning probe which can be as low as a few nanometres. This high resolution means it can be used to extract the chemical properties of single molecules and surfaces as described in section 3.2.2 [5, 6]. Another advantage to AFM is its ability to image any surface unlike similar techniques such a scanning tunnelling microscopy which requires electrically conductive samples [7]. AFM can also image under air, a vacuum or in liquid. The last condition is hugely important for biological samples which usually need to be immersed in liquid to behave as they would in their natural environment. AFM therefore has the ability to image biological molecules in their natural environment. Because of these features AFM was the tool used to investigate CAL B in this thesis.

3.1.1 Principles of Operation

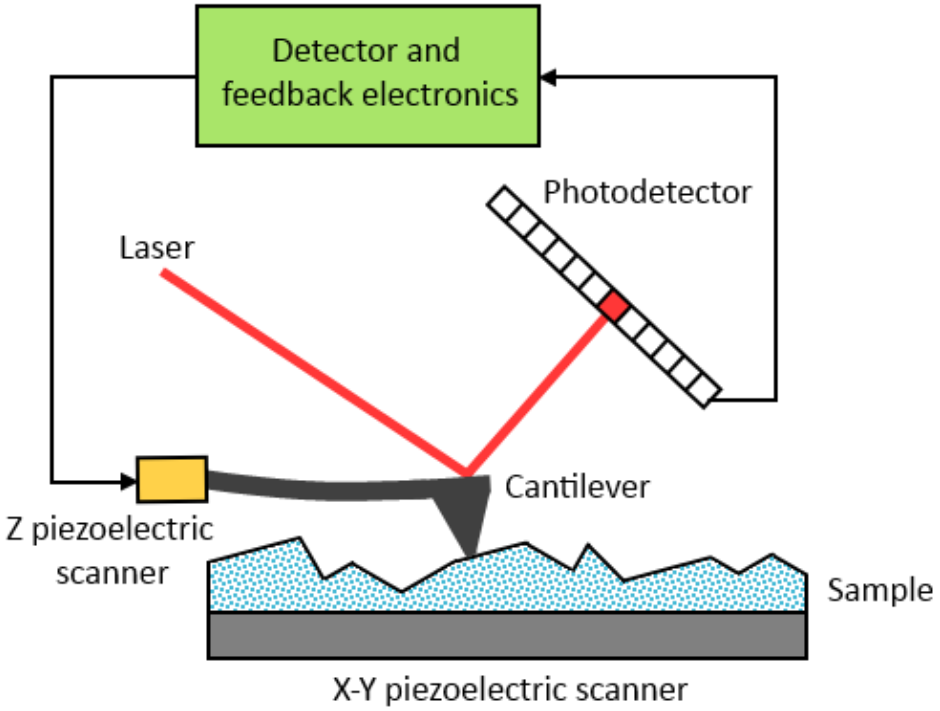

Figure 3.1: Schematic of basic AFM operation.

Atomic force microscopy is based on a small, sharp tip attached to a flexible cantilever which is raster scanned across the sample as seen in figure 3.1. The end of the cantilever is attached to a piezo scanner that controls the height of the tip above the surface. A feedback loop, discussed more in the following section, is used to keep the tip in steady contact with the surface by moving the piezo. The change in height required is stored and from this a topography image of the sample can be created.

The cantilever and tip are usually made from silicon or silicon nitride. The cantilever is 100-500 µm long with the tip mounted on the underside [8]. The radius of a standard tip is around 10 nm. An infrared laser is shone on to the

back of the cantilever and reflected into a split photodetector which measures the deflection of the cantilever by finding the difference in laser intensity between the top photodiode and bottom photodiode normalised to their sum. This deflection is proportional to the force acting on the tip and can be described by Hooke's law.

There are two general modes of AFM which are commonly used: contact or static mode and intermittent contact or tapping mode.

Contact Mode

Contact mode is the first scanning mode developed for AFM. Whilst imaging the tip remains in contact with the surface at all times. In the constant force mode of operation the feedback loop repeatedly samples the deflection of the cantilever (and so the force on the tip) and will change the height of the piezo to keep the force constant. This type of feedback loop means that the force acting on the sample can be controlled by the user and so reduces the damage of the sample. Contact mode suffers from a problem due to the lateral forces created by dragging the tip across the surface. This can lead to tears in soft samples or damage a tip being used to image hard, bumpy surfaces. Because of this it is reserved for flat and rigid samples [9].

Tapping Mode

To reduce the lateral forces acting between the surface and tip tapping mode can be used. In tapping mode the tip is oscillated vertically above the surface and only comes into contact with the surface at the lowest point of the oscillation cycle. The oscillation of the cantilever can be achieved using a number of

methods such as oscillating magnetic fields on a magnetised cantilever but it is usually controlled using piezo drivers [10]. The tip is oscillated at or just below its resonance frequency with an amplitude somewhere in the range of 20-100 nm [11]. As the tip nears the sample interactions such as van der Waals, electrostatic and dipole-dipole cause the oscillation to decrease. The feedback loop corrects for this by moving the cantilever piezo in the z axis to maintain the target amplitude. This movement of the piezo actuator can be read as the variation in height of the sample. Tapping mode inflicts much less force onto the sample than contact mode so it is widely used on biological or fragile samples.

3.1.2 Image Artefacts

There are a number of artefacts that occur when carrying out atomic force microscopy which give rise to undesirable effects in the resulting images. Some artefacts, such as drift and tip convolution, are intrinsic to the hardware used. Others occur due to poor image settings or environmental effects [10].

Feedback

It is important to be able to enter the correct settings when imaging to produce the best data possible. The feedback set point depends on which mode of AFM is being used. How quickly the feedback loop responds to changes in the sample's topography is dependent on the integral and proportional gains for all imaging modes.

If the gain is too low the tip will not trace the surface correctly and it will spend too long out of contact with the sample as shown in figure 3.2a. This is because

the tip will take a long time to respond to a reduction in the sample height. If the gain is too high the piezo height will change too quickly and which produces a ringing effect (figure 3.2b). For small flat surfaces the gain should be set low but usually it is a balancing act between ringing and not tracing the surface.

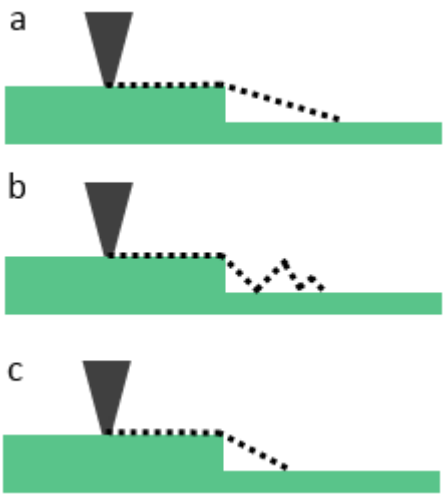

Figure 3.2: How gain affects the path of the cantilever. a) shows too low gain, b) too high gain and c) ideal gain.

Vibration Noise

There are a number of sources of noise for atomic force microscopy. Due to the size of the cantilever it is sensitive to thermally induced fluctuations. This becomes more pronounced when imaging in liquid making it common practice to leave the system to thermally equilibrate for up to 30 minutes. A major source of noise is from acoustic vibrations from the surrounding building. The way to reduce the effect from acoustic noise is to place the microscope on an air table or suspend it from elastic cords. Another considerable source of noise comes from the electrical components of the microscope. This source of noise can produce repeating oscillations in the data and is usually due to broken

components or an ungrounded scanning stage. If noise is present during imaging it can cause the image to be blurred or create underlying repeating patterns throughout the image as seen in figure 3.3.

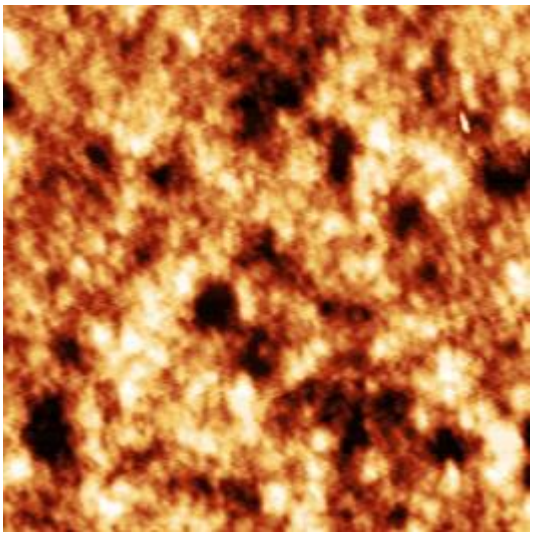

Figure 3.3: Example of noise in an AFM image [12].

Piezo Scanner Effects

Both the sample X-Y scanner and the cantilever height controller are based on piezoelectric ceramic scanners. Whilst the technology has been greatly improved since the first microscopes they still cause a number of artefacts in the final images. Firstly they are sensitive to temperature changes and expand when warmed. This means that if the environment temperature is fluctuating the sample can drift relative to the tip movement [13].

The piezoelectric scanners are driven by applying a voltage to them. However the extension is not linearly dependent on the driving signal which results in some unwanted effects. If not properly corrected, images can appear smaller at one edge than the other due to the sample scanner and inaccuracies in height

measurements from the cantilever piezo [10]. There is also hysteresis involved in piezoelectric materials which mean that the forward and backward scanning movements are not identical.

Tip Effects

The tip has an apex of fixed radius that is used to image the surface. If the size of the apex is much greater than the features on the sample you are imaging this will reduce the resolution you can achieve and mean that some detail can be lost as the tip is not small enough to register it. This usually does not affect the height measurements of the sample but the lateral shape of the objects if they have steep sides [13]. It can cause small objects to appear much larger than their intrinsic size or holes much shallower than they actually are. Figure 3.4 illustrates this effect. Using a sharper tip for smaller features can overcome this problem.

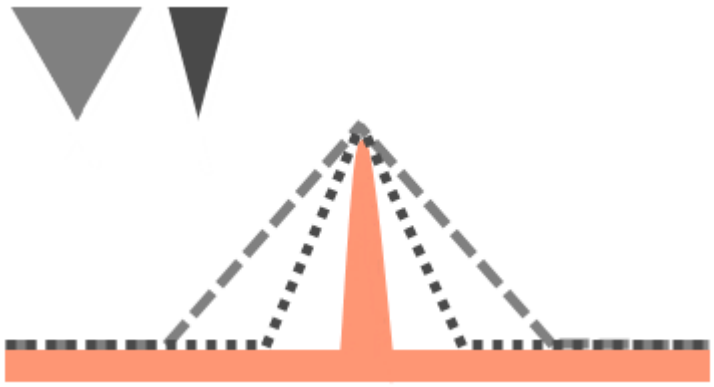

Figure 3.4: How tip shape can affect the perceived size of a feature.

Tips can also be contaminated or broken during imaging. Sections of soft samples such as biological molecules can be picked up by the tip which changes its shape and can introduce unexpected shapes in the images such as those seen

in figure 3.5. If the contaminant is dragged along the surface it can cause very distinct streaks in the final image. Tips can be broken by hard or rough surfaces and will produce similar effects to contaminated probes [10].

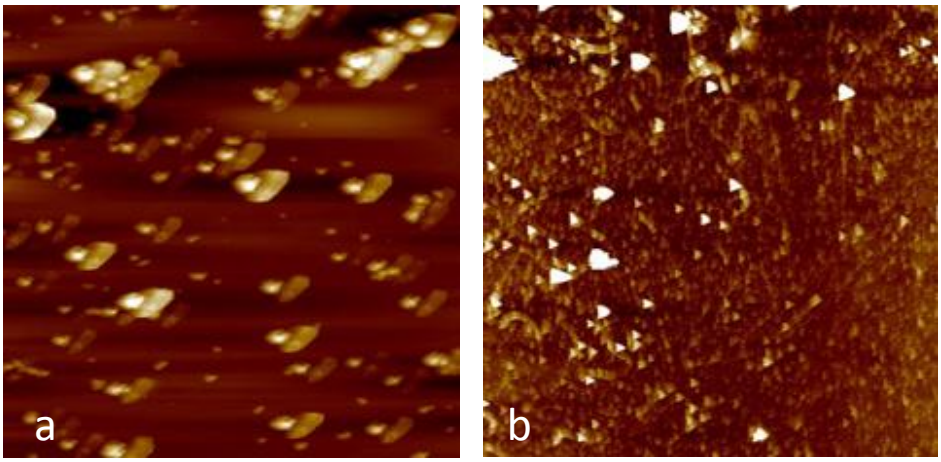

Figure 3.5: Example of an image taken with a) a contaminated tip and b) a broken tip. Both effects cause repeating patterns on the surface [14].

3.2 AFM Force Measurements

3.2.1 Force Curves

As mentioned in the previous section the force acting on the tip is proportional to the deflection of the cantilever, d [15]. They are related by Hooke's Law where k is the spring constant of the cantilever [16]:

$$F = -k\,d$$

A force-distance curve is produced by lowering and retracting the tip down to the surface at constant x and y whilst constantly measuring the force the cantilever experiences. The distance can either be defined as the distance between the tip and the surface or between the tip and its starting location away

from the surface. While the tip is not in contact with the surface the cantilever experiences no deflection. As the tip touches the surface the cantilever will experience an increasing positive deflection until the tip is withdrawn and the cantilever goes back to the equilibrium position. With a lot of surfaces however the tip will experience attractive forces as it approaches such as Van der Waals, capillary or Coulomb forces. This causes the tip to snap down towards the surface and produces a negative deflection in the force curve.

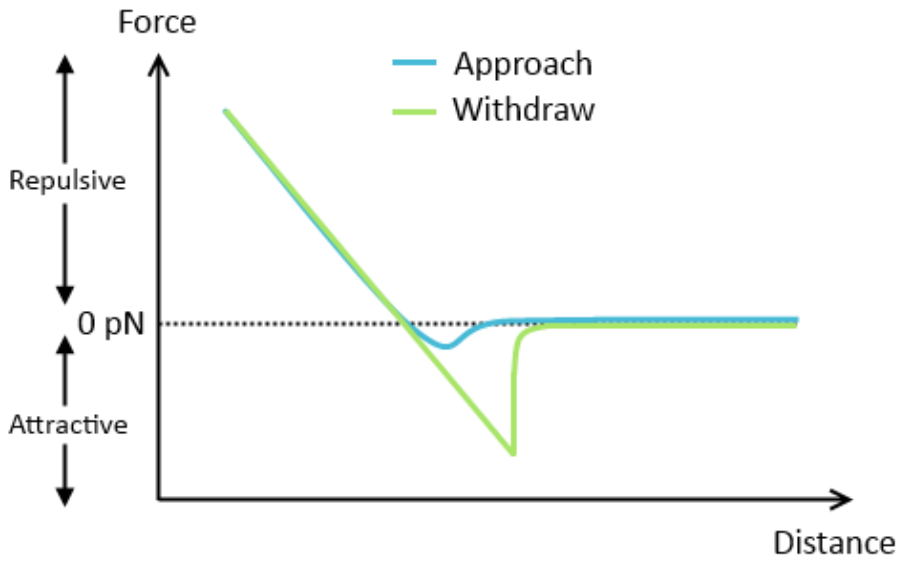

Figure 3.6: Example force curve over one cycle of approach and withdraw. Here the distance is defined as the distance between the surface and the tip.

The tip can also adhere to the surface where it will remain until the force from the retracting cantilever is large enough to overcome the tip-surface binding force. This again causes the cantilever to experience a negative deflection [17]. A force curve with attractive and adhesive forces can be seen in figure 3.6.

Analysis of these force curves can give values for some of the mechanical properties of the surface which is talked about in section 3.2.3.

The feedback system set point for force curves is known as a trigger which will tell the system when to start retracting the cantilever. There are two types of trigger – absolute and relative [18]. With an absolute trigger the tip and sample are brought together until a predetermined cantilever deflection is reached. A relative trigger is similar but the tip approaches the surface until the cantilever experiences a deflection greater than the trigger relative to the deflection at the non-contact part of the curve [15].

3.2.2 Calibration

The deflection of the cantilever can be measured to sub angstrom values leading to a force resolution of piconewtons but force curves initially give the measured forces in arbitrary units. This is because the system measures the cantilever deflection by calculating the laser beam movement across the photodetector which is measured as a voltage. The system needs to be calibrated to convert this laser movement into the cantilever deflection and then the force in the correct units [19].

Calibration is done in two steps. First the deflection sensitivity needs to be measured. This tells the system how much voltage corresponds to a set deflection of the cantilever. This is done by obtaining a force curve on a hard surface that will not be deformed by the tip such as glass or sapphire. As well as this the spring constant of the cantilever needs to be calculated which turns the deflection into a force. AFM tips come with a manufacturer's stated spring

constant but these are a general value stated for all tips. Variations in the fabricating process can cause these stated values to be wrong by a large percentage (sometimes by as much as 300%) [20].

Spring Constant Calibration

There are three main methods of calibrating the spring constant of a cantilever; dimensional models, static deflection and dynamic deflection. The first method looks at the geometry of the cantilever and tip and creates a full theoretical model of the cantilever based on its shape and dimensions. This technique has the largest error on it as the dimensions such as thickness and radius are just nm in size and so are hard to measure accurately which can give errors between 10-25% [21, 22].

Static deflection involves loading a known force onto the cantilever and obtaining k whilst dynamic deflection is based on the resonance behaviour of the cantilever. It is the most accurate method with errors between 5-10% but it is also the least user friendly and the technique most likely to damage the tip [22].

One dynamic method is thermal tuning which is the most commonly used technique as it is simple and usually an inbuilt function on the imaging software. First the deflection sensitivity is measured and then the cantilever is oscillated at a range of frequencies. At the resonant frequency the cantilever oscillation will have a sharp peak in amplitude. A simple harmonic model is fitted to this resonance curve which allows the spring constant to be calculated. Thermal tunes can be used for cantilevers with spring constants below 5 Nm^{-1} and is accurate to within 15-20% where the main uncertainty is from noise from other

sources. Thermal tuning also only requires the deflection sensitivity and the temperature of the room so is the method which requires the smallest number of prior measurements [9, 22, 23].

3.2.2 Analysing Force Curves

As mentioned force curves allow the mechanical properties of a surface to be calculated. Once the tip is calibrated these values will be in their correct units. There are four main properties that can be extracted from the sections of a force curve highlighted in figure 3.7:

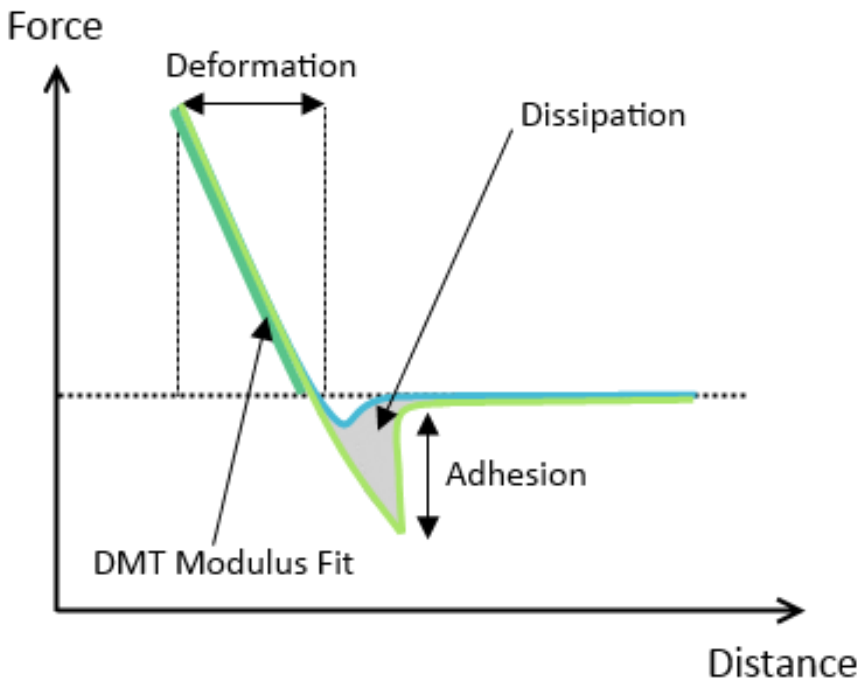

Figure 3.7: Force curve showing where all the mechanical properties are extracted.

Elastic Modulus

The elastic modulus calculation involves fitting the DMT (Derjaguin, Muller and Toporov) model of deformation to the curve. This model, like the classical Hertzian model, assumes elastic deformation between a spherical object and a surface however the DMT model also takes into account that the tip might experience an adhesive force from the surface. The elastic modulus calculation works over a large range between 700kPa and 70GPa.

Dissipation

The dissipation is defined as the area between the trace and retrace curves. It is the force multiplied by velocity integrated over time. If the trace is equal to the retrace there will be no energy lost. The adhesion majorly affects the dissipation. Once calibrated the dissipation is given in eV lost per force curve [24, 25].

Adhesion

Adhesion comes from forces between the tip and sample such as van der Waals and other electrostatics and forces from capillary meniscus [18]. Adhesion measurements are the basis of SMRFM and will be talked about in greater detail in section 3.3.

Deformation

The deformation is the penetration of the tip into the surface at peak force. As the load on the sample increases the deformation will increase. It includes both elastic and plastic deformation. It is the difference in separation from contact point to the peak force point but errors are introduced due to the jump to

contact point which will increase the value of the deformation unnecessarily [26].

3.2.4 Force Volume

Force volume AFM is an imaging technique that captures force curves. In force volume, also known as force spectroscopy, each pixel of the image contains a force curve as shown in figure 3.8 [27]. Analysis of all the force curves can produce images of mechanical properties. This allows the user to see how the mechanical properties change over a material or a biological organism. A topography image can be created by estimating the contact point between the tip and sample from the force curves [28]. One force curve can take over a second to take making force volume a very slow process compared to tapping or contact mode. A 16x16 pixels image can be obtained in ~15 minutes and so force volume images tend to be low resolution.

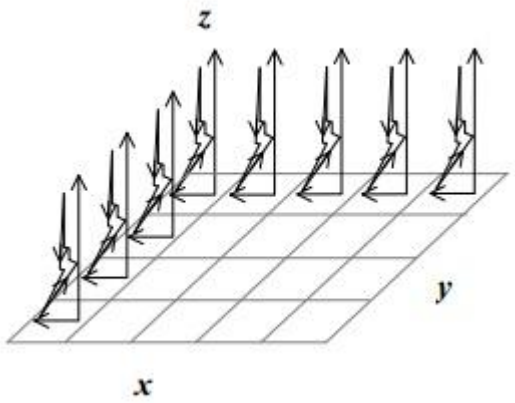

Figure 3.8: Schematic of how the cantilever and tip move during a force volume image. A force curve is taken at every point on the surface.

Force volume has been used for a huge range of applications. It has been used to measure the elasticity of cell cytoskeletons, investigate actin filaments, probe

electrostatic interactions between the tip and charged surfaces and the adhesion properties of a wide range of samples [29, 30, 31, 32].

3.2.5 PeakForce QNM

PeakForce Quantitative Nanomechanical property mapping (QNM) AFM is another, relatively new technique that combines the speed of tapping mode with the force curve capture of force volume. In QNM mode the tip is oscillated in a sinusoidal pattern and every time the tip touches the surface the height is measured and a force curve is taken [26]. These curves are analysed in real time to produce maps of the mechanical properties in figure 3.7. The raw data can also be extracted individually allowing the user to do their own analysis. It has a force resolution of down to 10 pN [33].

QNM produces force curve information with the resolution and speed of a standard tapping mode image. A high resolution image (512x512 pixels) will take 16 minutes in QNM which is a vast improvement on the slow capture time of force volume which would take many hours to take an image of the same resolution.

Tapping mode can give information about the mechanical properties of a sample by looking at the phase difference between the cantilever oscillation frequency and the drive frequency. These phase images can indicate a change in surface but the data is a combination of elasticity, hardness and adhesion. This means that it is impossible to extract the individual properties from the phase data giving QNM a large advantage [26].

A major benefit of QNM mode is that the feedback loop is based on the peak force acting on the tip. The user can define a maximum force for the tip to experience and the system will make sure it is not exceeded. This reduces damage to the sample and the tip by allowing for much smaller deformations. This also increases the resolution of the images by lowering the tip area which comes into contact with the surface.

PeakForce QNM has been shown to be a good alternative to other force measurement AFM techniques and has been used for a number of purposes. It has successfully measured the Young's modulus of polymers, amyloid fibrils and proteins as well as the mechanical properties of biofuels and other molecules [33, 34, 35, 36, 37, 38].

3.3 Single Molecule Recognition Force Microscopy

Atomic Force Microscopy has a force resolution of piconewtons which makes it ideal for measuring the small intramolecular forces which are typically around 150 pN [39]. This technique is called single molecule recognition force microscopy (SMRFM). It can be used on virtually any two binding molecules but it is most commonly used for biological samples. This is because AFM can be carried out in solutions which allow the biological molecule to remain *in vivo*. It has been used on molecules such as antibody-antigen pairs, proteins, DNA, oils and many more [40, 41, 42, 43, 44].

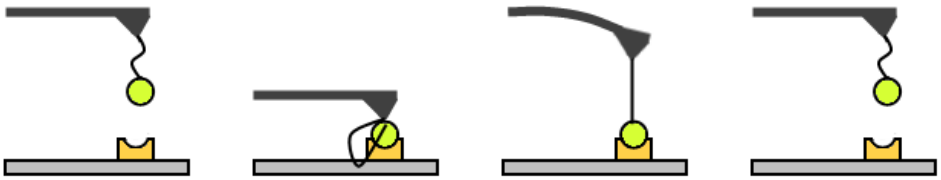

Figure 3.9: One force curve cycle during single molecule recognition. The binding molecule is attached by a tether to the AFM tip. When it binds to its substrate the tether is stretched and the cantilever bends towards the surface.

The premise is to attach one molecule, usually the ligand, to the AFM tip. The other molecule, usually the receptor, is immobilised on a flat surface. The functionalised tip is used to image the receptor and take force curves. As the tip, and therefore the ligand, comes into contact with the surface the ligand will bind to its receptor. As the tip is withdrawn the ligand-receptor bond will pull the tip down towards the surface causing a large deflection of the cantilever. Eventually the retracting piezo will be far enough away that the force applied to the ligand-receptor bond will overcome the binding force and the bond will break. This causes the deflection of the cantilever to snap back to the equilibrium position. The deflection of the cantilever through this process is demonstrated in figure 3.9. The adhesion in the force curve is now equal to the binding force of the ligand and receptor [45].

Although it is possible to attach the ligand directly to the AFM tip it is not particularly efficient as if the molecule is not aligned with the receptor's binding site there will be no interaction. Because of this it is very common to attach the ligand to the tip using a molecular linker such as a poly(ethylene glycol) (PEG) chain [41]. These linkers allow the ligand to rotate and move across the surface so they can find the binding site of the receptor. This increases the binding

probability during imaging [46]. They also do not interact with proteins and many other molecules which make them a good choice for molecular recognition experiments [42]. They do however make the chemistry involved in the attachment of the ligand to the tip more complicated.

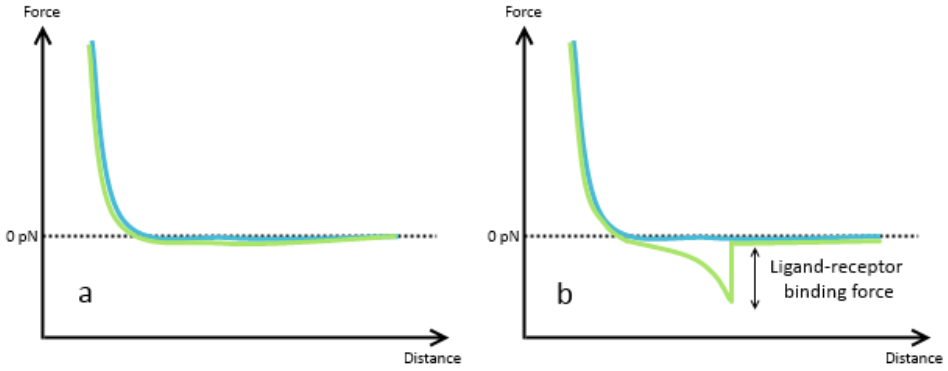

Figure 3.10: a) shows a force curve with no surface adhesion and no binding event. If the binding molecule is attached via a PEG linker the unbinding force curve will look similar to b). There will be a period of non-linear extension when the tip has left the surface caused by the stretching of the tether. This shape is very distinctive of a specific unbinding event.

Consideration needs to be given to the length of the linker. Too short and the ligand will not be able to rotate and move fully but the linker must be shorter than the oscillation amplitude of cantilever so that it can be stretched enough to break the ligand-receptor bond. Usually lengths between 5-9 nm are used in experiments as this gives the ligand enough space to move but still means the oscillation amplitude of the tip can be relatively small.

Another benefit of attaching the ligand via a tether is that it will alter the shape of the force curve and make it easier to distinguish between specific and background events. Because of the linker the tip will initially deflect as it would if it had not adhered to the surface until it is far enough away that the linker

becomes taught. This will create a change in gradient of the adhesion curve which creates a different shape in the curve overall. A background event will look like that in figure 3.10a while a specific event will look like figure 3.10a [47, 48].

3.3.1 Dependence on Loading Rate

Consideration needs to be given to the fact that the binding force between two molecules is dependent on the loading rate applied [40]. For these types of AFM force pulling measurements the loading rate is defined from Hooke's Law.

$$L_R = k\, V_{Ret}$$

Where L_R is the loading rate, V_{Ret} is the retraction velocity and k is the spring constant of the cantilever.

The rupture force dependence on the loading rate is given by the Bell-Evans model which states the force is directly proportional to the logarithm of the loading rate [49]. The cause of this dependence is due to thermally driven collisions the surrounding solvent and the binding molecules. These collisions will transfer energy from the solvent into the ligand-receptor bond and help dissociate the pair.

When a low loading rate is applied the tip moves away from the surface slowly. This increases the chance of a high energy collision from a solvent molecule which will break the bond prematurely and register as a small binding force. When a high loading rate is applied there is less chance of a collision and so the

bond is broken when the tip is further away from the surface resulting in a larger measured binding force [50]

3.3.2 Criteria for SMRFM

Dufrêne and Hinterdorfer outline a set of criteria needed for single molecule recognition force microscopy [44]. These are:

1. The tip binding force should be greater than the ligand receptor force so that the ligand will not break away from the tip.
2. Biomolecules need to have mobility so they can orientate themselves in the correct way for binding.
3. Non-specific interactions should be minimised.
4. There should be a low number of ligands on the tip to increase the chance of getting just one binding pair.
5. All the molecules being imaged should be orientated in the same way to increase the chances of binding to as many molecules as possible.

In practice it is not possible to fully fulfil all five of the criteria and a compromise between them is needed. The two most important criteria to consider are the top two as without them the chances of specific binding is greatly reduced or non-existent.

3.4 Functionalisation Chemistry

There are a number of ways to attach the ligands to the tip each with their own advantages and drawbacks. The three most common methods, absorption, gold

and silicon chemistry, are explained below along with any problems they present.

3.4.1 Absorption Chemistry

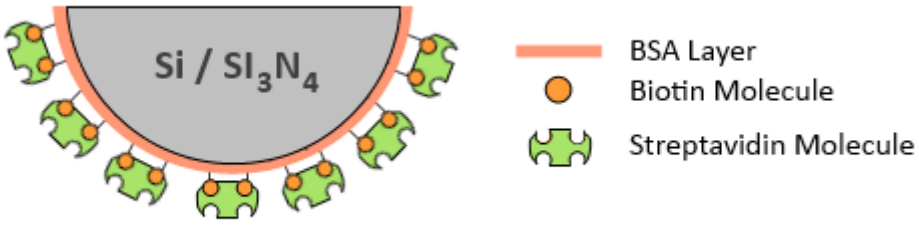

Figure 3.11: Schematic of absorption chemistry.

One way to attach ligands to AFM tips is via absorption [51]. Van der Waals and electrostatic forces cause the molecules to adhere to the hard surface [52]. Proteins are forced to expose their positive or negative amino acids which then bind with the oppositely charged parts of the tip. One reaction uses bovine serum albumin (BSA) which binds to silicon nitride. Amine groups (common in many biological molecules) can then be bound to the BSA as shown in figure 3.11 where biotin has been bound to the BSA. Streptavidin is then bound to the biotin to be used as the molecule of interest for imaging [53].

This is an easy reaction to carry out but it results in very weak bonds from Van der Waals and electrostatic forces. It is also not very accurate as force curves taken with tips functionalised with this method have been shown to show a large number of specific events when ideally there should be just one per curve [53].

3.4.2 Gold Chemistry

Another way to attach ligands is using the reaction that occurs between gold and thiol molecules. The gold atom and the thiol molecule bind via covalent bonds which are significantly stronger than absorption bonds meaning that the ligands do not come free when imaging. The reaction is simple to carry out and uses commercially available reagents [52]. Figure 3.12 displays a schematic of the process.

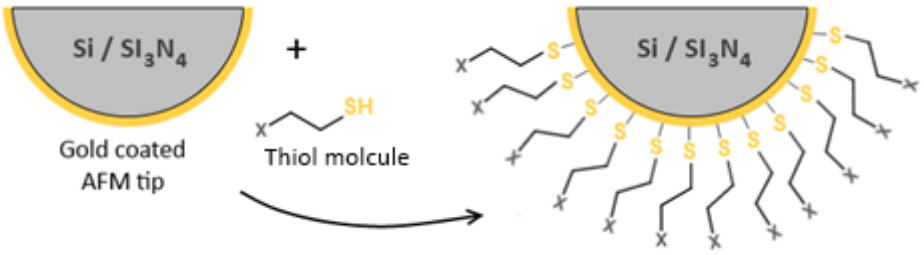

Figure 3.12: Schematic of gold chemistry. The sulphur atoms bind covalently with the gold layer on the AFM tip's surface.

To begin the reaction the AFM tips first needed to be coated in gold (with sputtering or evaporation) which is an expensive process and can leave the tips damaged and blunt. Also the gold coating on the AFM will be exposed to stress during imaging which can cause the layer to come loose from the silicon nitride tip which makes it unstable [45]. Thiolated PEG linkers can then be attached to the gold layer.

3.4.3 Silicon Chemistry

Silicon chemistry involves introducing amine groups onto the surface of silicon or silicon nitride AFM tips. Amine groups bind easily to functional groups such as carboxylic acids and NHS esters. Gold-thiol chemistry produces strong bonds but they have a high cost and it is difficult to coat the tips without damaging them [53]. For amine derivation the tips do not need to be coated with metals and all reagents used are fairly low cost [52].

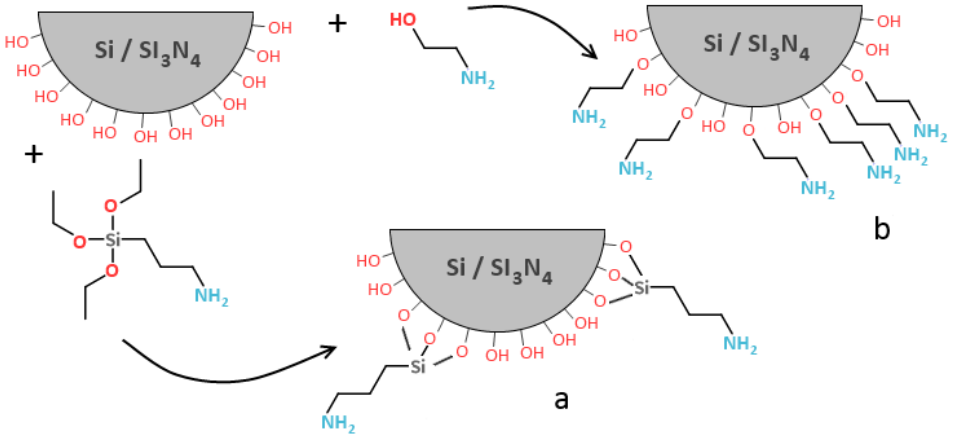

Figure 3.13: Schematic of silicon nitride chemistry. a) shows the APTES method whilst b) shows the ethanolamine HCL method.

When exposed to air a silicon nitride surface has a thin layer of silicon dioxide mixed with silanol and silylamine groups. There are a number of ways to introduce the amine groups into this layer, as seen in figure 3.13, by attaching the amine groups to the silanols [54].

APTES Method

3-(aminopropyl)triethoxysilane (APTES) can be used to modify the surface layer on the tips. There are multiple ways to do this but the two most frequently used processes have the APTES in either the gas phase or the aqueous phase.

When using the gas phase APTES amine derivitisation is done via chemical vapour deposition. The tips are cleaned and then put into an ozone cleaner to produce a more complete layer of silanol groups on the surface. The APTES and tips are then put into a desiccator (either under a vacuum or in argon gas) for two hours to introduce the amine groups. In aqueous phase the tips are cleaned and subjected to ozone cleaning before being briefly put into a solution of APTES and toluene.

In both procedures it is very important to reduce the moisture the APTES comes into contact with as it will hydrolyse and create ethanol and trisilanols when it meets water molecules. This can be difficult, especially ensuring the desiccator is free of any moisture when the cantilevers and APTES are put inside it.

Ethanolamine Method

Another amine derivitisation technique uses ethanolamine hydrochloride (HCL) dissolved in dimethyl sulfoxide (DMSO). The cantilevers are cleaned with chloroform and ozone before being left in the solution over night. After being cleaned with ethanol and DMSO they are ready to be functionalised. This process is much simpler than the gas phase APTES method and you do not need to worry about humidity which gives it an advantage over both APTES methods.

The APTES method does give three molecular bonds with the silanol groups whilst ethanolamine only provides one meaning a weaker bond.

For the SMRFM experiments carried out in this thesis the ethanolamine HCL chemistry on silicon nitride tips was chosen as the functionalisation method as absorption chemistry is not very accurate and gold chemistry is expensive and difficult. Ethanolamine HCL was chosen over APTES as it is a simpler reaction and found to be a very effective functionalisation method [48]. This choice is discussed further in section 5.1.1.

3.5 Alternatives to AFM

There are a number of different techniques to measure binding forces between molecules such as manipulation force microscopy, biomembrane force probes and optical tweezers.

Optical tweezers can be used to measure forces acting on particles but have only recently been used for biological purposes [55, 56]. They have been used to probe a variety of biological molecules in the last few years including DNA, antibodies, bacteria and cells [57, 58]. They can be used to investigate the binding force between two molecules by attaching the ligand to the polystyrene beads. The substrate is attached to a glass slide. The optical tweezers are used to pry the ligand away from the substrate by applying an increasing pull force to the ligand. Eventually the ligand-receptor bond will break away giving a measurement for the binding force. This has been successfully done for a number of binding pair molecules such as staphylococcus aureus bacteria and proteins, ATP and DNA and antibodies and proteins [58, 59]. The optical

tweezers method is more time consuming and convoluted than using SMRFM which is why it was not chosen for the work carried out in this thesis.

Another technique that is commonly used is manipulation force microscopy which is another force measuring system that uses AFM [60]. The substrate is immobilised onto a flat surface such as plain glass or polystyrene. The target molecule is either allowed to attach to the substrate directly (in the case of human cervical carcinoma cells on polystyrene) or attached to microspheres (as done with a number of different proteins) which then bind to the substrate [61]. The AFM tip is then used to dislodge the binding molecule from the substrate by moving the molecule towards the tip at a constant rate. As the tip unbinds the molecule it will be deflected which is measured and converted into a force via Hooke's law. As it is an AFM technique manipulation force microscopy can be carried out in liquid and therefore on living cells and it is less sensitive to mechanical noise and thermal drift than SMRFM [62]. However it is not as fast a process as SMRFM and therefore is usually applied to systems that have slow dynamics. Because of this SMRFM is the more suitable for studying the binding between an enzyme and its substrate as it is a fast process compared to un-catalysed reactions.

3.6 Confocal Microscopy

Confocal microscopy is an optical technique established in the 1950s by Marvin Minsky. It is based on fluorescence imaging which is the process of labelling certain parts of the sample with a specific fluorophore. When illuminated with the correct wavelength of light the fluorophore will be excited and undergo

spontaneous emission and emit photos of a longer wavelength. This is collected by a photo detector and an image is produced that shows the spatial distribution of the fluorophores and therefore the distribution of the labelled areas of the sample.

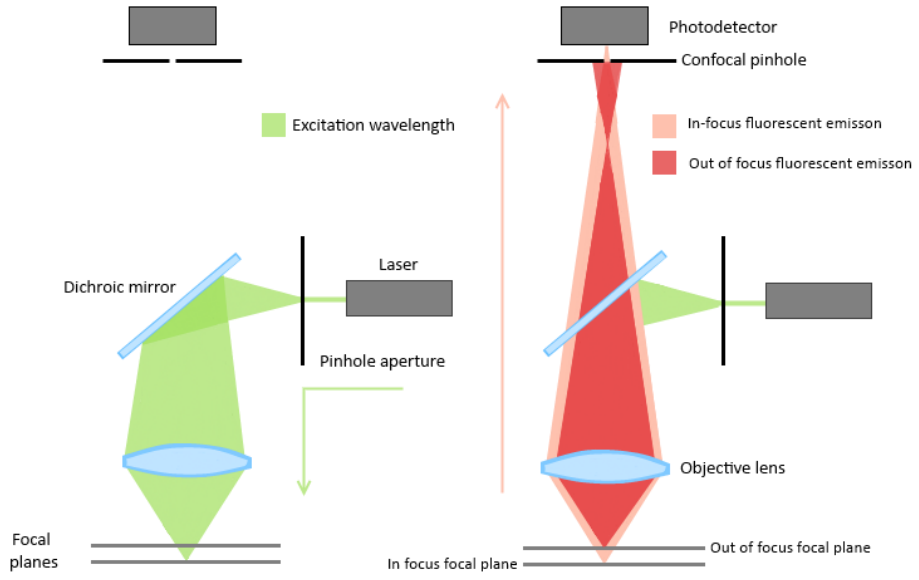

Figure 3.14: Schematic of a confocal microscope.

In a conventional epifluorescence microscope the entire sample is illuminated simultaneously. This can lead to blurring as light from fluorophores outside the focal plane can be picked up by the photodetector [63]. Also the light source itself can introduce extra noise in the final image due to scattering which can obscure sections of the final image [64].

The principle behind confocal microscopy is similar to epifluorescence imaging but with added measures that aim to reduce the unwanted, out of focus light. In confocal microscopy a much smaller laser spot size is used which illuminates just one point on the surface. The final image is then built point by point by raster

scanning the laser over the sample. The diameter of this laser spot can be as low as 0.25 µm and it has a field depth between 0.5 - 1.5 µm [65].

Because it has a shallower field depth and only one point is illuminated at a time there is a lot less background light produced. Areas above and below the focal plane have less illumination and therefore emit less photons. Out of focus light is further reduced using pinhole apertures as seen in figure 3.14. The first, in front of the light source, is used to limit scattering of light. The second is positioned in front of the photodetector. Out of focus light will be unable to pass through into the detector leaving only the light from the desired focal plane. This produces a much crisper image with higher resolution and contrast.

Confocal microscopy can be used on many biological samples without damaging them like transmission electron microscopy does. If the fluorophores are exposed for too long or the intensity of the light is too high they can be photo bleached which causes them to stop working. As the system works by building the image point by point there is the same illuminating angle for each pixel which creates a more uniform image. It also means a greater field of view can be obtained as it is limited by scanner measurements, not the size of the laser spot. This does mean however that it can take between 0.1 – 1 second per image which can be too long to image fast biological processes [64]. Confocal microscopy is employed in section 5.3.2.

3.7 References

[1] G. Binning, C. F. Quate and C. Gerber, “Atomic force microscope,” *Physical review letter,* vol. 56, no. 9, p. 930, 1986.

[2] G. Binning, C. Gerber, E. Stoll, T. R. Albrecht and C. F. Quate, “Atomic resolution with atomic force microscope,” *Europhysics Letters,* vol. 3, no. 12, p. 1281, 1987.

[3] N. Jalili and K. Laxminarayana, “A review of atomic force microscopy imaging systems: applications to molecular metrology and biological sciences,” *Mechatronics,* vol. 14, no. 8, pp. 907-945, 2004.

[4] E. R. Beach, G. W. Tormoen, J. Drelich and R. Han, “Pull-off force measurements between rough surfaces by atomic force microscopy,” *Journal of colloid and interface science,* vol. 247, no. 1, pp. 84-99, 2002.

[5] L. Gross, F. Mohn, N. Moll, P. Liljeroth and G. Meyer, “The Chemical Structure of a Molecule resolved by Atomic Force Microscopy,” *Science,* vol. 325, no. 5944, pp. 1110-1114, 2009.

[6] F. Ostendorf, C. Schmitz, S. Hirth, A. Kühnle, J. J. Kolodziej and R. M., “Evidence for potassium carbonate crystallites on air-cleaved mica surfaces,” *Langmuir,* vol. 25, no. 18, pp. 10764-10767, 2009.

[7] G. Binning, “Atomic force microscopy,” *Physica Scripta,* vol. 19, pp. 53-54, 1987.

[8] W. H. Alonso and J. L. Goldmann, “Feeling the forces: atomic force microscopy in cell biology,” *Life Sciences,* vol. 72, pp. 2553-2560, 2006.

[9] A. Alessandrini and P. Facci, “AFM: a versatile tool in biophysics,” *Measurement science and technology,* vol. 16, no. 6, p. R65, 2005.

[10] P. J. Eaton and P. West, Atomic force microscopy, Oxford University Press, 2010.

[11] R. García and R. Perez, “Dynamic atomic forcce microscopy methods,” *Surface science reports,* vol. 47, no. 6, pp. 197-301, 2002.

[12] AZoNano, “Vibration Isolation Solutions to Eliminate Noise in AFM and SPM,” March 2013. [Online]. Available:

http://www.azonano.com/article.aspx?ArticleID=3254. [Accessed 2014].

[13] D. Ricci and P. C. Braga, "Recognizing and avoiding artifacts in AFM imaging," in *Atomic Force Microscopy*, Humana Press, 2004, pp. 25-37.

[14] Australian Microscopy & Microanalysis Research Facility, "Tip Artefacts," June 2014. [Online]. Available: http://www.ammrf.org.au/myscope/spm/background/convolution.php/1401071839. [Accessed 2014].

[15] W. F. Heinz and J. H. Hoh, "Spatially resolved force spectroscopy of biological surfaces using atomic force microscopy," *Trends in biotechnology,* vol. 17, no. 4, pp. 143-150, 1999.

[16] R. Hooke, *Micrographia,* 1665.

[17] H. J. Butt, B. Cappella and M. Kappl, "Force measurements with the atomic force microscope: Technique, interpretation and applications," *Surface science reports,* vol. 59, no. 1, pp. 1-152, 2005.

[18] E. Santner and E. Stegemann, "Adhesion measurements by AFM - a gateway to the basics of friction," in *Meeting of the International Research Group on Wear of Engineering Materials*, 2005.

[19] W. Han and F. M. Serry, Force Spectroscopy with Atomic Force Microscopy, Agilent Technologies, 2008.

[20] J. L. Hutter and J. Bechoefer, "Calibration of atomic-force microscope tips," *Review of Scientific Instruments,* vol. 64, no. 7, pp. 1868-1873, 1993.

[21] E. L. Florin, M. Rief, H. Lehmann, M. Ludwig, C. Dornmair, V. T. Moy and H. E. Gaub, "Sensing specific molecular interactions with the atomic force microscope," *Biosensors and Bioelectronics,* vol. 10, no. 9, pp. 895-901, 1995.

[22] C. A. Clifford and M. P. Seah, "The determination of atomic force microscope cantilever spring constants via dimensional methods for nanomechanical analysis," *Nanotechnology,* vol. 16, no. 9, p. 1666, 2005.

[23] S. M. Cook, T. E. Schäffer, K. M. Chynoweth, M. Wigton, R. W. Simmonds and K. M. Lang, "Practical implementation of dynamic methods for measuring atomic force microscope cantilever spring constants," *Nanotechnology,* vol. 17, no. 9, p. 2135, 2006.

[24] B. Anczykowski, B. Gotsmann, H. Fuchs, J. P. Cleveland and V. B. Elings, "How to measure energy dissipation in dynamic mode atomic force microscopy," *Applied Surface Science,* vol. 140, no. 3, pp. 376-382, 1999.

[25] P. M. Hoffmann, S. Jeffery, J. B. Pethica, H. Ö. Özer and A. Oral, "Energy dissipation in atomic force microscopy and atomic loss processes," *Physical review letters,* vol. 87, no. 26, p. 265502, 2001.

[26] B. Pittenger, N. Erina and C. Su, Quantitative Mechanical Property Mapping at the Nanoscale with PeakForce QNM, Veeco Instruments Inc., 2010.

[27] W. F. Heinz, E. A-Hassan, J. H. Hoh and F. M. Serry, Application of Force Volume Imaging with Atomic Force Microscopes, Veeco Instruments Inc., 2010.

[28] C. Soussen, D. Brie, F. Gaboriaucf and C. Kessler, "Modeling of force-volume images in atomic force microscopy," in *Biomedical Imaging: From Nano to Macro*, IEEE, 2008, pp. 1605-1608.

[29] L. Wilson, P. T. Matsudaira, R. B. and J. Hörber, Atomic force microscopy in cell biology, Academic Press, 2002.

[30] C. Rotsch and M. Radmacher, "Mapping local electrostatic forces with the atomic force microscope," *Langmuir,* vol. 13, no. 10, pp. 2825-2832, 1997.

[31] M. Radmacher, M. Fritz, J. P. Cleveland, D. A. Walters and P. K. Hansma, "Imaging adhesion forces and eleasticity of lysozyme adsorbed on mica with the atomic force microscope," *Langmuir,* vol. 10, no. 10, pp. 3809-3814, 1994.

[32] P. Polyakov, C. Soussen, J. Duan, J. F. Duval, D. Brie and G. Francius, "Automated force volume image processing for biological samples," *PLoS One,* vol. 6, no. 4, p. e18887, 2011.

[33] T. J. Young, M. A. Monclus, T. L. Burnett, W. R. Broughton, S. L. Ogin and P. A. Smith, "The use of the PeakFroceTM quantitative nanomechanical mapping AFM-based method for high-resolution Young's modulus measurements of polymers," *Measurement Sciene and Technology,* vol. 22, no. 12, p. 125703, 2011.

[34] J. Adamcik, A. Berquand and R. Mezzenga, "Single-step direct measurement of amyloid fibrils stiffness by peak force quantitative nanomechanical atomic force microscopy," *Applied Physics Letters,* vol. 98, no. 19, p.

193701, 2011.

[35] A. N. Frone, S. Berlioz, J. F. Chailan and D. M. Panaitescu, "Morphology and thermal properties of PLA-cellulose nanofibers composites," *Carbohydrate polymers,* vol. 91, no. 1, pp. 377-384, 2013.

[36] S. M. Morsi, A. Pakzad, A. Amin, R. S. Yassar and P. A. Heiden, "Chemical and nanomechanical analysis of rice husk modified by ATRP-grafted oligomer," *Journal of colloid and interface science,* vol. 360, no. 2, pp. 377-385, 2011.

[37] O. Krivosheeva, M. Sababi, A. Dedinaite and P. M. Claesson, "Nanostructured Composite Layers of Mussel Adhesive Protein and Ceria Nanoparticles," *Langmuir,* vol. 29, no. 30, pp. 9551-9561, 2013.

[38] J. Adamcik, C. Lara, I. Usov, J. S. Jeong, F. S. Ruggeri, G. Dietler, H. A. Lashuel, I. W. Hamley and R. Mezzenga, "Measurement of intrinsic properties of amyloid fibrils by the peak force QNM method," *Nanoscale,* vol. 4, no. 15, pp. 4426-4429, 2012.

[39] V. T. Moy, E. L. Florin and H. E. Gaub, "Adhesive forces between ligand and receptor measured by AFM," *Colloids and Surfaces A: Physicochemical and Engineering Aspects,* vol. 93, pp. 343-348, 1994.

[40] M. de Odrowąż Piramowicz, P. Czuba, M. Targosz, K. Burda and M. Szymoński, "Dynamic force measurements of avidin-biotin and streptavidin-biotin interactions using AFM," *Acta Biochimica Polonica,* vol. 53, no. 1, pp. 93-100, 2006.

[41] T. Strunz, K. Oroszlan, R. Schäfer and H. J. Güntherodt, "Dynamic force spectroscopy of single DNA molecules," *Proceedings of the National Academy of Sciences,* vol. 96, no. 20, pp. 11277-11282, 1999.

[42] N. A. Alcantar, E. S. Aydil and J. N. Israelachvili, "Polyethylene glycol-coated biocompatible surfaces," *Journal of biomedical materials research,* vol. 51, no. 3, pp. 343-351, 2000.

[43] A. Gromer and A. P. Gunning, Interactions Between Oil Droplets Probed by Force Spectroscopy with the MFP-3D AFM, Asylum Research, 2010.

[44] Y. F. Dufrêne and P. Hinterdorfer, "Recent progress in AFM molecular recognition studies," *Pflügers Archiv-European Journal of Physiology,* vol. 456, no. 1, pp. 237-245, 2008.

[45] A. R. Bizzarri and S. Cannistraro, "The application of atomic force spectroscopy to the study of biological complexes undergoing a biorecognition process," *Chemical Society Reviews,* vol. 39, no. 2, pp. 734-749, 2010.

[46] C. K. Riener, F. Kienberger, C. D. Hahn, G. M. Buchinger, I. O. Egwim, T. Haselgrübler, A. Ebner, C. Romanin, C. Klampfl, B. Lackner, H. Prinz, D. Blaas, P. Hinterdorfer and H. J. Gruber, "Heterobifunctional crosslinkers for tethering single ligand molecules to scanning probes," *Analytica chimica acta,* vol. 497, no. 1, pp. 101-114, 2003.

[47] U. Dammer, O. Popescu, P. Wagner, D. Anselmetti, H. J. Guntherodt and G. N. Misevic, "Binding strength between cell adhesion proteoglycans measured by atomic force microscopy," *Science,* vol. 267, no. 5201, pp. 1173-1175, 1995.

[48] C. K. Riener, C. M. Stroh, A. Ebner, C. Klampfl, A. A. Gall, C. Romanin, Y. L. Lyubchenko, P. Hinterdorfer and H. J. Gruber, "Simple test system for single molecule recognition force microscopy," *Analytica Chimica Acta,* vol. 479, no. 1, pp. 59-75, 2003.

[49] Y. S. Lo, Y. J. Zhu and T. P. Beebe, "Loading-rate dependence of individual ligand-receptor bond-rupture forces studied by atomic force microscopy," *Langmuir,* vol. 17, no. 12, pp. 3741-3748, 2001.

[50] Y. S. Lo, J. Simons and T. P. Beebe, "Temperature dependence of the biotin-avidin bond-rupture force studied by atomic force microscopy," *The Journal of Physical Chemistry,* vol. 106, no. 38, pp. 9847-9852, 2002.

[51] C. Yuan, A. Chen, P. Kolb and V. T. Moy, "Energy landscape of streptavidin-biotin complexes measured by atomic force microscopy," *Biochemistry,* vol. 39, no. 33, pp. 10219-10223, 2000.

[52] S. Lee, Chemical functionalization of AFM cantilevers, Massachusetts Institute of Technology, 2005.

[53] R. Barattin and N. Voyer, "Chemical modifications of AFM tips for the study of molecular recognition events," *Chemical Communications,* vol. 13, pp. 1513-1532, 2008.

[54] A. Berquand and B. Ohler, Common Approaches to Tip Functionalization for AFM-Based Molecular Recognition Measurements, Bruker Nano Surfaces Business, 2010.

[55] K. H. Simpson, G. Bowden, M. Höök and B. Anvari, "Measurement of Adhesive Forces between Individual Staphylococcus aureus MSCRAMMs and Protein-Coated Surfaces by Use of Optical Tweezers," *Journal of bacteriology,* vol. 185, no. 6, pp. 2031-2035, 2003.

[56] M. C. Williams, "Optical tweezers: measuring piconewton forces," *Biophysics Textbook,* 2002.

[57] K. C. Neuman and A. Nagy, "Single-molecule force spectroscopy: optical tweezers, magnetic tweezers and atomic force microscopy," *Nautre methods,* vol. 5, no. 6, p. 491, 2008.

[58] C. Wagner, D. Singer, O. Ueberschär, T. Stangner, C. Gutsche, R. Hoffmann and F. Kremer, "Dynamic force spectroscopy on the binding of monoclonal antibodies and tau peptides," *Soft matter,* vol. 7, no. 9, pp. 4270-4378, 2011.

[59] H. Clausen-Schaumann, M. Seitz, R. Krautbauer and H. E. Gaub, "Force spectroscopy with single bio-molecules," *Current opinion in chemical biology,* vol. 4, no. 5, pp. 524-530, 2000.

[60] G. Sagvolden, "Protein adhesion force dynamics and single adhesion events," *Biophysical journal,* vol. 77, no. 1, pp. 526-532, 1999.

[61] G. Sagvolden, I. Giaever and J. Feder, "Characteristic protein adhesion forces on glass and polystyrene substrates by atomic force microscopy," *Langmuir,* vol. 14, no. 21, pp. 5984-5987, 1998.

[62] G. Sagvolden, I. Giaever, E. O. Pettersen and J. Feder, "Cell adhesion force microscopy," *Proceedings of the National Academy of Sciences,* vol. 96, no. 2, pp. 471-476, 1999.

[63] D. M. Shotten, "Confocal scanning optical microscopy and its applications for biological specimens," *Journal of Cell Science,* vol. 94, no. 2, pp. 175-206, 1989.

[64] D. Semwogerere and E. R. Weeks, "Confocal microscopy," *Encyclopedia of Biomaterials and Biomedical Engineering,* pp. 1-10, 2005.

[65] B. Matsumoto, Cell biological applications of confocal microscopy, Academic Press, 2003.

Chapter 4 - Analysis Program

4.1 Motivation

As described in section 3.3 AFM force curves can be used to measure the binding force between two molecules [1, 2]. The process is random so to get an accurate value for the rupture force and the binding probability it is important to take a large sample size of a few thousand curves [3]. As each force curve needs to be inspected individually for evidence of specific binding events and then analysed to measure the unbinding force it can be very time consuming to analyse the large number of curves resulting from each captured image. Commercially available software either does not have the required features to detect binding events versus background surface adhesion so returns incorrect force values, as with SPIP (The Scanning Probe Image Processor) software, or does not have the ability to deal with more than thirty force curves at once which is the case for Nanoscope Analysis. This means that the analysis of a high resolution image could take up to a day to complete. Because of this there was large motivation to automate the procedure and so bespoke software was created in Matlab.

Matlab was chosen for a number of reasons. Firstly the AFM imaging software Nanoscope comes with Matlab support which allows for the extraction of the raw data from the force curves. The Matlab software is powerful and can handle large arrays of data easily meaning thousands of force curves would not be a problem. It also has many inbuilt functions, such as line fitting and convolutions of data, which would make producing the algorithm less time consuming. Lastly

it is also simple to display graphs with Matlab which would make it easier to see how effectively the code was working during the development process.

Three different iterations of the analysis software were produced over the course of this work. This chapter discusses their analysis algorithm, advantages and shortcomings. A test force volume image was analysed using the slow method with commercially available software. The results were compared to the results given by the Matlab software to see how accurately the new software could locate specific events and measure the rupture forces.

4.2 Criteria and Considerations

There were a large number of criteria that the software needed to achieve and a few important considerations to take into account to make certain that it was more efficient than the current way of analysing force curve images.

The main criterion for the software was to reduce the time taken to do the analysis process by hand in the existing software whilst maintaining the same level of accuracy on the force measurements. It was also desirable to have as little user interaction as possible. The software needed to be able to correctly distinguish between specific events and false background events and then measure the unbinding force with a high precision. It should then return the average binding force as well as all the individual values so that they could be exported into other programs for further analysis. Extra data cuts were required on the binding location. A 'binding event' 50 nm away from the surface is not realistic when an 8 nm PEG tether is being used so there needed to be a user defined cut off point.

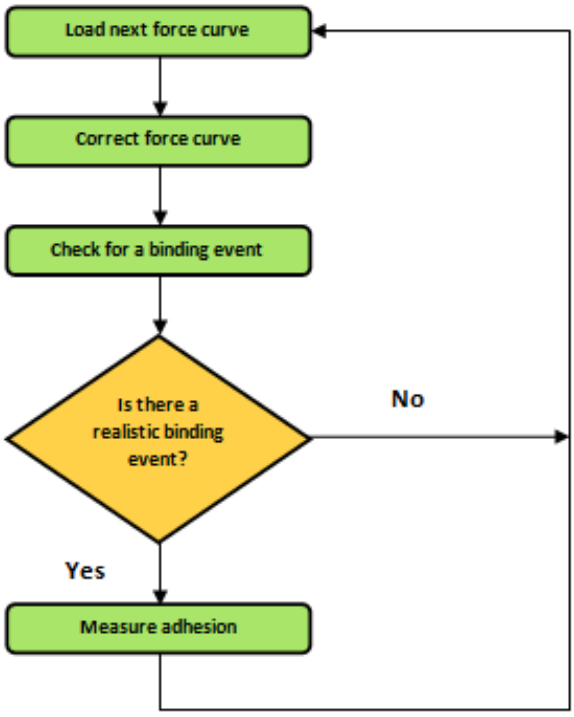

Figure 4.1: Simple flow chart of the basic program.

A summary of key points that the software should address can be seen below. These were used as a checklist to see how effective each iteration of the software was. The software should be able to:

- Handle thousands of force curves in one go
- Be faster than the current analysis time
- Maintain the high accuracy of the current method
- Have limited user interaction
- Locate all specific events
- Check events have a plausible binding location
- Remove background curves
- Convert deflection into Newtons
- Correct the baseline

- Return average binding force
- Return individual force values

With these criteria in mind a flow chart of the basic algorithm was created as seen in figure 4.1. There are two sections of this flow chart that are non-trivial - the force curve correct and the identification of binding events.

4.3 Corrections

Several corrections needed to be carried out on the force curves before they were ready to analyse. Firstly a baseline correction needs to be applied which straightens out the non-contact region of the curve and sets it to zero deflection or force [4]. To correct the baseline a linear polynomial (an example of which can be seen in figure 4.3a) was fitted to the non-contact region of the curve. The retrace and approach curves have 512 data points. By fitting the line to the last 100 data points of the retract curve it means that no adhesion signatures are included in the fit whilst still giving a large sample to fit to. Removing this line from the deflection values completes the baseline correct as seen in figure 4.2.

When force curves are first extracted from the AFM images they are a plot of the deflection verses the piezo position, Z, where the zero point is where the tip is furthest away from the surface. Before analysis it is advantageous to convert the piezo position data into the separation between the tip and the sample, denoted d [5, 6]. This is done using the following equation:

$$d = C_p - Z + \delta \tag{10}$$

Where C_p is the contact point and δ is the deflection of the cantilever which corrects for the additional distance added by the deflection of the cantilever. By subtracting the piezo position from the C_p it sets the contact point to 0 nm. This makes limiting the distance that potential binding features can be from the sample a much simpler process.

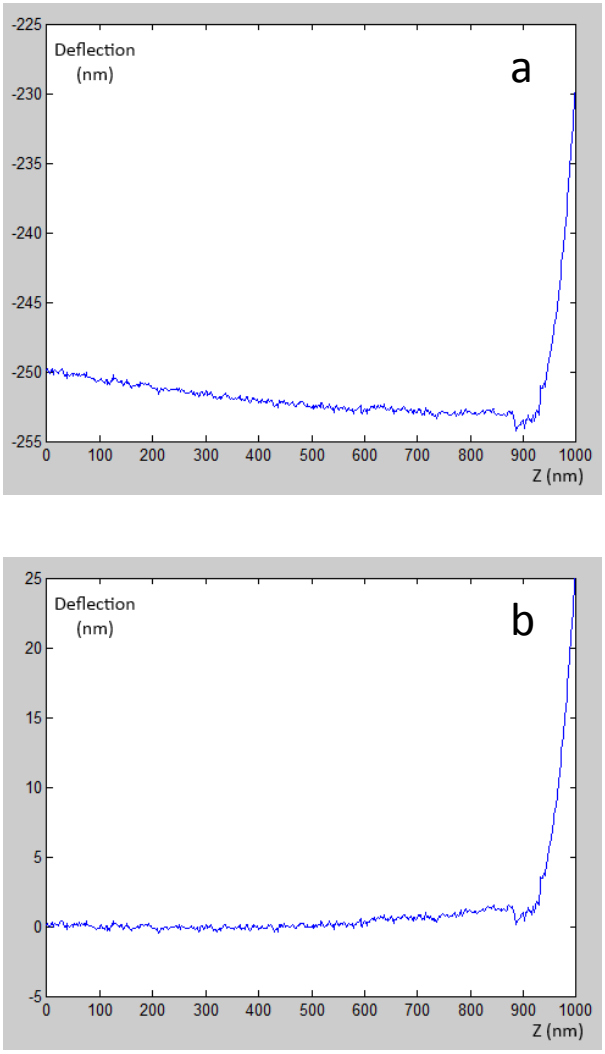

Figure 4.2: Example of a force curve before a) and after b) a baseline correct. The non-contact region is significantly straighter than it was previously and the non-contact section is at 0nm deflection.

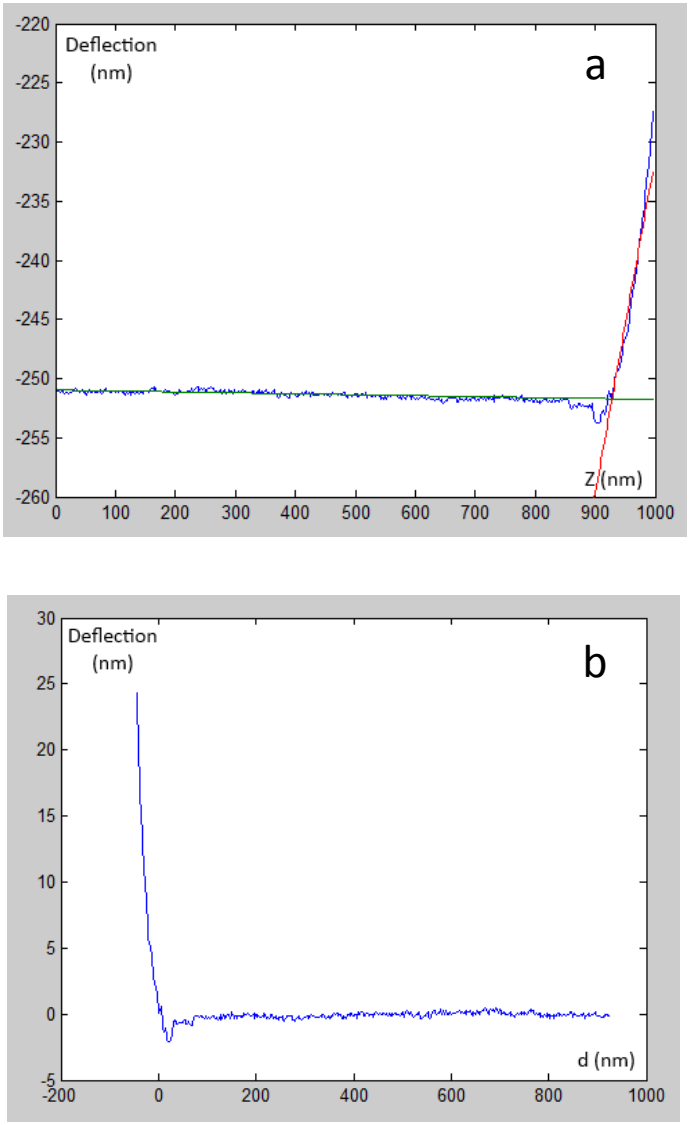

Figure 4.3: a) An example of the fits used to find the contact point of the surface and b) the outcome of setting the contact point as the origin and correcting for deflection of the cantilever.

The tip contact point was defined as where the baseline crosses the line of best fit through the contact section of the curve as shown in figure 4.3a [6]. The first 50 data points of the contact region were chosen for this fit so as to ensure no non-contact regions were accidentally included.

Finally, when the curves are extracted from the force volume image it is the deflection in nanometres that is plotted against the height above the surface so the deflection data needs to be converted into a force measured in Newtons. To do this the deflection array simply needs to be multiplied by the spring constant, as stated by Hooke's Law, which is measured during calibration of the AFM system via a thermal tune [6]. By carrying out a unit change the curve in figure 4.3b becomes that in figure 4.4.

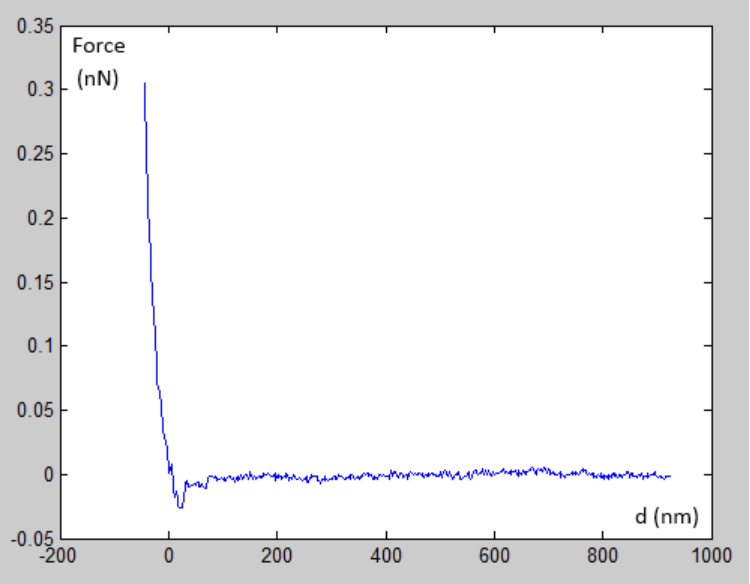

Figure 4.4: Example of a force curve after the unit change.

4.4 Binding Event Identification

As mentioned in section 3.3 a non-linear adhesion feature is indicative of a specific binding event occurring [7, 8]. A way of implementing the detection of this signal within the software was developed. There is no comprehensive model that accurately describes the shape of these force curve features. The worm-like chain model (WLC) (equation 11) is sometimes used but this is a complicated fit

to apply to the force curve data and requires the calculation of the contour length (L) and persistence length (l_p) of the tether [9, 10, 11].

$$F(x) = \frac{k_B T}{l_p}\left(\frac{1}{4\left(1-\frac{x}{L}\right)^2} - \frac{1}{4} + \frac{x}{L}\right) \quad (11)$$

The contour length is defined as the length of the tether at its maximum extension. The persistence length is a measure of the tether's stiffness, or more accurately the length over which correlations between the directions of the tangent are lost, and can be calculated by fitting complex mathematical models [12]. It has also been found that the WLC model becomes less accurate as the strength of the ligand-receptor bond decreases [13].

In its simplest form the program needs to be able to differentiate between specific and background events. One way would be to look for good candidate events by searching for large troughs in the desired range away from the contact region. These could then be shown on screen to undergo a final check by the user. This would save a large amount of time as a substantial portion of the current analysis time is spent opening files, waiting for them to load and the actual measurements of the adhesion. Checking the force curve shape by eye is a fairly speedy process and it would be even faster if the force curves that have no features had already been rejected.

However the criteria states that user interaction should be limited so another method was tried. Kasas *et al* highlight a way of locating the desired features by convolving the force curve with three very specific shapes that all binding events should contain [9] . These shapes are a vertical section where the ligand breaks

free, a sharp right angle where the vertical section meets the baseline and a 'V' section at the bottom of the feature [9]. If a curve shows a high convolution with these three shapes in the appropriate distance from the 0 nm mark then it is very likely to be a specific event. It is then a simple case of locating the exact coordinates of the vertical section of the event and then finding its magnitude to give the adhesion value.

4.5 Method of Testing

A force volume image taken using a tip functionalised with biotin on an avidin substrate was used as a test image for the program. Experiments using avidin and biotin are the subject of Chapter 5 where the experimental details are given discussed in more detail. The image consists of 256 curves which when analysed by hand gave 26 specific binding events and an average binding force of 34.12 ± 6.02 pN. Sorting through all 256 curves and then measuring the binding force of the 26 events using Nanoscope Analysis took approximately 90 minutes. All iterations of the program are compared to these values for time taken, number of curves, the particular force curves chosen (labelled 0-255) and the accuracy of the measured adhesion values.

4.6 Results

All versions of the software used the inbuilt Nanoscope Analysis Matlab files to export the force curve data into the workspace. They also all use the same baseline correct and unit conversion code which can be found in the appendix at the end of this thesis.

4.6.1 Version 1

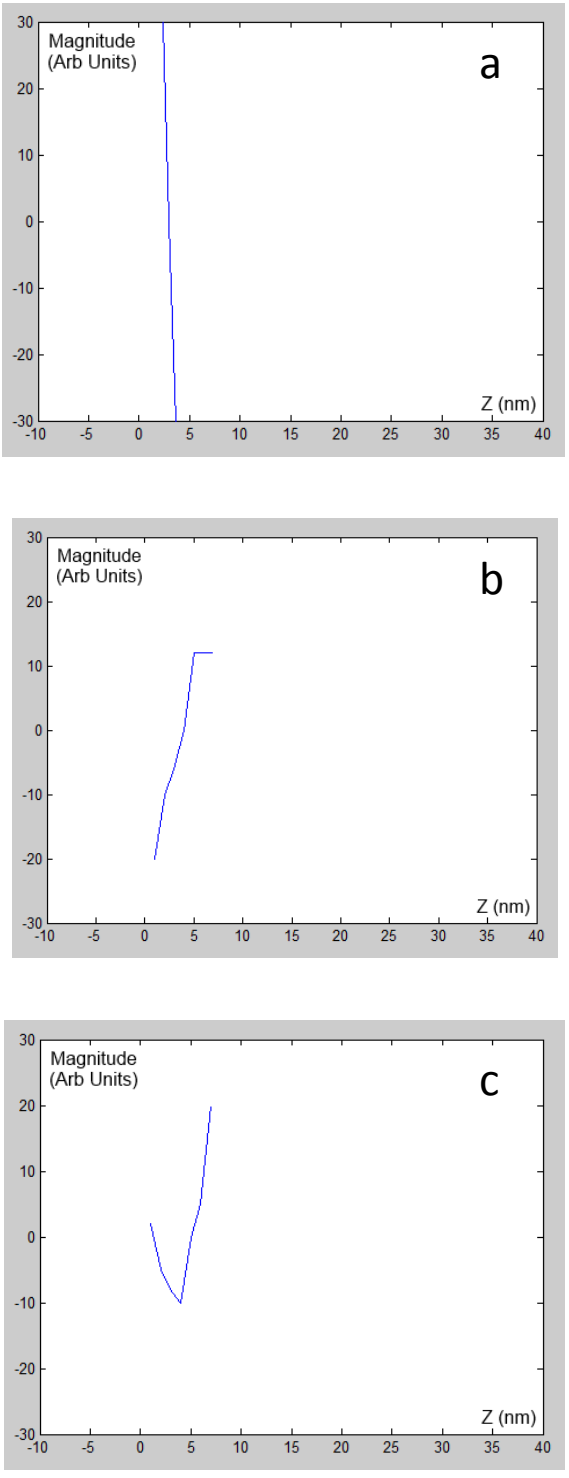

Figure 4.5: Images of the convolution vectors used to distinguish a) vertical sections, b) right angles and c) 'V' sections in the force curves.

After the corrections had been made the next step was to try the three convolutions described above. The same three vectors as Lara *et al* used were set up which can be seen in figure 4.5 [9]. They were as follows:

Vertical section: [100 50 0 -50 -100]

Right angle: [-20 -10 -6 0 12 12 12]

'V' shape: [-2 -5 -8 -10 0 5 20]

The inbuilt Matlab convolution function conv(u,v) was applied which produced a set of data for each convolution that gave peaks when the force curve was similar to the convolution shape. Figure 4.6 shows an example of a vertical convolution on a force curve where a peak in the convolution magnitude is clearly visible at 75 nm which corresponds with the jump in the force curve. However when applied, the 'V' and right angle convolutions showed no difference between a binding event and a background adhesion event.

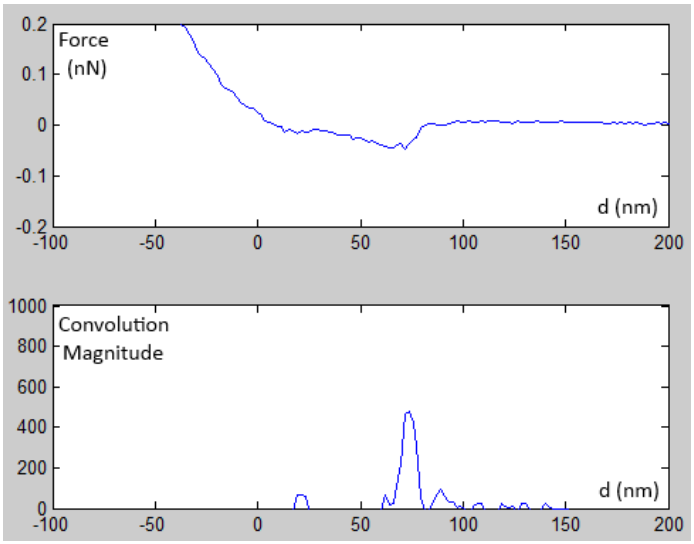

Figure 4.6: An example of a vertical convolution on a force curve. The convolution correctly identifies a vertical section around the 75nm distance.

Time was spent altering the vector sizes to make them have a stronger convolution with specific events than background curves but all attempts were unsuccessful. The vertical convolution could not show the difference between the events but it could distinguish the magnitude of the jumps in force very well. This feature became the basis of version 2.

4.6.2 Version 2

It was decided that the vertical convolution would be used to try and identify candidate force curves. Figure 4.7 slows a flow chart of the program. To speed up the convolutions all data not in the 0 - 16 nm region was discarded. The first decision was made after the vertical convolution. Matlab's peak finder function was used to count the number of troughs larger than a user defined magnitude over the region of interest. If there were more than four troughs the force curve was deemed too noisy and was discarded. If there was more than one trough but less than five it was displayed on screen along with the number of troughs present in the curve. The user could then input 0 if there was no event present or supply the program with the trough number of the vertical section that showed a specific event. The location of the vertical section was found to a greater accuracy and then the adhesion value was calculated.

The program took roughly two minutes to analyse the 256 curves which is an enormous decrease in the analysis time. It does however require fairly constant user interaction but it was still quick enough to be acceptable.

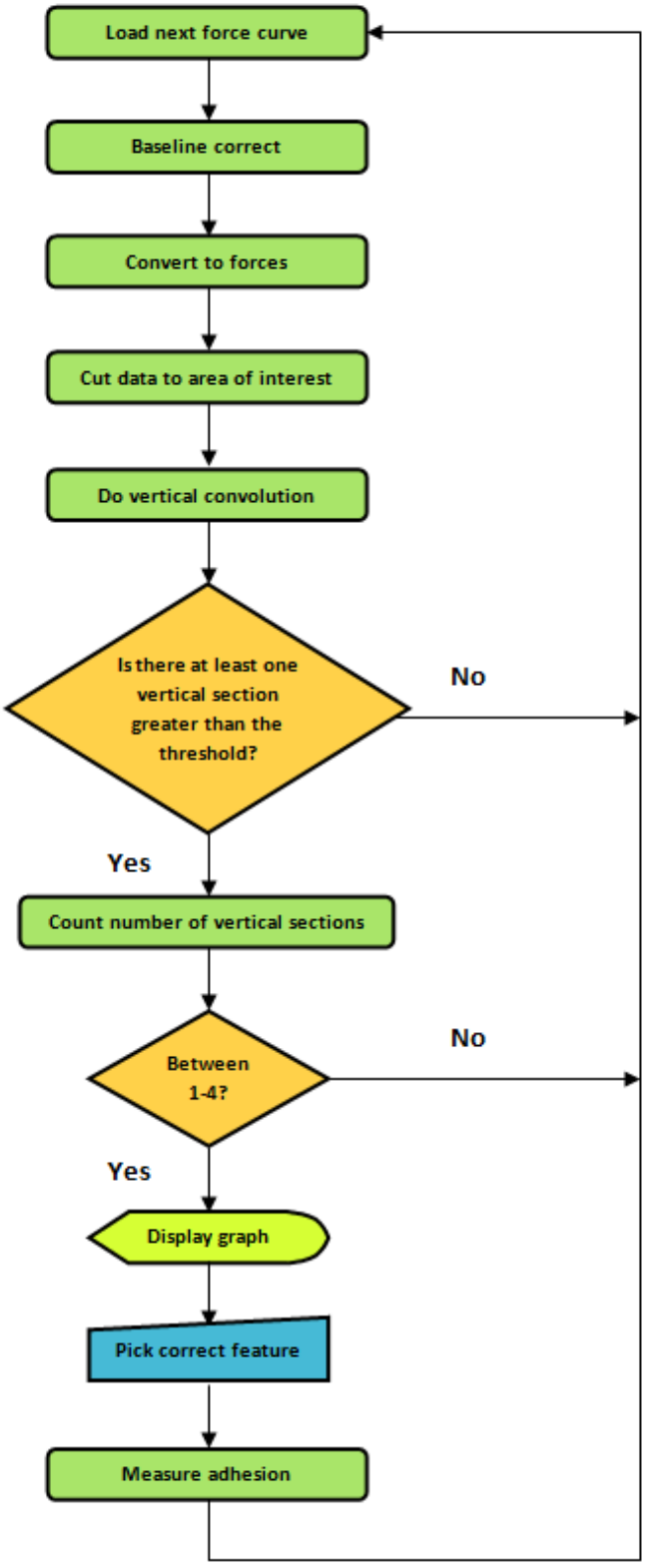

Figure 4.7: Flow chart highlighting the algorithm used in version 2 of the software.

	Version 2.0	Version 2.1	Version 2.2	Manual Analysis
Average force (pN)	21.84 ± 3.8	24.5 ± 3.7	38.4 ± 7.0	34.12 ± 6.02
Total Number of Files	20	22	27	26
Missing Files	14	15	15	-
Extra Files	8	11	16	-

Table 4.1: Summary of the results obtained using the vertical convolution method of identifying binding features from three different iterations of the program compared to manual analysis carried out with commercial software.

Different variations in the vertical shape that was being used for the convolution and the cuts used to define a specific event were used to try and optimise the analysis and the results are summarised in table 4.1. By looking at the average force and the total number of files it appears that the optimisation of the parameters was improving the accuracy of the analysis as Version 2.2 has a similar average force as the results found from manual analysis with the commercial software. However by comparing the actual force curve files that were analysed it became clear that many files that should have passed were not being measured by the algorithm and many files that should have been discarded were kept and analysed. Each version of the software was run multiple times to account for human error when identifying specific curves but each run gave the same result.

4.6.3 Version 3

Although version 2 was very quick it was not as efficient as desired so a third version of the software was created which was based on the basic program outlined in section 4.4. It was decided that if it could analyse a whole image file

in a few minutes and be very accurate then the constant user interaction was acceptable.

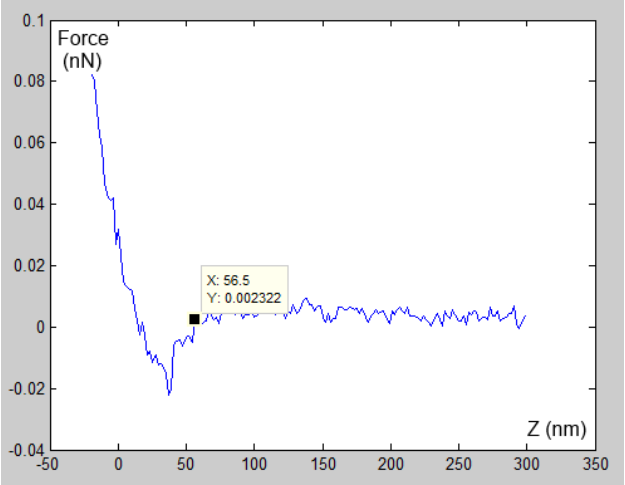

Figure 4.8: Example of a curve having its adhesion feature measured using cursors - the main principle behind version 3 of the software.

The area of interest set by the user e.g. 0-16 nm was extracted from the retract curve. The first point in this data was selected and then the algorithm checked that the points either side of it were larger in value. By cycling through all points on the curve the troughs were found. The magnitudes of the troughs were then compared with the thermal noise to check that it was not just a random fluctuation in the curve. The noise was calculated from taking the average spread of the non-contact region data points. By comparing the magnitude of the trough to the thermal noise which is intrinsic to each force curve and not to a user defined size, as was the case for version 2, it would mean less time would be spent working out the optimal data cuts.

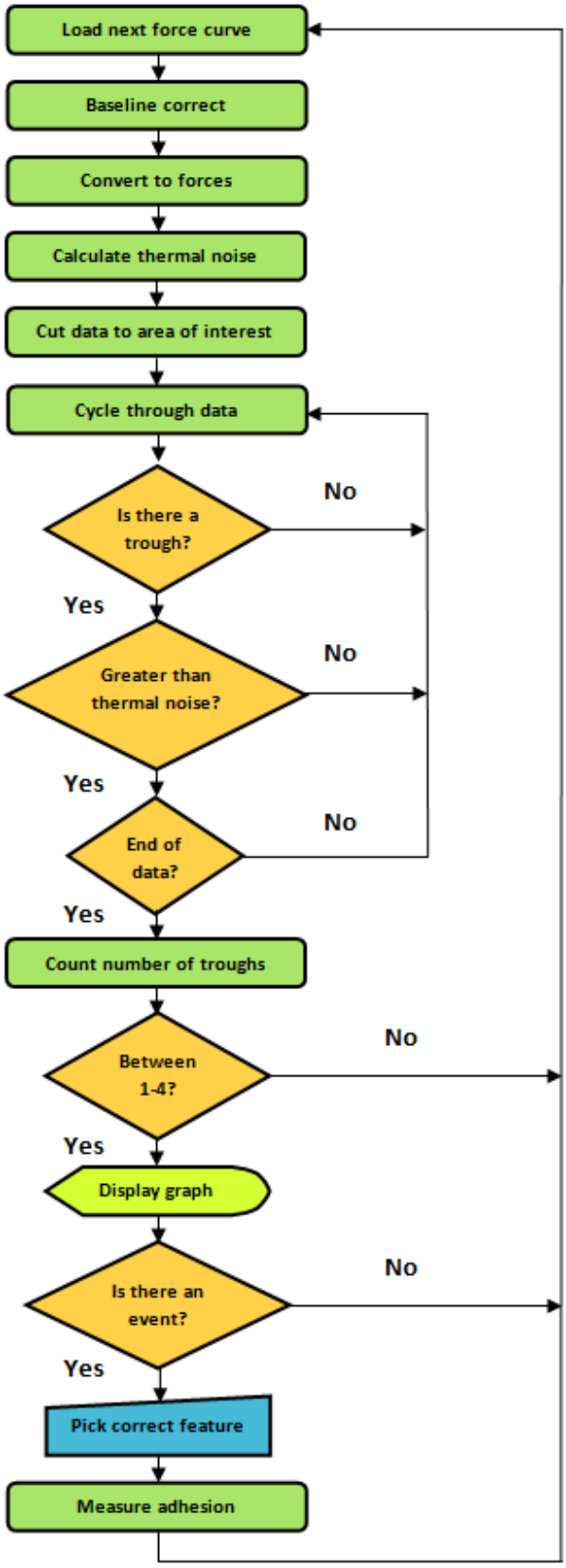

Figure 4.9: Flow chart highlighting the algorithm used in version 3 of the software.

Troughs that passed the inspection were counted and, as with version 2, if there was 1-4 troughs present the curve was displayed to the user. However instead of the user entering the trough number the user was asked to say if there was an event present. If the force curve did show a binding event cursors were used to allow the user to identify the top and bottom of the binding feature so the adhesion could be measured. This, although slower and required more user input than version 2, gave significantly more accurate adhesion values shown in table 4.2.

	3.1	**Commercial software**
Average force (pN)	35.4 ± 5.9	34.12 ± 6.02
Total Number of Files	25	26
Missing Files	2	-
Extra Files	1	-

Table 4.2: Summary of the results obtained from the point and click method of calculating adhesion.

Just two force curves were missed and only one was incorrectly identified. This was likely to be due to the two curves having very small events that were similar in size to the thermal fluctuations which meant they were discarded. The average force measured was very similar to that calculated using Nanoscope analysis. When the measured force value of a particular curve was compared directly with the value from Nanoscope the smallest difference was 0.03 pN and the largest was just 7 pN which, when averaged with many data points, does not introduce a large error.

The whole image analysis took 8 minutes which improves the measurement time by approximately 82 minutes therefore despite version 3 taking four times as

long as version 2 it is still significantly faster than the current method, required the same amount of user input per file and was more accurate in the force measurements. For these reasons version 3 was the code that was used for real analysis of files in Chapters 5, 6 and 7. The final code can be found in the Appendix section.

4.7 Conclusion

Over the course of the work outlined in this chapter three different pieces of Matlab algorithms were written. One version did not work, one was too inaccurate and the last worked very effectively. It should be noted that smoothing the curves before analysis was tried in all versions of the software but made no difference to the outcome. The results produced by version 3 matched very well to the results obtained by analysing each curve individually using Nanoscope Analysis. The measured rupture force varied by 1 pN.

For completeness it would have been good practice to compare the results from the Matlab program to previously published results from literature as well in case the manual method was incorrect. However as the loading rate for the data was obtained at the default setting for Nanoscope there were no results that the average forces calculated here could be compared to. In Chapter 5 the final program written in this chapter, version 3, was used to analyse a larger force volume image that was compared directly to literature values and produces very similar results which is a good indication that the Matlab program is analysing the data correctly.

Of the criteria set out in section 4.2 all but three were fulfilled. The criteria dictated that there should be limited user interaction. Although the user must be active by making decisions and giving inputs frequently the amount of interaction is reduced. The binding force measurements do not have to be written down one by one. Instead all values are returned at the end which saves a lot of time. The user only has to input a Boolean to say if the curve has passed and then click on the binding feature to measure the adhesion. Also, because force curves can be noisy and vary a bit between images, having the user make the final decision will be more accurate as they can adapt to changes easily and quickly. Although making it fully automated would make it a lot quicker there will always be a trade off between speed and accuracy.

The second criterion that version 3 failed to address was that it should be able to 'locate all specific events'. Two force curves were missed but missing curves will not alter the average significantly as long as the sample size is large enough. It was also unsuccessful at removing all background events as one incorrect event was included. However as the program is set up so the final decision comes down to the user this would be a user mistake as opposed to a problem with the algorithm. The same human error would be present when analysing images using commercial software too.

Overall an efficient piece of code was written that can accurately detect specific binding events, measure the force accurately and reduced analysis time by 82 minutes meaning the core objective outlined in this chapter was accomplished.

4.8 References

[1] V. T. Moy, E. L. Florin and H. E. Gaub, "Adhesive forces between ligand and receptor measured by AFM," *Colloids and Surfaces A: Physicohemical and Engineering Aspects,* vol. 93, pp. 343-348, 1994.

[2] M. de Odrowąż Piramowicz, P. Czuba, M. Targosz, K. Burda and M. Szymoński, "Dynamic force measurement of avidin-biotin and streptavidin-biotin interactions using AFM," *Acta Biochimica Polonica,* vol. 53, no. 1, pp. 93-100, 2006.

[3] J. Friedrichs, K. R. Legate, R. Schubert, M. Bharadwaj, C. Wener, D. J. Müller and M. Benoit, "A practical guide to quantify cell adhesion using single cell force spectroscopy," *Methods,* vol. 60, no. 2, pp. 169-178, 2013.

[4] JPK Instruments, A practical guide to AFM force spectroscopy and data analysis, JPK Instruments, 2011.

[5] H. J. Butt, "Measuring local surface charge densities in electrolyte solutions with a scanning force microscopy," *Biophysical journal,* vol. 63, no. 2, pp. 578-582, 1992.

[6] W. F. Heinz and J. H. Hoh, "Spatially resoled force spectroscopy of biological surfaces using the atomic force microscope," *Trends in biotechnology,* vol. 17, no. 4, pp. 143-150, 1999.

[7] U. Dammer, O. Popescu, P. Wagner, D. Anselmetti, H. J. Guntherodt and G. N. Misevic, "Binding strength between cell adhesion proteoglycans measured by atomic force microscopy," *Science,* vol. 267, no. 5201, pp. 1173-1175, 1995.

[8] C. K. Riener, C. M. Stroh, A. Ebner, C. Klampfl, A. A. Gall, C. Romanin, Y. L. Lyubchenko, P. Hinterdorfer and H. J. Gruber, "Simple test system for single molecule recognition force microscopy," *Analytica Chimica Acta,* vol. 479, no. 1, pp. 59-75, 2003.

[9] S. Kasas, B. M. Riederer, S. Catsicas, B. Cappella and G. Dietler, "Fuzzy logic algorithm to extract specific interaction forces from atomic force microscopy data," *Review of scientific instruments,* vol. 71, no. 5, pp. 2082-2086, 2000.

[10] J. Fritz, A. G. Katopodis, F. Kolbinger and D. Anselmetti, "Force-mediated

kinetics of single P-selectin/ligand complexes observed by atomic force microscopy," *Proceedings of the National Academy of Sciences,* vol. 95, no. 21, pp. 12283-12288, 1998.

[11] A. Valiaev, S. Zauscher and S. C. Schmidler, "Statistical Analysis of Single-Molecule AFM Force Spectroscopy Curves," *Biophysical Journal,* 2006.

[12] C. Bouchiat, M. D. Wang, J. F. Allemand, T. Strick, S. M. Block and V. Croquette, "Estimating the Persistence Length of a Worm-Like Chain Molecule from Force-Extension Measurements," *Biophysical Journal,* vol. 76, pp. 409-413, 1999.

[13] N. W. Moore and T. L. Kuhl, "The Role of Flexible Tethers in Multiple Ligand-Receptor Bond Formation between Curved Surfaces," *Biophysical Journal,* vol. 91, pp. 1675-1687, 2006.

Chapter 5 - Single Molecule Force Spectroscopy Test System

As described in section 3.3, single molecule recognition force microscopy uses AFM force curves to measure the rupture force between two molecules. It is this technique that will be used to study the effects the environment has on Cal B's capacity to break down lipid substrates [1]. AFM force curves can be obtained using a variety of AFM modes such as force volume and QNM. At the time of carrying out this work the majority of single molecule experiments used force volume. One objective of the work discussed in this chapter was to compare QNM and force volume as QNM has the potential to be a quicker, simpler alternative to force volume imaging.

Force volume has a number of disadvantages. Each force curve can take seconds to capture due to the slow approach and withdraw speeds and a small intrinsic dwell time of 2-4ms at the surface. It is possible that some biological binding half-lives are less than a few milliseconds and so processes can be missed as force volume would be too slow to observe them [2]. A force volume image with 64x64 pixels is low resolution and yet takes approximately 90 minutes to capture. Because of this poor resolution identifying the location of binding sites on a large substrate such as a cell can be very inaccurate. Force volume imaging involves a lot of post data capture analysis as each force curve needs to be examined individually for evidence of a binding event. Those that do then need additional analysis to measure the binding force of the molecules.

Section 3.2.5 discussed the new technique of QNM which has the potential to solve some of the problems associated with force volume. The technique is a significantly faster than force volume with a 512x512 pixel image takes around 16 minutes to capture. It produces simultaneous images of topography and the mechanical properties of the sample with another key feature being instantaneous feedback via real time analysis of the force curves. The adhesion images captured can show almost immediately if binding is occurring between the molecules and give quantitative force values. This quick identification of unbinding events is a useful tool for establishing the quality of the functionalised tip. The fact that the raw force curves can be extracted, using the high speed data capture feature, means that the more in depth and tailored analysis that force volume provides can be carried out with QNM too.

Figure 5.1: Ribbon structure diagram of the protein avidin. Avidin has a molecular weight of 60kDa.

A second objective of this work was to develop a test system to investigate the practical aspects of single molecule recognition experiments such as tip functionalisation chemistry and force curve analysis.

The binding molecules chosen were the protein avidin, which is found in egg white, and biotin, also known as vitamin H. Biotin has a high affinity for avidin along with other proteins such as streptavidin [3, 4]. Avidin can be immobilised onto a flat surface for imaging with a tip that has been functionalised with biotin. Avidin and biotin have been used extensively in force volume experiments and are regularly used as an introductory system for users that are new to the technique [5, 6, 7, 8, 9]. The binding force between avidin and biotin is one of the strongest known protein-ligand interactions making their binding signatures easily observable [10].

They also have a number of additional advantages which make them a good test system which are highlighted in Ebner's paper:

1) "*robust and reliable,*

2) *well known in terms of binding properties,*

3) *easy to prepare with commercially available components,*

4) *avidin can easily be absorbed to mica*" [11].

Because the binding properties have been so widely studied avidin and biotin are the perfect molecules to use to compare force volume and QNM AFM.

5.1 Challenges and Considerations

5.1.1 Tip Chemistry

Section 3.4 discusses the different types of chemistry that are available for functionalising an AFM tip with the desired ligand. Because the avidin and biotin interaction is so well known and frequently used heterobifunctional PEG tethers with biotin pre-attached are commercially available in a range of lengths. These tethers come with a wide variety of molecules attached to the other end allowing for a large variety of tip-PEG chemistry to be used.

Binding via gold-thiol reactions was rejected due to the high cost and difficulty involved with coating AFM tips in gold without damaging them [12]. Instead amino functionalisation of silicon nitride was chosen as previous experiments reported in the literature have had a high level of success with attaching an NHS ester on the end of the PEG using this method [5, 11, 13].

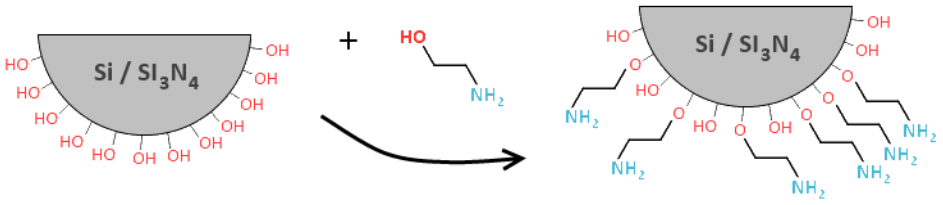

Figure 5.2: Schematic of the binding chemistry that occurs during aminofunctionalisation with the ethanolamine HCL method.

Riener *et al* investigated which of the two amine-derivitisation methods (APTES or ethanolamine HCL) were best for single molecule recognition microscopy [5]. They compared gas phase and aqueous phase APTES methods of amino

functionalisation with the ethanolamine HCL method carried out at room temperature and at 100^{o}C for attaching NHS-PEG-Biotin tethers to silicon tips.

They found that whilst all four techniques gave a suitable number of ligands on the AFM tip, the ethanolamine method at 100^{o}C gave the highest number of PEG linkers attached to the silicon whilst the gas phase APTES gave the least. Having a high density of PEG chains can be detrimental as the tightly packed ligands can block each other and actually lower the binding probability. The room temperature ethanolamine HCL method gave the highest binding probability of 0.246 ± 0.155 during imaging whereas the APTES method was 0.168 ± 0.072 for gas phase. The APTES method gave marginally lower levels of non-specific adhesion compared to ethanolamine HCL with a difference of 0.01.

From the work by Riener *et al* the room temperature ethanolamine HCL process was chosen for biotin functionalisation for a number of reasons. Firstly, as mentioned above, it is capable of giving enough ligand coverage to be used in molecular recognition experiments and has been used in a number of previous experiments using other molecules besides biotin [14, 15, 16]. Secondly it does not require any specialist equipment as the work is carried out in glassware and all the reagents used are cost effective and easily available. It is much simpler to carry out than the APTES method as the humidity of the environment does not need to be considered however it does take more time as it requires the tips to be left overnight in the ethanolamine HCL solution.

5.1.2 Loading Rate

A significant challenge with comparing QNM and force volume AFM is the dependence of the binding force on the loading rate of the cantilever as discussed in section 3.3.1. Due to the difference in the way the cantilever moves in the two techniques it is hard to achieve the same loading rate for both as the loading rate is linearly dependent on the retraction velocity. As force volume is slower than QNM it is expected that the measured binding forces would be lower in force volume mode. Force volume mode has the option to specifically set the desired retraction velocity so the loading rate can be easily established accurately once the spring constant is known. QNM does not have the ability to explicitly set the retraction velocity, only linear scanning velocity.

The motion of the cantilever oscillation in QNM is sinusoidal. This motion causes the retraction velocity, and therefore loading rate, to change throughout one cycle. The retraction velocity can be estimated using the known oscillation amplitude and frequency, the latter of which can be obtained from the linear scan speed and the number of force curves per line. By modelling the path of the tip as a sine wave the differential of this could be used to calculate the velocity. It is also important to calculate the retraction velocity at the correct distance from the surface. This was chosen to be 16nm as it takes into account the length of the PEG tether and the size of avidin and biotin.

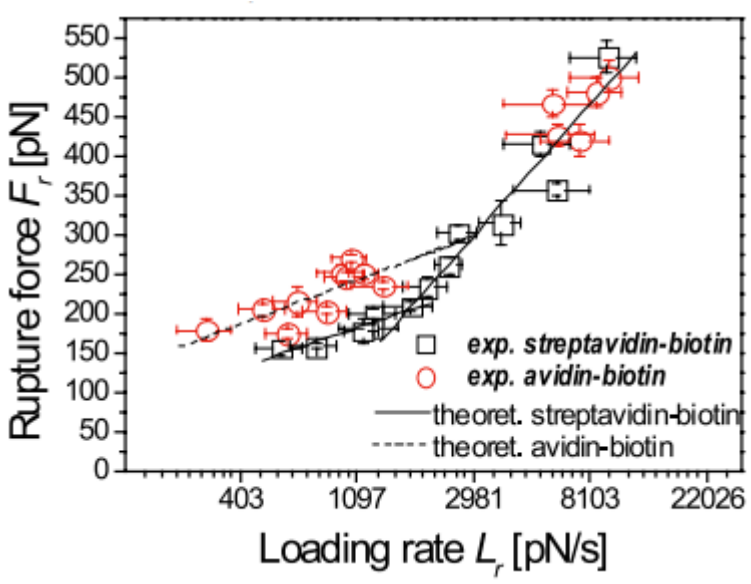

Figure 5.3: Binding force verses loading rate for avidin and biotin and streptavidin and biotin [17].

A benefit of avidin and biotin being widely studied is that the binding force between the two molecules at different loading rates has been well documented (as shown in figure 5.3) in a number of experiments meaning there are many results to compared to which is useful check for seeing if the system is working effectively [8, 17, 18].

5.2 Experimental Method

All reagents were obtained from Sigma Aldrich unless otherwise stated.

5.2.1 Avidin Immobilisation

Avidin was immobilised onto the silicate mica. Mica is extremely flat substrate, which makes it a good platform for AFM imaging, and it has almost perfect cleavage meaning single layers of mica can be pulled off easily leaving a very

smooth and clean surface to work on. Avidin is affixed to mica using electrostatic interactions. Avidin's basic isoelectric point, meaning it has positively charged residues on its surface at neutral pH, and mica's negative charge allows the avidin to bind to the mica [5]. This is a very simple reaction and a great improvement on the previous way to immobilise avidin which involved covering a gold substrate with a monolayer of the ester 11, 11'-dithiodiundecanoic acid bis-succinimidyl in a time consuming process to which avidin was then bound [8].

To carry out the mica absorption process a stock solution of avidin in phosphate buffered saline (PBS) was made at a concentration of 1 $mgmL^{-1}$ as recommended by Riener *et al* [5]. The PBS consisted of 10 mM phosphate, 2.7 mM potassium chloride and 127 mM sodium chloride at a pH of 7.4. This stock solution was diluted with 1 mM sodium chloride to an avidin concentration of 0.5 $mgmL^{-1}$.

Freshly cleaved mica was immersed in this diluted solution for 15 minutes and then washed with PBS.

5.2.2 Atomic Force Microscopy

In this work all atomic force microscopy was carried out using a Bruker BioScope Catalyst AFM which was attached to a Veeco Nanoscope V controller and run with the Nanoscope v8.15 software. All topography and adhesion images were created using the open source software package Gwyddion [19]. Force curves were analysed using the version 3 of the Matlab software discussed in Chapter 4.

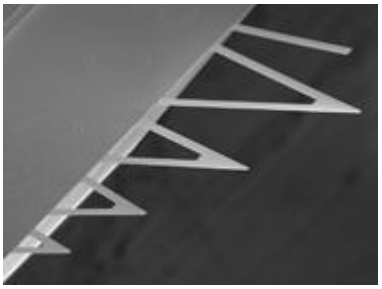

Figure 5.4: Electron microscope image of a set of MCLT cantilevers that were functionalised with biotin.

Unless otherwise specified all AFM images were taken using MLCT tips (figure 5.4) under a PBS buffer. These tips were chosen for functionalisation as they have six cantilevers which all have low spring constants meaning they are sensitive enough to detect the molecular interactions and can also be used effectively in liquid.

5.2.3 Amino Functionalisation

First the tips were washed with chloroform twice and then ozone-plasma cleaned for 15 minutes. This removed other contaminating molecules and introduced a layer of silanols onto the silicon nitride. Following this the tips were once again washed twice in chloroform and dried in a stream of nitrogen.

To introduce the amine groups onto the silicon nitride surface a solution of 2.2 g of ethanolamine HCL in 4 mL of dimethyl sulfoxide (DMSO) was made. Once the ethanolamine HCL has dissolved 4 Å molecular sieve beads were added to remove any water present in the solution. The tips were then left in the solution

overnight. The following morning they were washed with DMSO three times, ethanol three times and then dried in nitrogen.

5.2.4 PEG Attachment

The next step was to attach the biotin. 8 nm NHS-PEG-Biotin chains (with a molecular weight of 3.4 kDa) were obtained from Creative PEGWorks in the USA. The structure can be seen in figure 5.5. The tethers were put into a solution of chloroform at a concentration of 1 $mgmL^{-1}$. Triethanolamine (TEA) was then added at a concentration of 0.5 volume %. The TEA acts as a catalyst for binding the NHS to the NH_2 molecules now on the silicon nitride surface. From the work by Riener *et al* the silicon nitride should be left in this solution for three hours [5]. After three hours the tips are rinsed in chloroform and then dried under air.

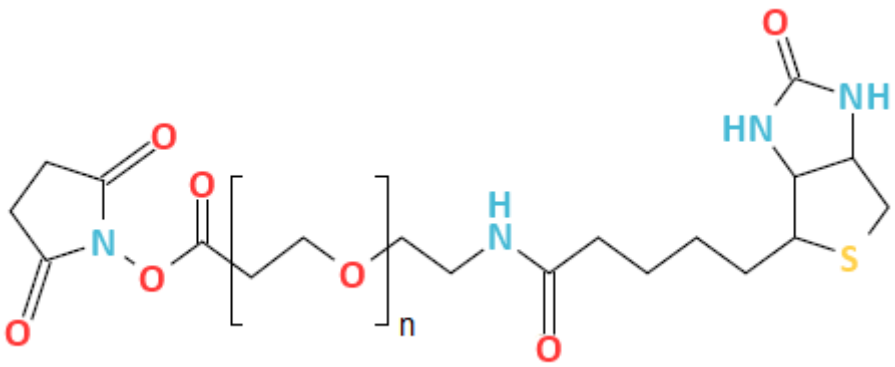

Figure 5.5: Structure of a NHS-PEG-Biotin linker that was used to bind the biotin to the AFM tips.

5.3 Results - Chemistry

5.3.1 Avidin Immobilisation

The first challenge was to attach the avidin to mica. The mica was submerged in the 0.5 $mgmL^{-1}$ avidin solution for 15 minutes as suggested by Riener *et al* and then immediately imaged [5]. These images showed a very low concentration of avidin on the surface as shown in figure 5.6a. Instead fresh mica was immersed in the 1 $mgmL^{-1}$ avidin solution for 30 minutes which produced a higher concentration of avidin molecules as seen in figure 5.6b.

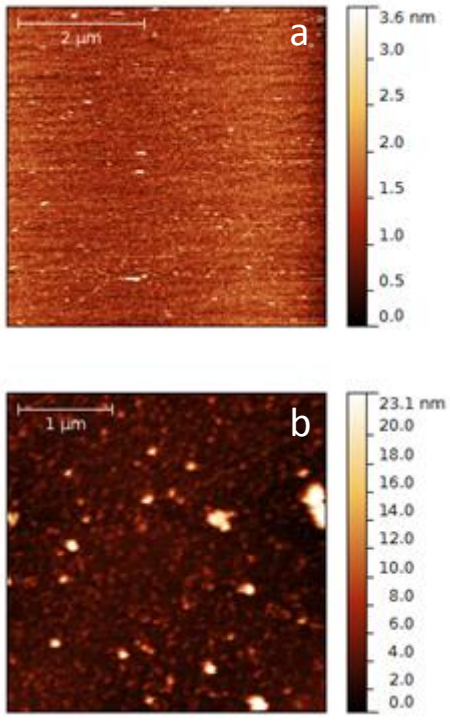

Figure 5.6: Freshly cleaved mica left a) for 15 minutes in 0.5$mgmL^{-1}$ and b) for 30 minutes 1$mgmL^{-1}$ avidin solutions. The higher concentration avidin solution and longer wait time results in much more avidin on the mica surface.

Avidin particles are between 6.5 nm and 8.5 nm in size which compares well with the size of the observed features on the mica surface however there are some large aggregates on the surface too [20].

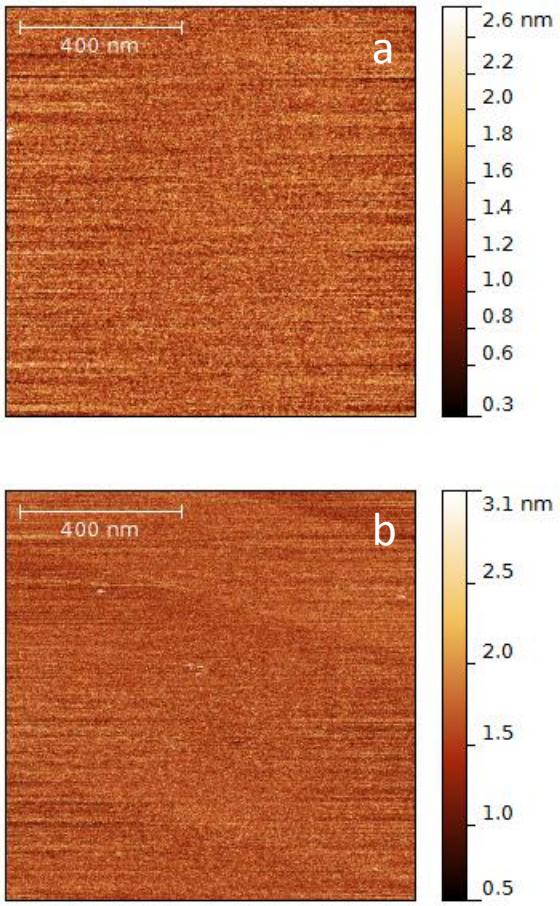

Figure 5.7: AFM images of a) freshly cleaved mica and b) treated mica without any avidin. The mica was left in the solution for 30 minutes - the same wait time that produced figure 5.6b. The solution does not deposit anything on the mica surface indicating the structures seen in figure 5.6b are in fact avidin aggregates.

To confirm the presence of avidin on the surface two control images were acquired which can be seen in figure 5.7. One was of freshly cleaved mica (figure 5.7a). This control showed there were no objects on the surface of the mica. The

second control experiment was to make the same NaCl avidin solution but without the avidin in it. The mica was immersed in this for 30 minutes and imaged to check that PBS and NaCL were not contaminated and depositing molecules on the surface of the mica. As seen in figure 5.7b it remained feature free. This is a good indication that the items on the surface in figure 5.6b are avidin molecules and aggregates.

5.3.2 Attaching PEG Tethers to Silicon

To confirm the PEG linkers could be attached to silicon/silicon nitride a number of control experiments were carried out. Biotin molecules are small in size and as such are difficult to image directly. Instead NHS-PEG linkers were acquired from Creative PEGWorks that had the fluorophore fluorescein attached to the end rather than biotin. These were also 8 nm in length and could be attached to silicon and then imaged using a confocal microscope as described in section 3.6. Fluorescein, when excited with blue light of wavelength 494 nm, will emit in the green portion of the spectrum at 518 nm.

Instead of AFM tips fragments of silicon wafer were used as they were cheaper and easier to image due to their comparatively large size. A number of silicon wafers were amino functionalised and then left in the fluorescein-PEG-NHS, chloroform and TEA solution for a variety of times from 20 to 180 minutes in order to study the effect time had on the concentration of bound PEG tethers. They were washed with chloroform twice to remove any loose PEG tethers before imaging. A silicon wafer that had been covered with amine groups was imaged to check there was no intrinsic green emission from the surface already.

As can be seen from figures 5.8a to 5.8g there is progressively more fluorescein emission, and therefore increasing PEG tether numbers, on the silicon the longer it was left in solution, which is as expected. The control image, figure 5.8h, showed no evidence of green emission.

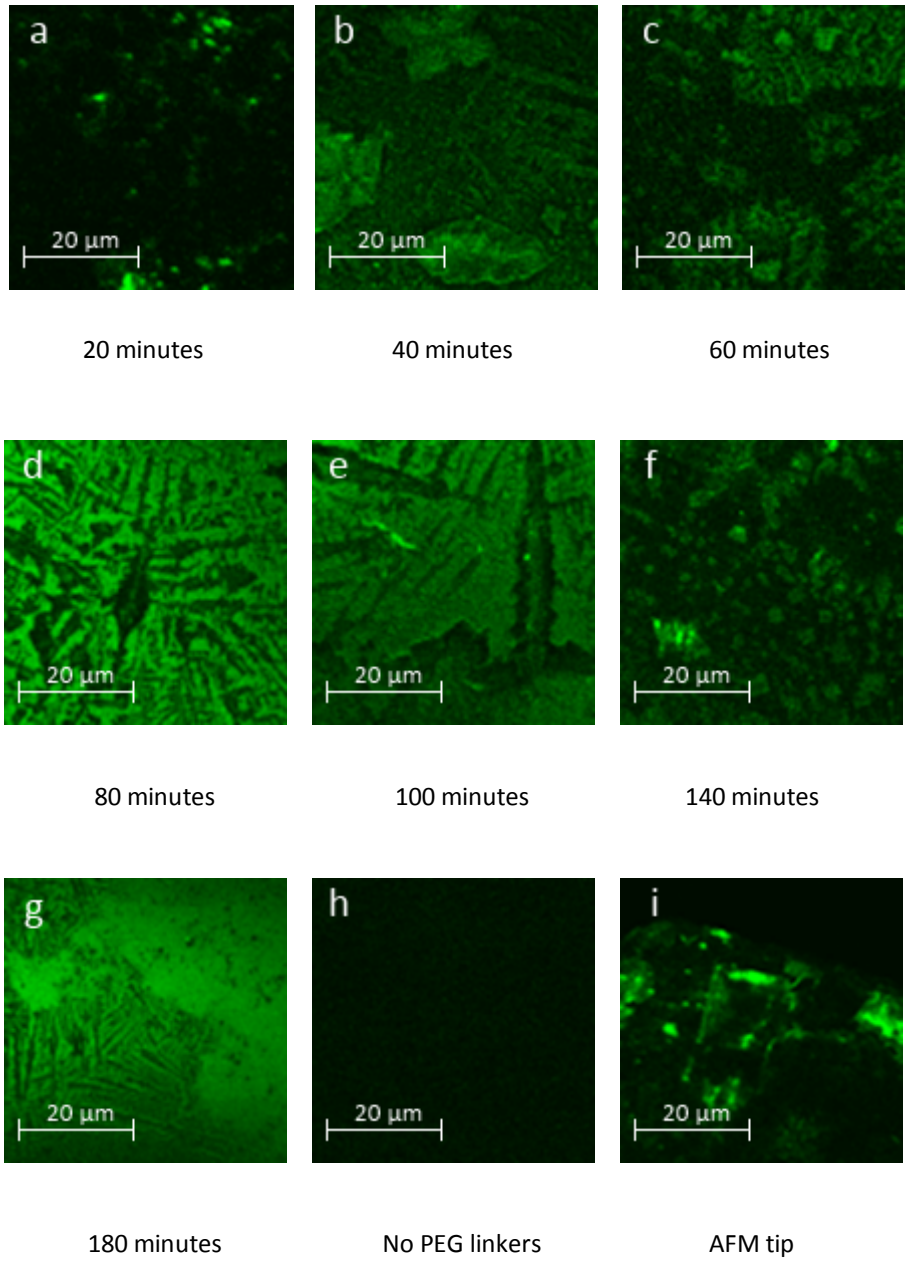

Figure 5.8: Confocal microscopy images looking for traces of fluorescein emission at 518nm.

From these images it was seen that the 140 minute and 180 minute silicon wafers have a good covering so a time between these two will be suitable for functionalisation. For future functionalisation 150 minutes was given for the PEG chains to bind to the AFM tips. One silicon nitride AFM tip was also functionalised with fluorescein to check that it worked on silicon nitride too (figure 5.8i).

5.4 Results - Molecular Recognition

5.4.1 PeakForce QNM

Because QNM has the ability to analyse force curves in real time and therefore produces an adhesion map during imaging they should show immediately when specific binding is occurring. This will only be the case if there is no intrinsic adhesion between the mica or avidin and the AFM which could produce false events.

To investigate this avidin was imaged with QNM with an unfunctionalised tip to measure the background adhesion values. As seen in figure 5.9b the adhesion from the avidin is lower for the avidin than for the mica substrate. This means if the avidin-biotin force is larger than the mica-tip adhesion any biding that occurs will be seen as areas of high adhesion correlating with avidin on the topography image.

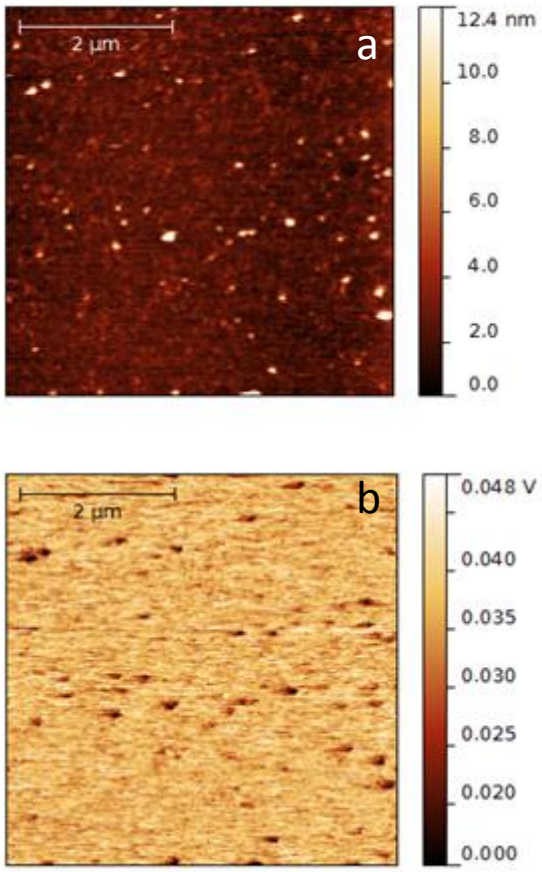

Figure 5.9: QNM images of a) topography and b) adhesion of avidin on mica taken with an unfunctionalised tip. The avidin (the higher features in the topography image) shows considerably less adhesion than the surrounding mica in the adhesion image.

In each functionalisation process 8-12 tips were coated with biotin-PEG chains but not every functionalisation was successful as the linker must be on the very end of the tip and this is statistically unlikely for every attempt. Also if the tip gets damaged any PEG chains can be removed from the tip. Figure 5.10 shows some QNM topography and adhesion images taken for one run of functionalisation. The adhesion images for tip set 2 cantilevers A and E show greater adhesion strength located on some of the avidin molecules which indicates specific binding is occurring. The lack of binding in some avidin

molecules can be understood by the random orientation of binding sites which leaves some sites inaccessible to the biotin.

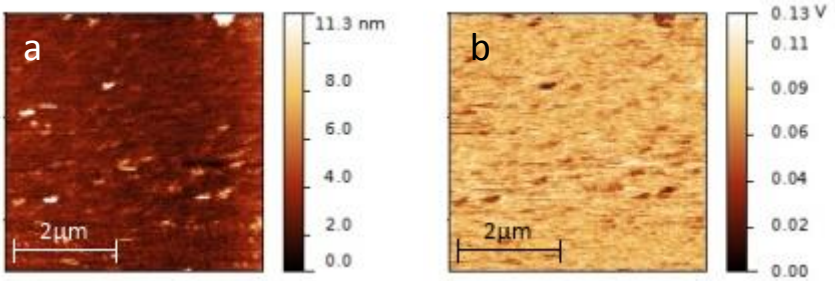

Tip set 1 - Cantilever A

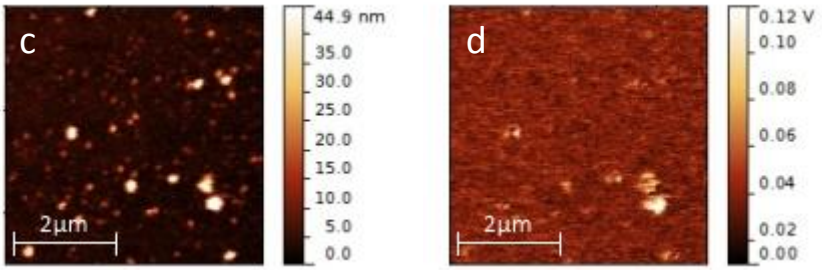

Tip set 2 - Cantilever A

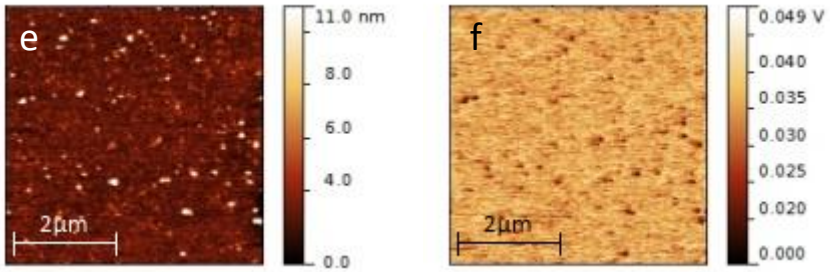

Tip set 3 - Cantilever F

Figure 5.10: Uncalibrated QNM images of height (left column) and adhesion (right column) for different tips. Image d) shows evidence of adhesion.

The tips that showed evidence of specific binding events were calibrated, using the thermal tune process explained in section 3.2.2. Figure 5.11 shows a calibrated adhesion image. The binding force is measured as being 244.5 ± 3.1 pN. The loading rate was estimated using the knowledge of the amplitude (27.82 nm) and the oscillation frequency (227 Hz). This gave a retraction velocity of 12.65 μms^{-1} at 16 nm away from the surface.

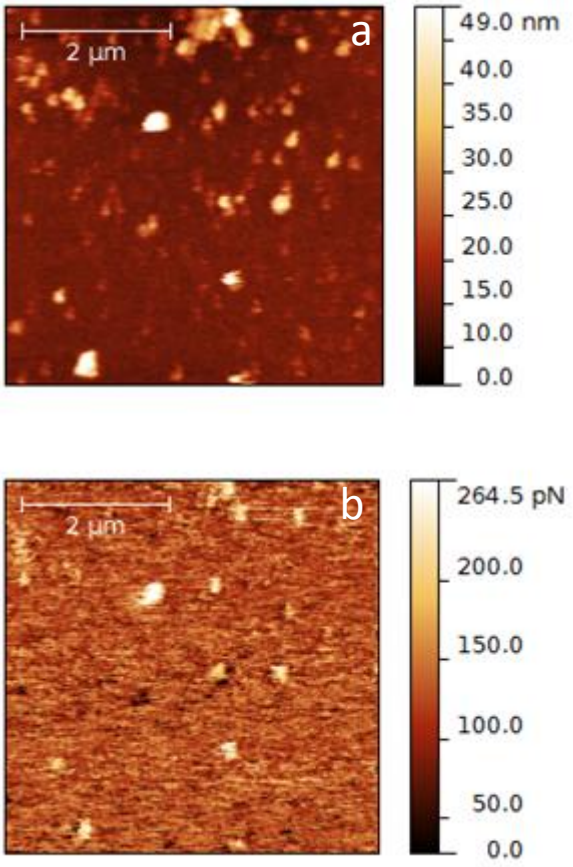

Figure 5.11: Calibrated QNM images of a) topography and b) adhesion. The adhesion images show binding between the biotin and avidin at a loading rate of 55420 pNs^{-1}.

The spring constant was calculated to be 4.381 x 10^{-3} Nm^{-1} which resulted in a loading rate of 55.4 nNs^{-1}. The individual binding force results were extracted

from the adhesion image and can be seen in figure 5.12. As the unbinding process is random a Gaussian distribution of the rupture forces is expected which is what is seen in the histogram.

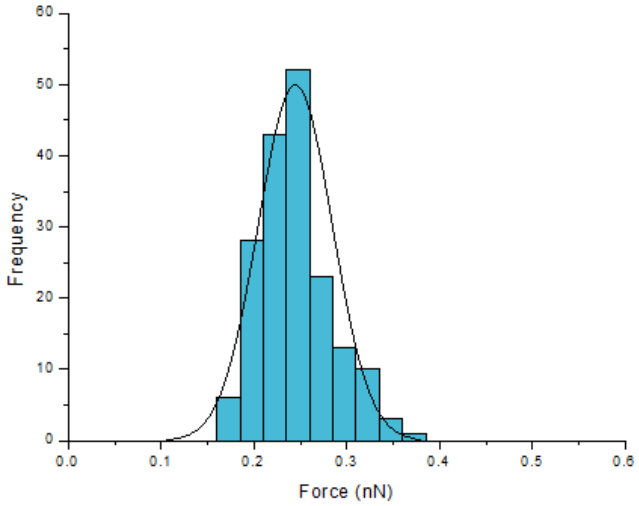

Figure 5.12: Histogram of binding events between avidin and biotin taken with QNM at a loading rate of 55420 pNs^{-1}.

The Nanoscope software allows the capture of an entire line of force curves for offline analysis. This creates a file of many force curves that can be split into the individual force curves and analysis separately. Force curves were captured for images that showed evidence of specific binding events so that they could be analysed in a comparable fashion to the force volume curves. This allowed for a more direct comparison between the two AFM techniques. It was also a good control for specific unbinding events as the force curve could be inspected for the signature shape.

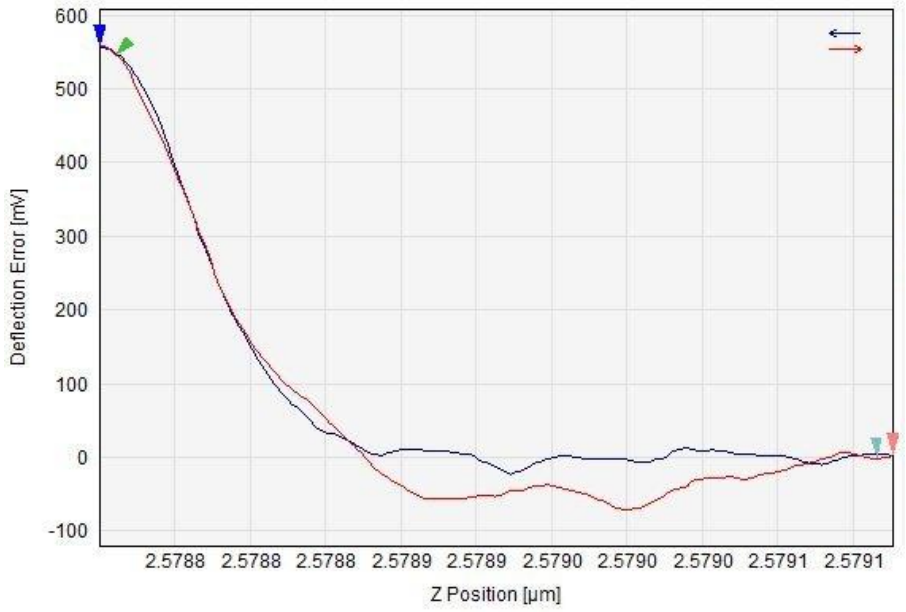

Figure 5.13: An example of a force curve from QNM's high speed data capture feature using a biotin functionalised tip at a loading rate of 55420 pNs^{-1} to image an avidin substrate. Due to the baseline being noisy it is hard to tell the difference between adhesion and noise.

During analysis of these force curves no evidence of specific binding was seen in the shape of the force curves. All curves looked very similar to the shape shown in figure 5.13 which is very noisy. This noise could have been caused by vibrations in the liquid from external sound or thermal energy. The oscillation frequency for the high speed data capture feature is much larger (of the order on kHz) than the 227Hz used for imaging. It is possible that this increase in cantilever speed is the cause of the noise in the force curves.

5.4.2 Force Volume

Alongside QNM experiments force volume images were taken with functionalised tips. Figure 5.14 shows the reconstructed adhesion map taken of

the avidin substrate using SPIP. Calibrated functionalised tips were also used and the force curves captured were analysed. An example of specific and unspecific curves can be seen in figures 5.15a and 5.15b. The binding forces were put into a histogram which can be seen in figure 5.16.

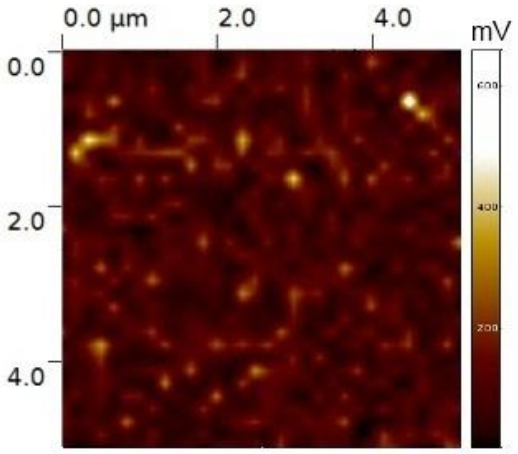

Figure 5.14: Image of adhesion between avidin and biotin created from the force volume curves examples of which can be seen in figure 5.15.

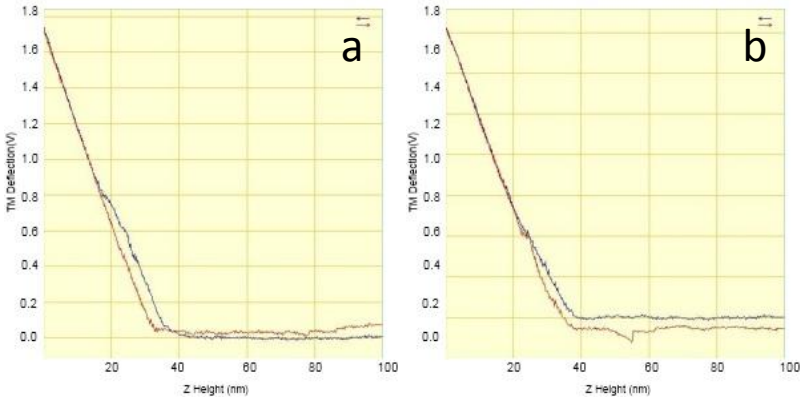

Figure 5.15: a) is similar to the majority of curves and shows no binding between the tip and the surface. b) is an example of an uncorrected curve showing binding between avidin and biotin which is recognisable due to the non-linearity of the adhesion section. Both curves were taken at a loading rate of 1400 pNs^{-1}.

Immediately after capturing the calibrated data, free avidin was introduced into the PBS imaging buffer. This avidin should bind with the biotin on the tip and block the interactions between the avidin on the mica. Specific interactions were identified and measured for this image and put onto the histogram in figure 5.16. This graph shows that the amount of specific interactions when free avidin is introduced is vastly reduced suggesting that the interactions shown in green are due to specific binding between the avidin and biotin.

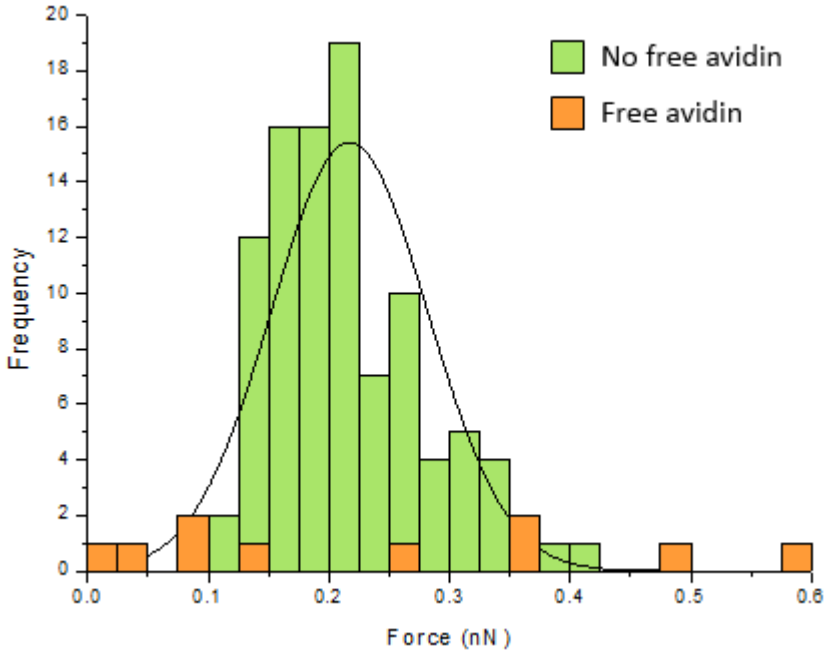

Figure 5.16: Histogram showing the binding force for each specific interaction between avidin and biotin at a loading rate of 1400 pNs^{-1}. The orange bars show data taken when free avidin was introduced into the PBS imaging buffer. There are a lot less interactions due to the blocking from the free avidin.

The loading rate for these images was 1400 pNs^{-1}. The average binding force at this loading rate was found to be 217.0 ± 3.6 pN. The binding probability was

also calculated and summarised in table 5.1. This compares well to Riener *et al*'s measurements [5].

	Results	Literature [5]
No free avidin	0.250 ± 0.109	0.246 ± 0.155
Free avidin	0.027 ± 0.014	0.058 ± 0.031

Table 5.1: Binding probability of avidin-biotin interactions found in this worked compared to those quoted in literature.

5.5 Comparison of QNM and Force Volume Results

The binding forces measured using both AFM techniques were compared with the results measured in literature. A summary of these results can be found in table 5.2. The force volume result at a loading rate of 1400pNs^{-1} compares very well to Odrowaz Piramowicz *et al*'s result of 236.05 ± 4.31pN [17]. Their results for the same loading rate can be seen in figure 5.17.

Loading Rate (pNs^{-1})	Rupture Force (pN)	QNM (pN)	Odrowaz Piramowicz *et al* (pN) [17]
1400	217.0 ± 3.6	-	236.05 ± 4.31
55420	-	244.5 ± 3.1	>550

Table 5.2: Binding forces measured with different AFM techniques compared to results published at similar loading rates.

figure 5.16.

Because QNM is such a fast technique there are no previously published results at such high loading rates for avidin and biotin as force volume cannot achieve the same retraction speeds. However literature suggests that the binding force should be greater than 550pN (figure 5.3). The QNM result presented here is less

than half the magnitude expected from the literature. It is very similar to the result found with force volume despite the loading rate being almost 40 times larger.

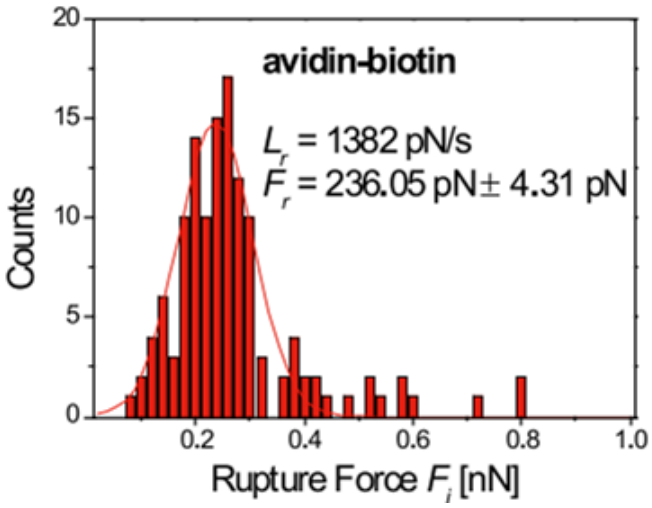

Figure 5.17: Previously published results showing binding force for avidin and biotin at a loading rate of 1382pNs^{-1} [17]. This compares very well with the results shown in figure 5.16.

This could indicate that the loading rate was overestimated and that the true loading rate is closer to 1400 pNs^{-1} or perhaps the speed with which QNM images is not giving the molecules long enough to bind. It is difficult to say exactly how long avidin and biotin take to bind but it may take a significant amount of time that causes QNM to miss the interactions whilst force volume, which is slower, can see them. If the interactions were not occurring it would explain why the QNM curves do not show the specific shape of unbinding events. However it does not explain why the adhesion maps match very well with the topography images. If there was a background interaction of this magnitude it

would likely have been seen on the force volume curves too unless it is something that only occurs at high loading rates.

Another possibility is that there is a problem in QNM's analysis algorithm which has led to an underestimate of the binding force. As the QNM force curves were too noisy to analyse in the same way as the force volume curves it is not possible to know if this is the cause of the discrepancies in results. It is uncertain whether the force curves that QNM analyses in real time to create the adhesion maps are as noisy as those produced using the high speed data capture feature.

Temperature, dissociation rate and other environmental factors can influence the measured binding force but these parameters are never stated in the literature so more investigations are needed at high loading rates before discarding QNM as a quantitative measurement tool for SMRFM.

5.6 Conclusion

The results presented in this chapter show very strong evidence for molecular recognition events between avidin and biotin. In force volume mode the theoretical force curve shape for specific events was observed repeatedly during analysis and the average unbinding force of 217.0 ± 3.6 pN corresponds to the results in the literature (236.05 ± 4.31 pN) well. There was a significant drop in binding probability from 0.25 to 0.027 when free avidin was introduced into the PBS buffer which is highly indicative of the binding between the bound avidin and the biotin on the tip being blocked. This means that the functionalisation chemistry used was suitable and therefore can be adopted for future experiments with CAL B and lipids.

An objective of this work was to see if QNM could be an alternative to force volume mode for single molecule recognition force microscopy. For avidin and biotin it was capable of showing when specific binding occurred. This was because the AFM tip did not stick to avidin as much as it adhered to mica meaning when specific binding took place between the two molecules the adhesion increase was very pronounced.

For quantitative measurements of the unbinding force QNM appears to be inaccurate as it gave a value of 244.5 ± 3.1 pN at a loading rate of 55.4 nNs^{-1} whilst literature suggests the average force should be greater than 550 pN [17].

Because of the unknown accuracy QNM mode is possibly more suited to looking at changes in the relative binding forces due to the conditions of the surroundings than measuring quantitative forces as it is quick and high resolution. For instance it should be very good at showing the sudden drop in an enzyme's ability to bind to its substrate due to an increase in temperature as the adhesion image should show less adhesion with the rise in temperature.

A big consideration with using QNM in this capacity is that the binding force being measured might be very similar to the background adhesion from the flat surface the substrate is immobilised on. This would make it very hard to distinguish between background and specific forces. Combined with the fact that the force curves that QNM can capture are too noisy to see binding signatures if the surface is too adhesive QNM will be an insufficient technique for SMRFM.

Overall QNM is not suitable to substitute force volume AFM for accurate measurements but it is a good supplementary technique that can be used to see

if binding is present before switching to force volume mode to get more quantitative information. This could save the time spent imaging with AFM tips that are not functionalised correctly in force volume mode.

5.7 References

[1] A. R. Bizzarri and S. Cannistraro, "The application of atomic force spectroscopy to the study of biological complexes undergoing a biorecognition process," *Chemical Society Review,* vol. 39, no. 2, pp. 734-749, 2010.

[2] C. Vasilev, A. A. Brindley, J. D. Olsen, R. G. Saer, J. T. Beatty and C. N. Hunter, "Nano-mechanical mapping of the interactions between surface-bound RC-LH1-PufX core complexes and cytochrome c 2 attached to an AFM probe," *Photosynthesis research,* pp. 1-12, 2013.

[3] N. Kresge, R. D. Simoni and R. L. Hill, "The Discovery of Avidin by Esmond E. Snell," *Journal of Biological Chemistry,* vol. 279, no. 41, pp. e5-e5, 2004.

[4] N. M. Green, "Thermodynamics of the Binding of Biotin and Some Analogues by Avidin," *Biochem J.,* vol. 101, pp. 774-780, 1966.

[5] C. K. Riener, C. M. Stroh, A. Ebner, C. Kampfl, A. A. Gall, C. Romanin, Y. L. Lyubchhenko, P. Hinterdorfer and H. J. Gruber, "Simple test system for single molcules recognition force microscopy," *Analytica Chimica Acta,* vol. 479, no. 1, pp. 59-75, 2003.

[6] R. Merkel, P. Nassoy, A. Leung, K. Ritchie and E. Evans, "Energy landscapes of receptor-ligand bonds explored with dynamic force spectroscopy," *Nature,* vol. 387, no. 6714, pp. 50-53, 1999.

[7] Y. S. Lo, N. D. Huefner, W. S. Chan, F. Stevens, J. M. Harris and T. P. Beebe, "Specific interactions between biotin and avidin studied by atomic force microscopy using the Poisson statistical analysis method," *Langmuir,* vol. 15, no. 4, pp. 1373-1382, 1999.

[8] R. De Paris, T. Strunz, K. Oroszlan, H. J. Güntherodt and M. Hegner, "Force spectroscopy and dynamics of the biotin-avidin bond studied by scanning force microscopy," *Single Molecules,* vol. 1, no. 4, pp. 285-290, 2000.

[9] E. L. Florin, V. T. Moy and H. E. Gaub, "Adhesion Forces Between Individual Ligand-Receptor Pairs," *Science,* vol. 264, no. 5157, pp. 415-417, 1994.

[10] Y. S. Lo, Y. J. Zhu and T. P. Beebe, "Loading-rate dependence of individual ligand-receptor bond-rupture forces studied by atomic force microscopy," *Langmuir,* vol. 17, no. 12, pp. 3741-3748, 2001.

[11] A. Ebner, F. Kienberger, G. Kada, C. M. Stroh, M. Geretschläge, A. S. M. Kamruzzahan, L. Wildling, W. T. Johnson, B. Ashcroft, J. Nelson, S. M. Lindsay and H. J. Gruber, "Localization of Single Avidin-Biotin Interactions Using Simultaneous Topogrphy and Molecular Recognition Imaging," *ChemPhysChem,* vol. 6, no. 5, pp. 897-900, 2005.

[12] S. Lee, Chemical functionalization of AFM cantilevers, Massachusettes Institute of Technology, 2005.

[13] A. Ebner, P. Hinterdorfer and H. J. Gruber, "Comparison of different aminofunctionalization strategies for attachment of single antibodies to AFM cantilevers," *Ultramicroscopy,* vol. 107, no. 10, pp. 922-927, 2007.

[14] J. Tang, A. Ebner, H. Badelt-Lichtblau, C. Völlenkle, C. Rankl, B. Kraxberger, M. Leitner, L. Wildling, H. J. Gruber, U. B. Sleytr, N. Ilk and P. Hinterdorfer, "Recognition imaging and highly ordered molecular templating of bacterial s-layer nanoarrays containing affinity-tags," *Nano Letters,* vol. 8, no. 12, pp. 4312-4319, 2008.

[15] D. Alsteens, V. Dupres, K. McEvoy, L. Wildling, H. J. Gruber and Y. F. Dufrênem, "Structure, cell wall elasticity and polysaccharide properties of living yeast cells, as probed by AFM," *Nanotechnology,* vol. 19, no. 38, p. 384005, 2008.

[16] A. Ebner, L. Wildling, A. S. M. Kamruzzahan, C. Rankl, J. Wruss, C. D. Hahn, M. Hölzl, R. Zhu, F. Kienberger, D. Blaas, P. Hinterdorfer and H. J. Gruber, "A new simple method for linking of antibodies to atomic force microscopy tips," *Bioconjugate Chem.,* vol. 18, no. 4, pp. 1176-1184, 2007.

[17] M. de Odrowąż Piramowicz, P. Czuba, M. Targosz, K. Burda and M. Szymoński, "Dynamic force measurements of avidin-biotin and streptavidin-biotin interactions using AFM," *Acta Biochimica Polonica,* vol. 53, no. 1, pp. 93-100, 2006.

[18] C. Yuan, A. Chen, P. Kolb and V. T. Moy, "Energy landscape of streptavidin-biotin complexes measured by atomic force microscopy," *Biochemistry,* vol.

39, no. 33, pp. 10219-10223, 2000.

[19] D. Nečas and P. Klapetek, “Gwyddion - Free SPM data analysis software,” [Online]. Available: http://gwyddion.net/. [Accessed August 2014].

[20] M. Berndt, M. Lorenz, J. Enderlein and S. Diez, “Axial nanometer distances measured by fluorescence lifetime imaging microscopy,” *Nano letters,* vol. 10, no. 4, pp. 1497-1500, 2010.

Chapter 6 - *Candida Antarctica* Lipase B and *Pseudomonas Aeruginosa 3859*

As previously discussed in section 2.4 CAL B is of high interest for low temperature applications in detergents due to it being from a psychrophilic organism [1]. The work in Chapter 5 showed that SMRFM could be deployed successfully with two modes of AFM using the molecules avidin and biotin. The next step towards investigating how temperature affects CAL B's ability to bind to a substrate was to use the knowledge from the avidin and biotin experiments on CAL B itself.

The main objective of this work was to detect specific events between CAL B and its substrate. The lipase PA38659 was studied as a precursor to CAL B to test substrates and binding chemistry whilst the CAL B enzyme was being produced. PA3859 could also be produced in a deactivated form and so provides a useful control molecule.

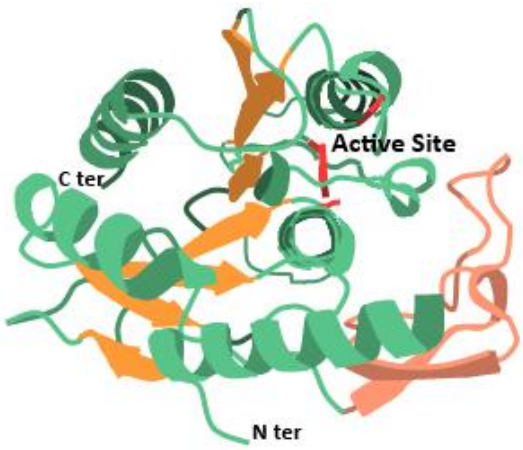

Figure 6.1: Ribbon structure diagram of PA3859 lipase. The active site is coloured red.

PA3859 is an enzyme with a molecular weight of 24.3 kDa and dimensions of approximately 10 x 10 x 7 nm created by the bacterium *Pseudomonas Aeruginosa* which is responsible for causing a number of diseases and infections in humans and other animals [2]. PA3859 is a carboxylesterase and so shares the same substrates as CAL B [3] . One of the defining features of carboxylesterases is that they share very similar properties with each other, especially those which contain an alpha-beta hydrolase fold [2, 4]. This is a standard fold that contains a number of beta sheets connected via alpha helices. Both PA3859 and CAL B contain this tertiary structure and so if a PA3859 system shows specific events then it is highly likely CAL B will show specific events with the same experimental system too. Unlike *Candida Antarctica*, *Pseudomonas Aeruginosa* is not an extremophile and so its enzyme will not work at the low temperatures CAL B should function at.

Both PA3859 and CAL B were used in the experiments carried out in this chapter. Firstly, to perform single molecule experiments with these lipases a number of alterations to the experimental method used to study avidin and biotin were made to account for different substrates and binding chemistry. These alterations were then thoroughly tested to make sure rupture events were still discernible by looking for non-linear adhesion events in the force curves. As with the avidin and biotin experiments free substrate was introduced into the imaging buffer to block interactions and see how that affected the number of binding events detected. It was also unknown how quickly PA3859 and CAL B would bind to their substrate and so the time the tip dwelt on the surface was varied to investigate the number of specific events witnessed as a function of dwell time.

6.1 Challenges and Considerations

6.1.1 Binding chemistry

As chapter 5 showed that the ethanolamine HCL amine chemistry was a suitable system for attaching biotin to silicon nitride tips the same chemistry was utilised for the lipases. Due to the specialised enzymes being used there were no commercially available PEG linkers with the enzymes pre-attached therefore a method was needed to bind the proteins to the PEG tether. In the literature there are a number of ways that proteins have been attached to PEG linkers using a wide variety of chemical bonds [5, 6]. These techniques either expose portions of the amino acids in the proteins or involve genetically engineering reactive groups onto the proteins for binding.

One method of attachment utilises amine bonds. Both the N-terminal of a protein and the amino acid lysine, which is one of the most abundant constituents of proteins, contains NH_2 molecules. NH_2 can be bound to NHS molecules on a PEG tether in the same reaction that bound the NHS-PEG-Biotin tethers to the tip in section 5.2.3 [7]. Another prevalent method of binding is via disulfide bonds. Cysteine, another amino acid found in many proteins, contains a thiol (sulfhydryl) side chain. Usually these side chains create disulfide bonds with other cysteine molecules in the protein's tertiary structure [7, 8]. Reducing agents can be used to break the disulfide bonds exposing the thiols such that they can bind to molecules including pyridyldithio propionate (PDP) or maleimide (MAL). NHS-PEG-NHS, NHS-PEG-PDP and NHS-PEG-MAL tethers are all

easily available in a variety of lengths so both the amine and thiol methods could be used.

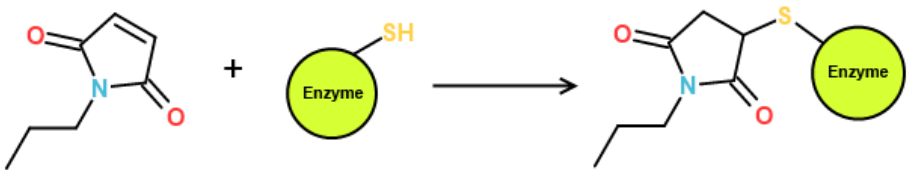

Figure 6.2: Process of attaching a malemide to a thiol on the enzyme's surface via disulfide bonds. In this diagram the PEG tether is not fully shown.

Due to the overabundance of lysine in proteins the binding location of the PEG tether is not specific and so could be too close to the active site which could limit the protein's activity. Finally with an NHS-PEG-NHS it is possible for the lower NHS molecule to bind to the tip as well as the upper one which creates loops of PEG tether on the tip surface and blocks some of the sites the enzymes could bind to. For these reasons it was decided that the enzymes would be attached to the PEG tethers via disulfide bonds. Maleimide was chosen over PDP as it is a faster reaction allowing a lower protein concentration to be used. The MAL-thiol bond is also irreversible so it cannot be broken unlike the PDP-thiol bond which can [9]. This is important as if the bond was reversed during imaging then the AFM tip would no longer be functionalised with the enzyme and specific events would cease to be observed.

6.1.2 Substrates

For the two enzymes a carboxylic ester substrate needed to be attached onto a flat surface for imaging. Due to its low surface roughness and ability to be easily

cleaved mica was the desired surface for this research. A number of experiments have shown that carboxylic acids can be immobilised onto a mica surface [10, 11]. With this knowledge the substrate ±-2-acetoxypropionic acid (APA) was chosen as it is an ester as well as a carboxylic acid. The two enzymes can hydrolyse this molecule and produce an acid and an alcohol as seen in figure 6.3.

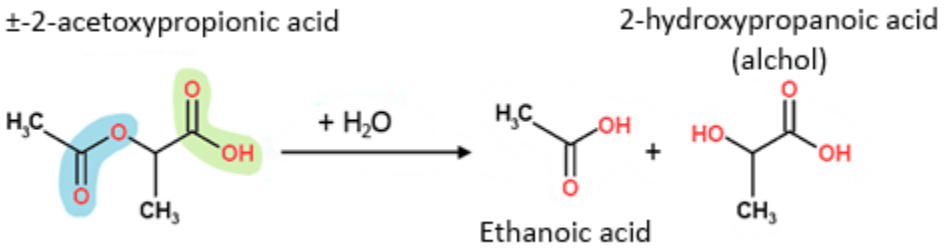

Figure 6.3: Structure of ±-2-acetoxypropionic acid and the hydrolysis process the enzymes catalyse. The blue section of the substrate is the ester and the green section is the carboxylic acid portion of the molecule.

6.1.3 AFM Technique

Based on the results from the previous chapter, it was decided that all CAL B and PA3859 experiments would be carried out using force volume AFM. The reason for this was that due to force volume's stable force curves it would be possible to study the shape of curves and therefore be certain that specific unbinding events being observed.

Force volume has the ability to set a dwell time for the tip on the surface which was important as it was unknown how long the enzymes would take to bind to the substrate. If the tip was withdrawn too quickly the molecules may not have enough time to bind and therefore no events would be seen. By varying the

dwell time of the tip it was possible to see how the number of specific events changed.

However this may negatively affect the results if the dwell time is longer than the natural binding time of the molecules as interactions will be missed. It could also reduce the values of the force measurements if non-stimulated unbinding occurs whilst the tip is in the process of retracting from the surface. This will cause it to measure a lower force but can be looked for as the curve would have less of a distinct unbinding shape as the tether would not be stretched fully.

6.2 Experimental Method

6.2.1 Binding Chemistry

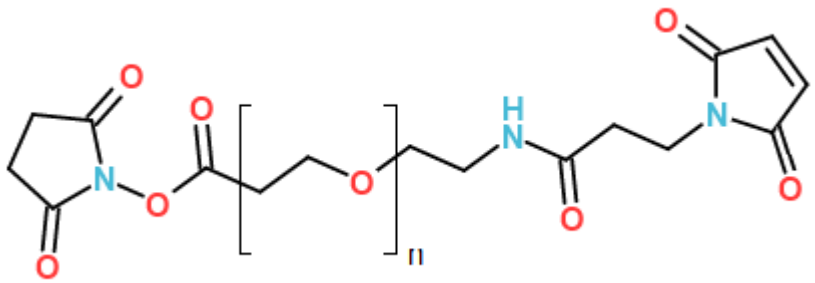

Figure 6.4: NHS-PEG-Mal tether. n was chosen to be 24 which gave a 9.52nm linker length.

NHS-PEG-MAL tethers were acquired from Thermo Scientific with length 9.52 nm. Extra cysteine sites were engineered onto both CAL B and PA3859 to make sure there were some cysteine present on the surface. This was carried out by colleagues from the University of Glasgow who also checked that the enzyme activity was unaffected by the added amino acids. They then used the reducing

agent TCEP.HCL (Tris(2-carboxyethyl)phosphine hydrochloride) to break the disulfide bridges.

MCLT AFM tips were functionalised using the same method set out in section 5.2.3. After the NHS end of the PEG tether was attached to the tips they were left in the enzyme solution for three hours to give time for the thiol groups on the enzymes to bind to the maleimide. After washing the tips with deionised water they were ready to be used for imaging.

6.2.2 Substrates

Substrate samples were prepared by creating a solution of ±-2-acetoxypropionic acid in chloroform. Freshly cleaved mica was immersed in 25 µL of the solution for 30 seconds before being left to dry under nitrogen for 2 minutes as described in Benitez et al's paper [11]. It was unknown what concentration of APA would give the best coverage on the mica surface so solutions of 1.5 mM, 5 mM and 15 mM were created and imaged. The results of this test can be found below

6.2.3 Temperature

As future experiments aim to see how CAL B is affected by environmental temperatures the room temperature was recorded during all the data collection in this chapter. It was found that the average temperature was 23^{o}C which is substantially above CAL B's proposed optimum temperature of 0^{o}C.

6.3 Results - Acetoxypropionic Acid Substrate

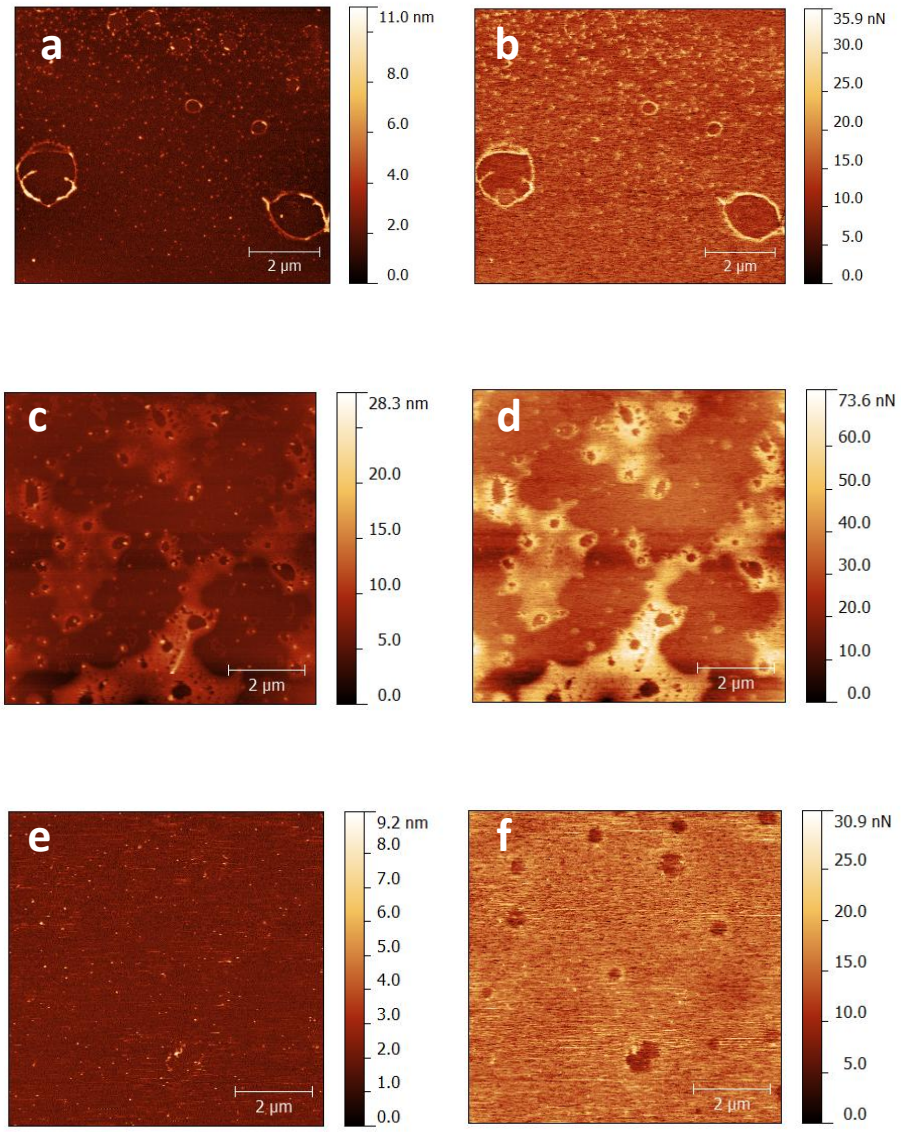

Figure 6.5: QNM height (left column) and adhesion (right column) images of APA on mica at concentrations of a) 1.5mM, c) 5mM and e) 15mM in chloroform. Taken at room temperature.

The three different APA concentrations substrates were prepared and then imaged straight away with QNM AFM in air to investigate distribution of the substrate on the mica surface. A tapping 105 tip was used throughout imaging.

Figure 6.5 shows the topography and adhesion images for all three concentrations.

The topography images show a small number of features on the mica for 1.5 mM APA (figure 6.5a), a fairly large coverage for 5 mM APA (figure 6.5c) and then very few features for 15 mM (figure 6.5e). However when the adhesion images are studied the amount of APA on the surface appears to increase with concentration as expected. In the 15 mM APA adhesion image (figure 6.5f) there are a few holes in the surface layer which could be incomplete coverage of APA on the mica. This suggests that the coverage of APA is fairly uniform and thin and therefore there are no visible features in the topography image.

6.3.1 Control Images

Images of freshly cleaved mica both on its own and immersed in chloroform for 30 seconds and dried in nitrogen were captured as controls which can be seen in figure 6.6. The plain mica images show a very uniform and flat surface. The images of mica treated with only chloroform shows a large number of small features on the surface of the mica. These features are also present in the 1.5 mM and 5 mM APA solutions and appear to account for most of the features present in the 1.5 mM APA substrate. The 15mM images do not show much evidence of these features both in the height and adhesion images which is beneficial as it removes a layer of background adhesion.

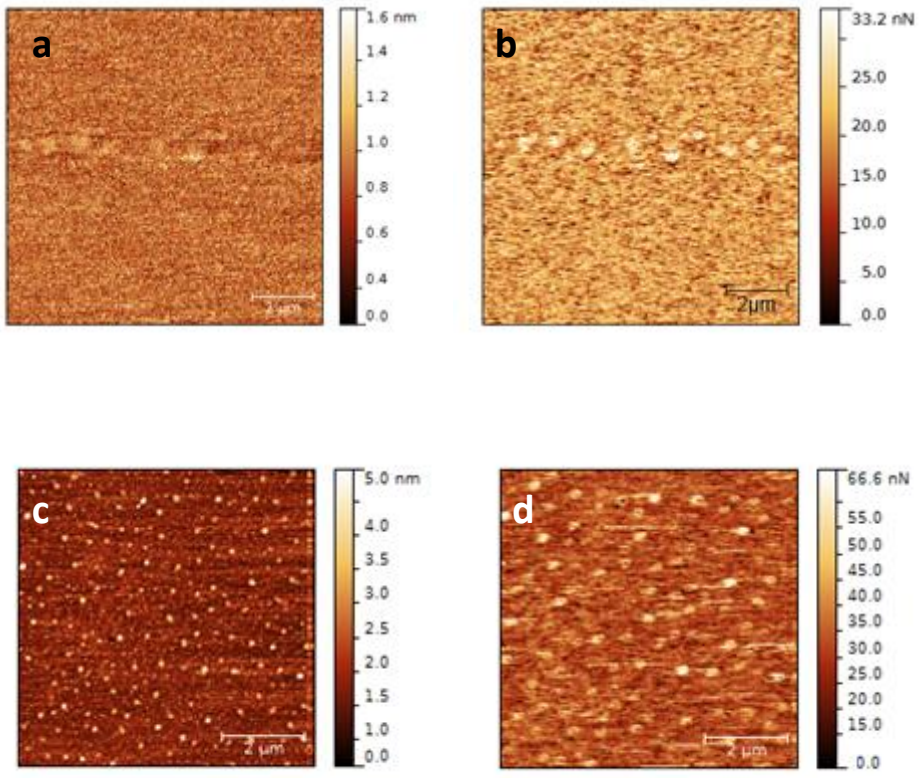

Figure 6.6: QNM height (left column) and adhesion (right column) of a) plain mica and c) mica left in chloroform for 30 seconds and dried in nitrogen at room temperature.

Both 5 mM and 15 mM APA substrates show suitable coverage for force spectroscopy measurements but it was decided that 15 mM would be the concentration used as the coverage was more complete and the adhesion from the chloroform residue was not present.

For all concentrations of APA the adhesion measured in each image is approximately 30 pN. If any specific events have unbinding forces near 30 pN then it is possible that they are background events incorrectly selected as specific events.

6.4 Results – Control Experiments

Before imaging with the two enzymes a number of control experiments were carried out to ensure there were no large sources of background events. This involved taking a number of 32 x 32 pixel force volume images with tips at various steps in the functionalisation process and measuring the binding probability. The different tips used were: plain tips, ones that had only been through the amino functionalisation stage with ethanolamine HCL and tips with only the NHS-PEG-MAL tethers attached to it. These were used to image both the plain mica and the APA substrate. The results presented in table 6.1 show that the binding probability is very low for all controls as expected and therefore there is no large source of background events.

	Binding Probability	
	No APA	**APA**
Plain Tip	0.0107 ± 0.0098	0.0093 ±0.0076
Ethanolamine HCL	0.0081 ± 0.0051	0.0024 ± 0.0009
PEG	0.0023 ± 0.0012	0.0071 ± 0.0065

Table 6.1: Summary of the binding probabilities for tips with different coatings on both plain mica and the APA substrate.

6.5 Results - PA3859

PA3859 was attached to the tip as described previously and used to image the APA substrate. The loading rate was set at to be 1400 pNs^{-1} and nine 32 x 32 pixel images were collected at varying dwell times. PA3859 has a size of ~10 nm so with a PEG linker of 9.52 nm features up to 19.5 nm away from the contact point were accepted. The unbinding forces and the binding probabilities have

been summarised in figure 6.8. All dwell times gave evidence of specific unbinding curves, an example of which can be seen in figure 6.7 and the binding probabilities are all greater than the maximum background levels of 0.0107 ± 0.0098 as seen in figure 6.8b.

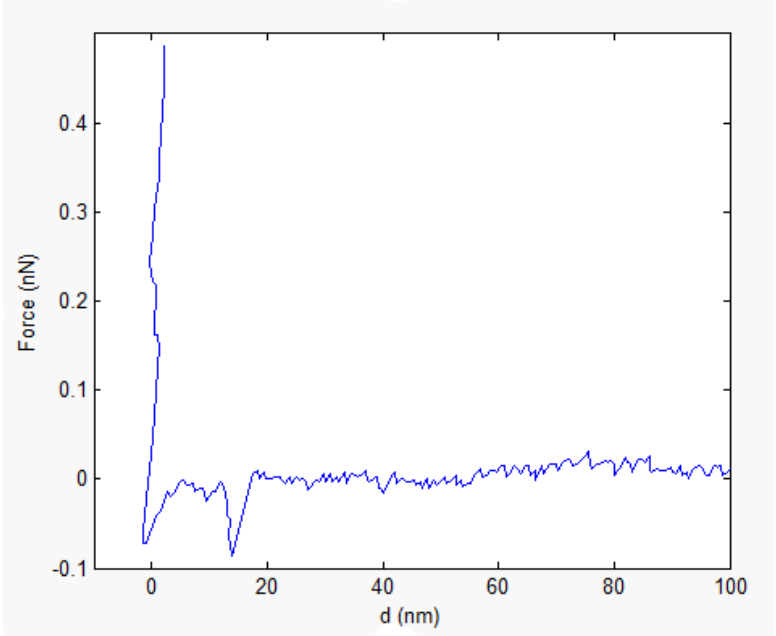

Figure 6.7: Specific PA3859 event at a dwell time of 250ms. Non-specific adhesion can be seen at d=0 nm and the specific adhesion of the binding event starts at 16nm giving an unbinding force in the region of 900pN. This image was taken at a loading rate of 1400 pNs^{-1} and at room temperature.

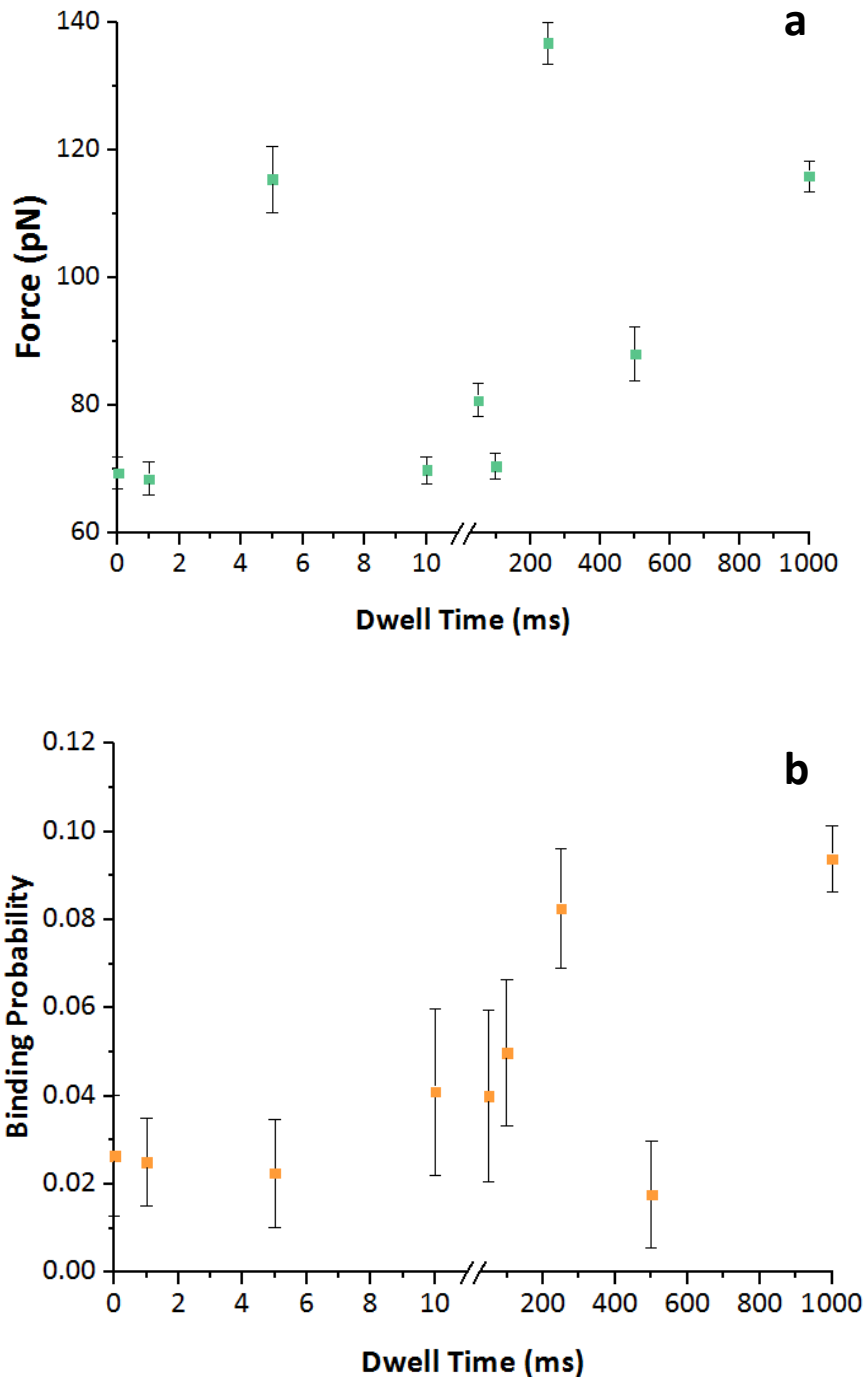

Figure 6.8: Dwell time versus a) unbinding force and b) binding probability for PA3859 at a loading rate of 1400 pNs^{-1}. 1000 ms was found to give the highest number of specific force curves.

The measured binding probabilities do increase with dwell time as expected with the exception of 500 ms dwell time. This was a very noisy force volume image and so is very likely to be an anomalous result caused by external acoustic noise. 250 ms and 1000 ms both show a large binding probability. The measured unbinding forces are quite disparate, ranging from 60-140 pN. This could be due to 32 x 32 pixels being a small sample size. Experiments with CAL B will use a greater sample size to measure unbinding forces.

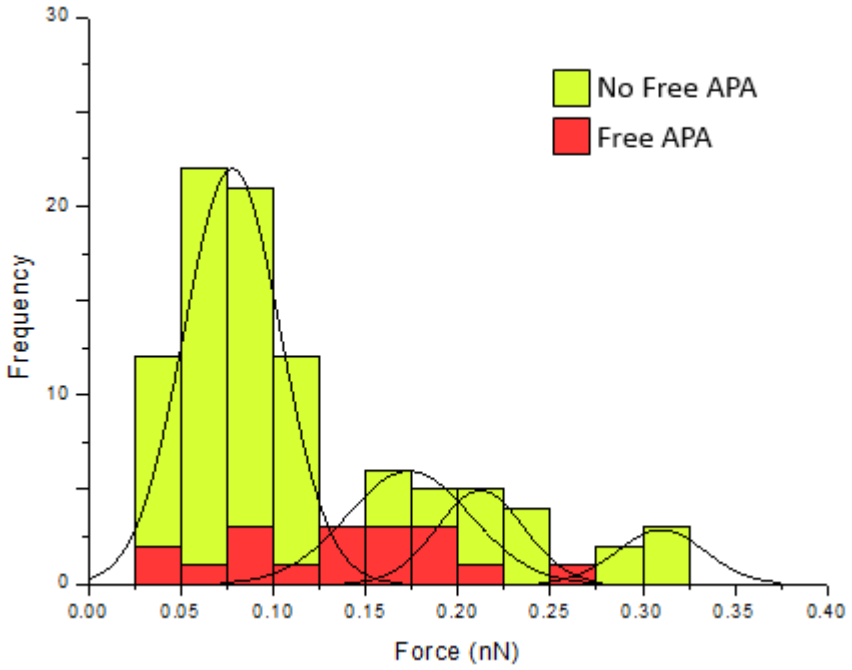

Figure 6.9: Histogram showing unbinding forces measured for PA3859 at a tip dwell time of 1 second at room temperature and loading rate of 1400 pNs^{-1} with both free and no free APA. Free APA reduces the number of vents significantly.

The data for 1000 ms is presented in the histogram in figure 6.9. It provides an explanation for the discrepancies between the measured rupture forces. The histogram shows four peaks centred on 77.7 ± 26.1 pN, 173.3 ± 33.4 pN, 212.3 ±

23.4 pN and 309.9 ± 23.7 pN. This could be due to the number of enzyme molecules that are binding in each force curve. It is known that multiple bonds dissociating at the same time will produce rupture forces that are integer values of the force for a single bond [12, 13]. In the results for 1000 ms the single bond rupture force is 78 pN which means two, three and four bonds should give measured values of 156 pN, 234 pN and 312 pN respectively which are all very similar to the centres of the corresponding peaks. It is progressively less likely to get a larger number of bonds which is reflected in the decreasing height of the peaks.

An unbinding force value of 78 pN corresponds very well with the majority of unbinding forces for shorter dwell times which only have one peak when presented as a histogram. The dwell times of 5 ms and 250 ms which both state rupture forces of over 100 pN are the only other histograms that show evidence of multiple bond peaks. Both data sets have their primary peak centred between 70-80 pN meaning that all of the results correspond very well and are not as diverse as they initially appear. Using the data for the first peak for all data sets the average rupture force for PA3859 at a loading rate of 1400 pNs^{-1} is 75.0 ± 6.7 pN.

6.5.1 Deactivated PA3859 and Free APA

	Binding Probability
Activated PA3859	0.0938 ± 0.0276
Deactivated PA3859	0.0095 ± 0.0029
Activated PA3859 with free APA	0.0107 ± 0.0012

Table 6.2: Binding probabilities for activated, deactivated and free APA single molecule force experiments at a dwell time of 1000 ms. The number of rupture events is much greater for activated, uninhibited PA3859 as predicted

After carrying out the dwell time experiments a number of controls were taken. It was possible to get a deactivated version of PA3859 that still had the engineered cysteine molecules on the surface to attach it to the PEG tether. By doing the same experiment with a 1000 ms dwell time with the deactivated lipase and looking at the binding probability it was possible to see if the observed events were due to PA3859's active site binding to the substrate or interactions between another part of the enzyme and the substrate. Free APA was also introduced into the PBS imaging buffer when using the activated version of PA3859 to block the enzyme-immobilised substrate interactions as free avidin did when looking at the avidin-biotin system.

Both of the control experiments above reduce the binding probability down to values similar to the control experiments carried out in section 6.3.1 which are just background noise events that look similar to specific events and so are incorrectly analysed. The binding data for free APA is included in figure 6.9. It shows that the number of specific events vastly reduces when free APA is

introduced leading to the conclusion that specific interactions between the enzyme and its substrate are being observed in the data featured in figure 6.9.

6.6 Results - CAL B

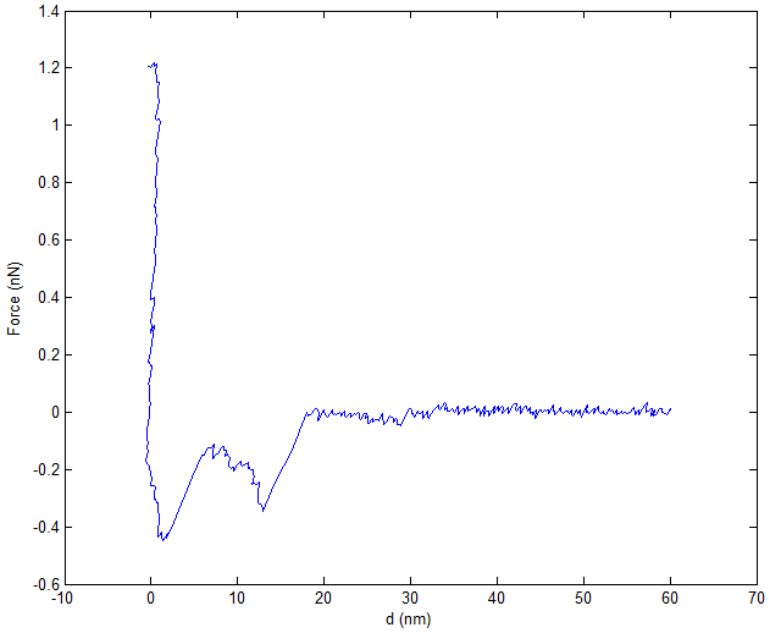

Figure 6.10: Specific event between CAL B and APA at a tip dwell time of 100ms, a loading rate of 1400 pNs^{-1} and at a room temperature of 23°C. Unspecific adhesion occurs at 0 nm and specific binding occurs at 12 nm giving an unbinding force of approximately 350 pN.

CAL B was attached to the PEG tether and similar experiments were repeated with the extremophile enzyme. The force volume images contained 64 x 64 pixels instead of 32 x 32 pixels which gave four times as many force curves to analyse. It was hoped this would increase the accuracy of the measured unbinding forces. The dwell time was varied and as with PA3859 all dwell times

showed evidence of specific events as shown in figure 6.10. CAL B is 3 x 5 x 4 nm in size so features located up to 15 nm were accepted.

The unbinding forces and binding probabilities are summarised in figure 6.11 and it can be seen that the peak in binding probability occurs at a 100 ms dwell time before the probability started to decrease. This could be due to one or more binding cycles being completed before the tip starts to retract. Completed hydrolysis means that there is less substrate available for the enzyme to bind to and therefore less specific events are observed at dwell times greater than the binding time which is close to 100 ms.

The graph in figure 6.11a also show that the rupture forces measured for each dwell time are fairly consistent with each other which is what was expected with the increase in sample size. 64 x 64 pixel images give four times the sample size than the 32 x 32 pixel images used for PA3859 which improves the statistics of the data.

The data for 100 ms is displayed in figure 6.12. Unlike PA3859 there is no evidence of multiple bonds in the data for any of the dwell times. This means the slight inconsistency in the measured unbinding forces for 0 ms, 5 ms and 500 ms are likely to be caused by the small number of specific events that were available for analysis. Discarding the anomalous results gives an average rupture force of 152.3 ± 5.3 pN for CAL B at a loading rate of 1400 pNs^{-1}.

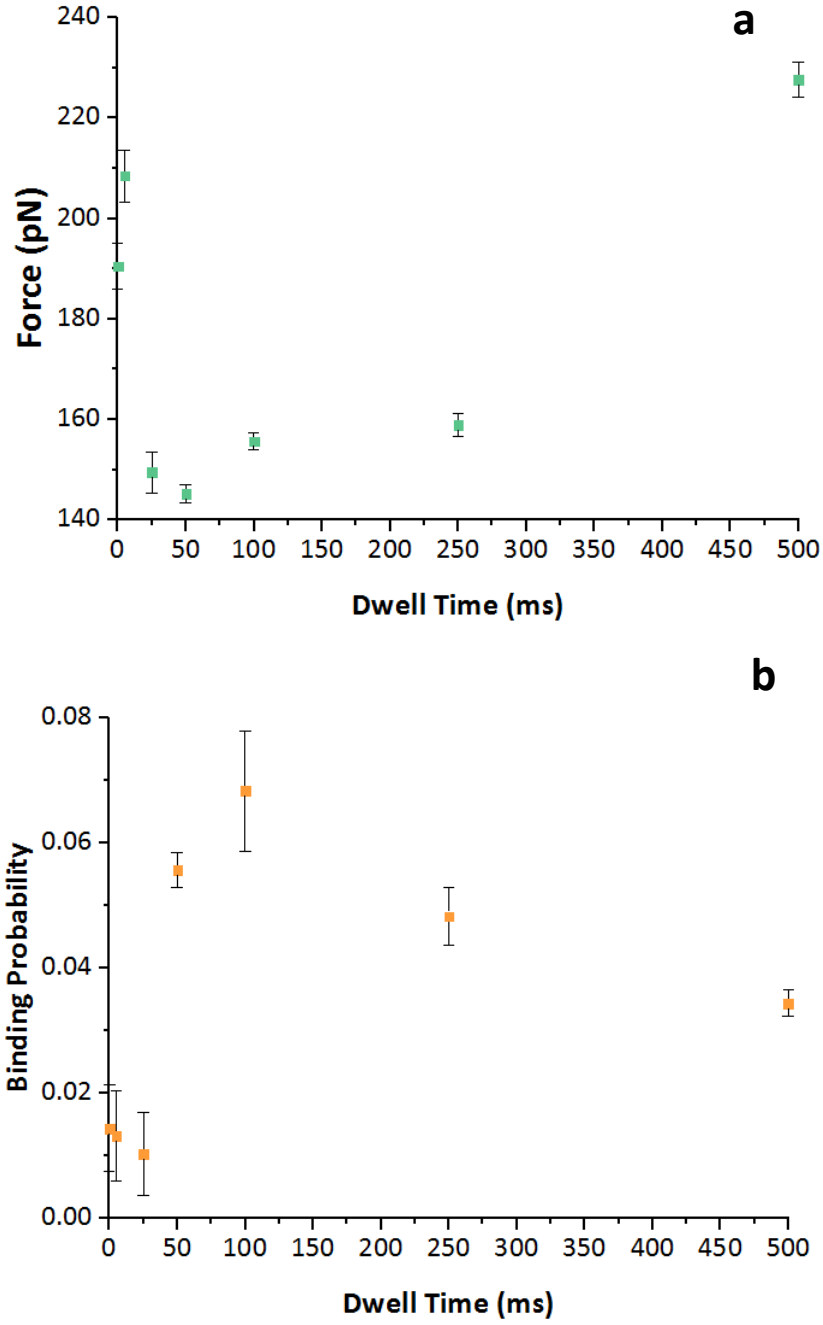

Figure 6.11: Dwell time versus a) unbinding force and b) binding probability for CAL B at a loading rate of 1400 pNs^{-1}. 100 ms was found to give the highest number of force curves.

6.6.1 Free APA

The next step was to introduce free APA into the imaging buffer to block the interactions. As shown in table 6.3 and figure 6.12 the number of specific events dropped significantly when the substrate was present in the buffer signalling that specific events were being seen for CAL B.

	Binding Probability
No free APA	0.0684 ± 0.096
Free APA	0.0093 ± 0.0024

Table 6.3: Binding probabilities for activated and free APA single molecule force experiments at a dwell time of 100 ms.

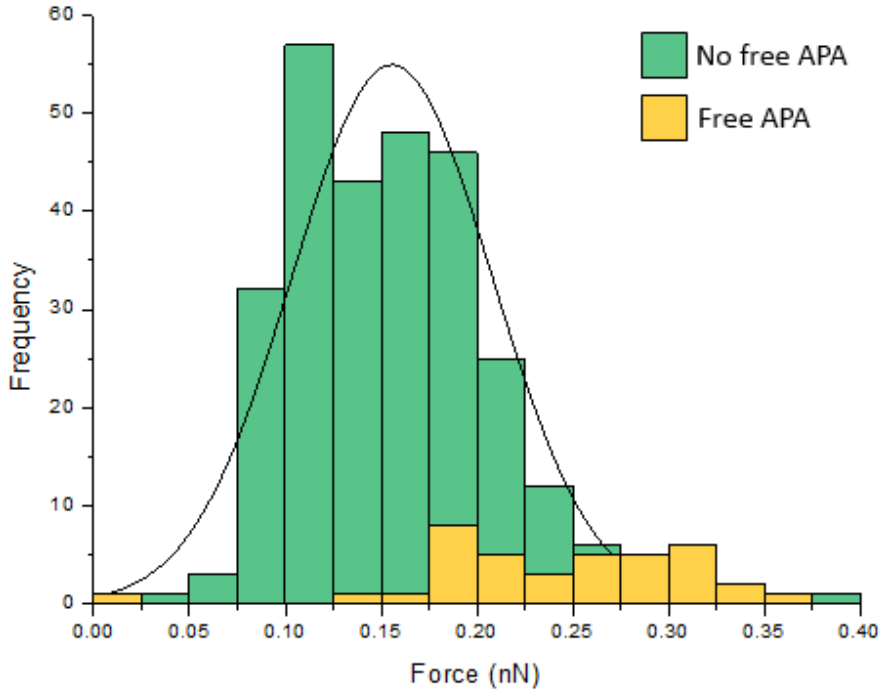

Figure 6.12: Histogram showing rupture forces measured for CAL B at a tip dwell time of 100ms, a loading rate of 1400 pNs^{-1} and at room temperature with both free and no free APA. Free APA reduces the number of events significantly.

6.7 Conclusion

The objective of this chapter was to successfully observe single molecule unbinding events between APA and both the PA3859 and CAL B lipases. Both enzymes were imaged at a range of tip dwell times, from 0 ms to 1000 ms, to see which produced the highest number of specific events. For PA3859 the best dwell times was 1000 ms, with a binding probability of 0.0938 ± 0.0276 whilst for CAL B 100 ms proved to be the most effective leading to a binding probability of 0.0684 ± 0.0096.

Average unbinding forces were measured for both proteins at all dwell times and for CAL B the forces were reasonably uniform with the majority of forces being in the region of 150 pN. This was not the case with the PA3859 measurements. It was initially thought to be due to a small sample size but, through looking at the histograms of the inconsistent results, it appears to be due to multiple binding events giving large unbinding forces which alter the average unbinding forces in figure 6.8a. By fitting multiple peaks to the data in figure 6.9 the new average rupture force for a single event becomes 78 pN which is consistent with other values.

Control experiments were carried out to measure the background level of 'unbinding events' when no enzyme was present. Both enzymes showed a significant decrease in binding probability to levels similar to the background level (0.0093 ± 0.0024 for CAL B and 0.0107 ± 0.0012 for PA3859) when free APA substrate was introduced into the imaging buffer. This presents good evidence that the events witnessed are due to binding between the enzyme's active site

and the substrate. Deactivated PA3859 was also used to demonstrate this further by reducing the binding probability from 0.0938 ± 0.0276 to 0.0095 ± 0.0029.

With the results presented in this chapter work could now start on measuring the temperature dependence of SMRFM experiments with CAL B to determine the effects on the binding.

6.8 References

[1] B. Joseph, P. W. Ramteke, G. Thomas and N. Shrivastava, "Standard Review Cold-active microbial Lipases: a versitile tool for industrial applications," *Biotechnology and Molecular Biology Review,* vol. 63, no. 6, pp. 39-48, 2007.

[2] A. Pesaresi and D. Lamba, "Crystallization, X-ray diffraction analysis and phasing of carboxylesterase PA3859 from Pseudomonas Aeruginosa," *Biochimica et Biophysica Acta (BBA)-Proteins and Proteomics,* vol. 1752, no. 2, pp. 197-201, 2005.

[3] A. Pesaresi and D. Lamba, "Insights into the fatty acid chain length specificity of the carboxylesterase PA3859 from Psudomonas Aeruginosa: A combined structural, biochemical and computational study," *Biochimie,* vol. 92, no. 12, pp. 1787-1792, 2010.

[4] D. L. Ollis, E. Cheah, M. Cygler, B. Dijkstra, F. Frolow, S. M. Franken, M. Harel, S. J. Remington, S. I. J. Schrag, J. L. Sussman, K. H. G. Verschueren and A. Goldman, "The α/β hydrolase fold," *Protein Engineering ,* vol. 5, no. 3, pp. 197-211, 1992.

[5] A. Berquand and B. Ohler, Common Approaches to Tip Functionalization for AFM-Based Molecular Recognition Measurements, Bruker Nano Surfaces Business, 2010.

[6] M. J. Roberts, M. D. Bentley and J. M. Harris, "Chemistry for peptide and protein PEGylation," *Advanced drug delivery reviews,* vol. 54, no. 4, pp. 459-476, 2002.

[7] L. Wildling, B. Unterauer, R. Zhu, A. Rupprecht, T. Haselgrübler, C. Rankl, A. Ebner, D. Vater, P. Pollheimer, E. E. Pohl, P. Hinterdorger and H. J. Gruber,

"Linking of sensor moelcules with amino groups to amino functionalized AFM tips," *Bioconjugate chemistry ,* vol. 22, no. 6, pp. 1239-1248, 2011.

[8] D. Haywork, "Sulfhydryl-reactive Crosslinker Chemistry," Thermo Scientific, 2014.

[9] D. Sinwel, M. Rangl, D. Höglinger, A. Scherfler, R. Zhu, E. Pohl, R. Tampé, A. Ebner, P. Hinterdorfer and H. J. Gruber, "Functionalization of AFM tips with native proteins or His6-tagged proteins," in *Linz Winter Workshop*, 2012.

[10] J. Chen, A. R. Murphy, J. Esteve, D. F. Ogletree, M. Salmeron and J. M. Fréchet, "Preparation and nanoscale mechanical properties of self-assembled carboxylic acid functionalized pentathiophene on mica," *Langmuir,* vol. 20, no. 18, pp. 7703-7710, 2004.

[11] J. J. Benítez, J. A. Heredia-Guerrero and A. Heredia, "Self-assembly of carboxylic acids and hydroxyl derivatives on mica. A qualitative AFM study," *The Journal of Physical Chemistry C,* vol. 111, no. 26, pp. 9465-9470, 2007.

[12] X. Zhang and V. T. Moy, "Cooperative adhesion of ligand-recptor bonds," *Biophysical chemistry,* vol. 104, no. 1, pp. 271-278, 2003.

[13] E. Evans, "Probing the relation between force lifetime and chemistry in single molecular bonds," *Annual review biophysics and biomolecular structure,* vol. 30, no. 1, pp. 105-128, 2001.

Chapter 7 – *Candida Antarctica* Lipase B Temperature Variation

After demonstrating that CAL B could be used for single molecule recognition force measurements in Chapter 6 the final phase of this project was to vary the temperature to investigate how CAL B functions in unheated water. The average temperature for household cold water in the UK is 7.3^{o}C so it was decided to see how the lipase would work in similar conditions for use in ambient temperature washing processes [1]. As previously stated CAL B has an optimum temperature close to 0^{o}C but from experiments carried out in the previous chapter it is known that it works at temperatures close to 23^{o}C [2].

To carry out these cold environment experiments the AFM imaging area needed to be cooled. There are a number of heating stages commercially available for the Bruker Catalyst AFM but there are no cooling stages. This meant that a custom-built cooler was required which introduced a number of difficulties.

A thermoelectric cooler (TEC) was used as the main cooling element as they can reach sub-zero temperatures so would be able to easily reach 0-20^{o}C temperatures of interest here. TECs operate based on the principles of the Peltier effect. The Peltier effect states that if a current is passed through a junction between two dissimilar materials a temperature difference is created [3, 4]. TECs are not as efficient as some cooling devices but they have the major benefits of being inexpensive, straightforward to control and simple to install [5].

They are also small which is an important requirement as the gap between the AFM scanning head and the X-Y stage is only a centimetre.

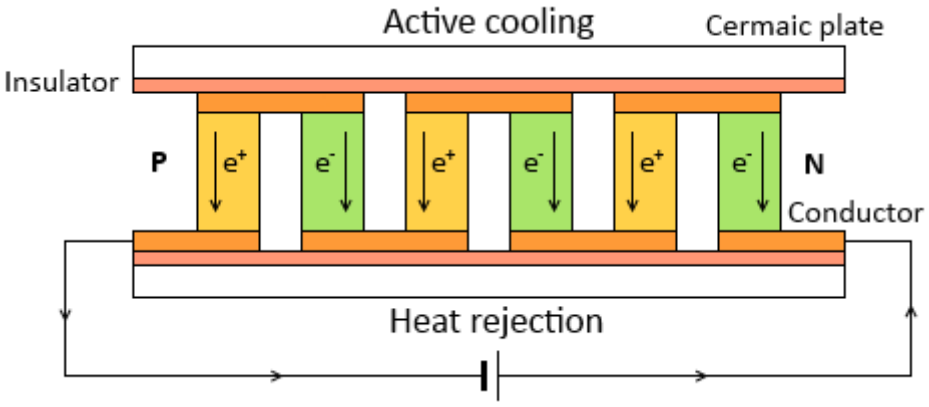

Figure 7.1: Schematic of the workings of a thermoelectric cooler.

TECs mainly comprise of semiconductors which are doped to make p-type and n-type materials. A circuit is set up of junctions between the two semiconductors connected in series. When a current is passed through a n-to-p junction the prevailing carriers in the two materials move away from the junction and take away heat as demonstrated in figure 7.1. The reverse happens at p-to-n junctions. This creates one cold side of the TEC and one warm side [5].

This chapter discusses the development of the cooling system and its application in rupture force measurements for CAL B on APA where the binding probability and unbinding force were measured at a range of temperatures to see how they were affected. It was decided that the enzyme would be examined at temperatures of 30^{o}C (using a commercial heating stage), 7^{o}C and temperatures in between to see how the activity of CAL B changed from current commercial washing temperatures to the target washing temperature for the UK.

It was predicted that at temperatures near 7°C the activity of CAL B should be higher, which would be reflected in the measured binding probabilities, and continue to improve as temperatures were reduced to 0°C. The optimum binding probability found in Chapter 6 at a temperature of 23°C 0.0684 ± 0.0096 so it is expected that the cooler temperatures will have larger binding probabilities. The measured rupture forces should also be consistent with the average result found in Chapter 6 of 152.3 ± 5.3 pN.

It was desirable to investigate how CAL B's activity changed at temperatures below 7°C as current literature on the enzyme only investigates two temperatures: 0°C and 40°C and simulations have investigated 5°C, 35°C and 50°C [6, 7]. Sub-zero temperatures were not looked at as this would require an imaging buffer that would not freeze below 0°C which was not possible without adding large amounts of salt to the PBS buffer. Salinity is a parameter that can affect and denature a protein so it is possible at these higher salt concentrations that CAL B will be unable to bind to the APA [8].

7.1 Challenges and Considerations

7.1.1 Cooling system

As discussed a cooling system needed to be created which was based on a TEC. Because TECs act as heat pumps they eject a large amount of heat which has to be removed. To do this a secondary cooler was required. The size of this secondary cooler needed to be relatively small. The area underneath the AFM scanning head is 35 x 35 x 10.5 mm so the entire cooling mechanism needed to

fit within this space. It was decided that a copper block would be placed under the TEC. The copper block contained a pipe through which cool water was passed. The heat from the TEC was then conducted through the copper and into the water which removed it away from the imaging area.

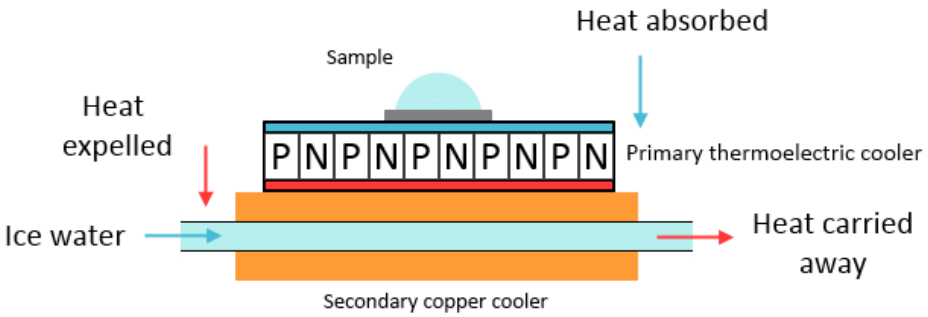

Figure 7.2: Schematic of the complete cooling system used to image at low temperatures.

7.2 Experimental Method

Functionalisation of tips with CAL B and the preparation of APA substrates were carried out using the same method set out in Chapter 6.

7.2.1 Cooling System

A TEC was purchased from FerroTec with dimensions of the TEC were 30 x 30 x 2.5 mm which meant that the copper block needed to be thinner than 8 mm. This was created and then adhered to the hot side of the TEC using thermally conductive paste to aid heat transfer.

The TEC was wired to a current generator purchased from VoltCraft which ranged from 0 to 5.8 A. A K-type thermocouple from

Farnell was immersed in the imaging solution and connected to a National Instruments Multifunction DAQ system. A LabVIEW program was created to sample the temperature of the buffer every 2 seconds and take an average. At the start of every AFM image the program was re-initialised so the temperature was measured only over the imaging time.

7.2.2. Heating Stage

For the warmer than room temperature conditions a heating stage for the Catalyst AFM was purchased from Bruker which replaced the usual sample holder on the X-Y scanning stage. This was connected to a temperature controller supplied by Veeco Instruments that allowed the desired temperature to be input. Two glass slides were put between the heating stage and the sample to damp vibrations from the stage which meant that setting the temperature directly with the controller became difficult and required the use of the thermocouple to know the exact conditions.

7.3 Results – Cooling System and Imaging Buffer

The first challenge to implementing the cooling system for SMRFM was to ascertain if the low temperatures could be reached whilst still producing high quality AFM images and force curves. There were a number of new sources of noise introduced by the cooling system which could affect the AFM images. Vibrations through the thermocouple could introduce movement in the imaging buffer which would create noise in the final image similar to that shown in figure 3.3. Water was passing through the copper block on which the sample was

placed potentially causing further vibrations and the current generator and TEC could be a source of electrical noise. Contact images and force curves of a sapphire sample were taken at three temperatures: 20°C, 7°C and 4°C using unfunctionalised tips to see if image noise was present.

During this experiment a number of issues became apparent when the temperature was reduced. Firstly it was hard to set the desired temperature to a high accuracy. It was possible to get within tens of a degree away from the target but hard to reach exactly 7°C. This was partly due to the current generator having an analogue control meaning it was hard to change the current by small amounts to alter the temperature.

Another problem was condensation. The liquid cantilever holder for the Catalyst AFM includes a pane of glass above the cantilever to let the laser pass through whilst protecting the electronics from the imaging buffer. When the underside of the glass came into contact with the cold buffer, water vapour in the air would condense on to the top of the glass and block the laser from reaching the cantilever. Without a high laser sum reaching the photodetector the AFM cannot function. To combat this effect washing up liquid was used to coat the topside of the glass to stop water condensing on it.

After solving the problem of condensation images could be obtained at 19.6°C, 7.7°C and 4.1°C. The contact images can be seen in figure 7.3 and the force curves in figure 7.4.

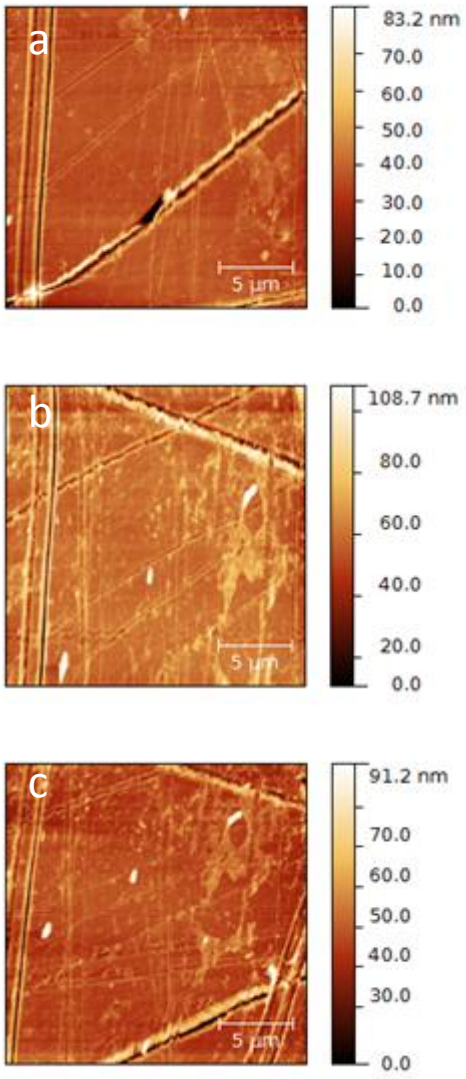

Figure 7.3: Contact images of sapphire at a) 19.6°C, b) 7.7°C and c) 4.1°C. The image quality is similar for all temperatures showing that cooling does not visibly alter the images.

It can be seen from figure 7.3 that the drop in temperature or the application of the cooling system itself does not introduce any noise into the contact images. There is a similar level of quality in all three images. This was not found to be the case with the force curves. The force data got progressively noisier with the reduction of temperature as seen in figure 7.4.

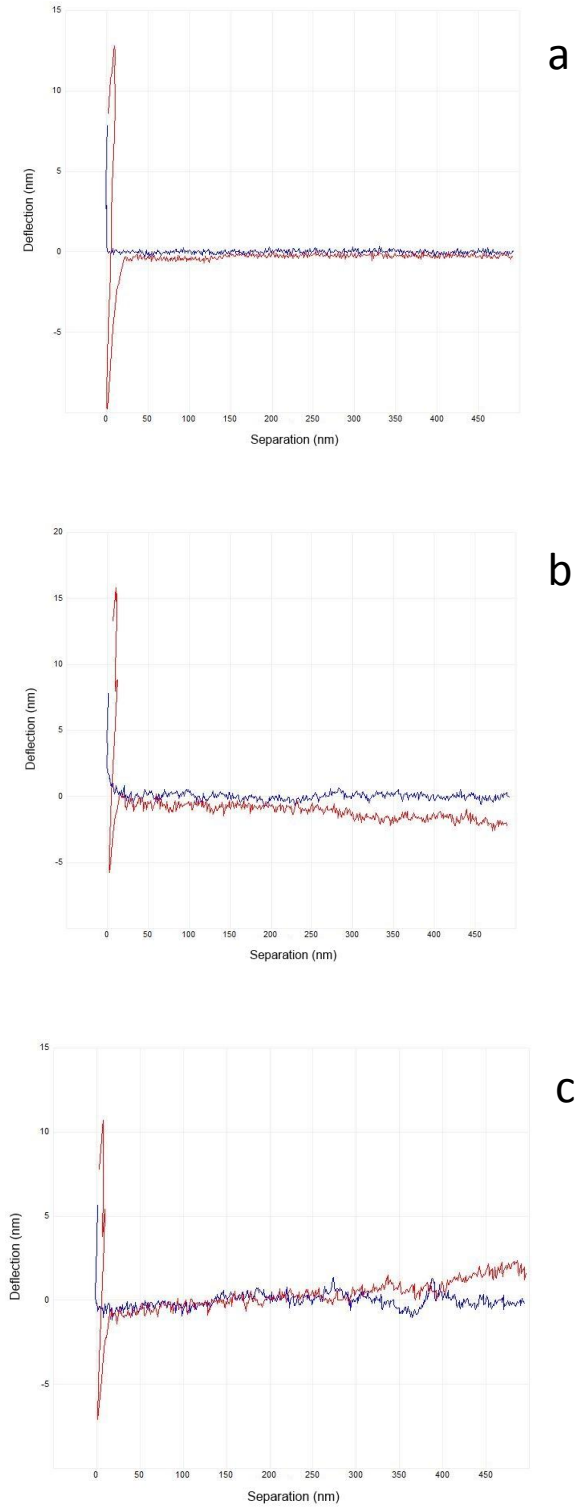

Figure 7.4: Force curves taken at a loading rate of 1400 pNs^{-1} on a sapphire sample at a) 19.6°C, b) 7.7°C and c) 4.1°C. It can be seen that the lower the temperature is the noisier the force curve becomes.

This is unlikely to be due to the background room noise, the thermocouple or the water flowing through the copper block under the sample as these were all present at 19.6^{o}C but this force curve (figure 7.4a) is fairly free from noise. The source of the noise could instead be due to the increase in the current passing through the TEC.

Despite the added noise both the low temperature force curves in figures 7.4b and 7.4c show stable enough force curves that specific unbinding events should be visible meaning that the cooling system can be used for the SMRFM experiments. However the measured unbinding forces are likely to be less accurate due to the extra noise.

7.4 Results – Temperature Variation

After the cooling system had been installed AFM tips were functionalised with CAL B to investigate what happened when the temperature was varied from 30^{o}C to 7^{o}C and below. For each temperature a 64 x 64 pixel force volume image on APA was collected which gave 4096 force curves. A surface delay of 100 ms was used as this was found to be the most favourable in Chapter 6 and the loading rate was set at 1400 pNs^{-1} to be consistent with previous results. From these force curves the binding probability and average binding force was calculated. The results have been displayed in figure 7.5.

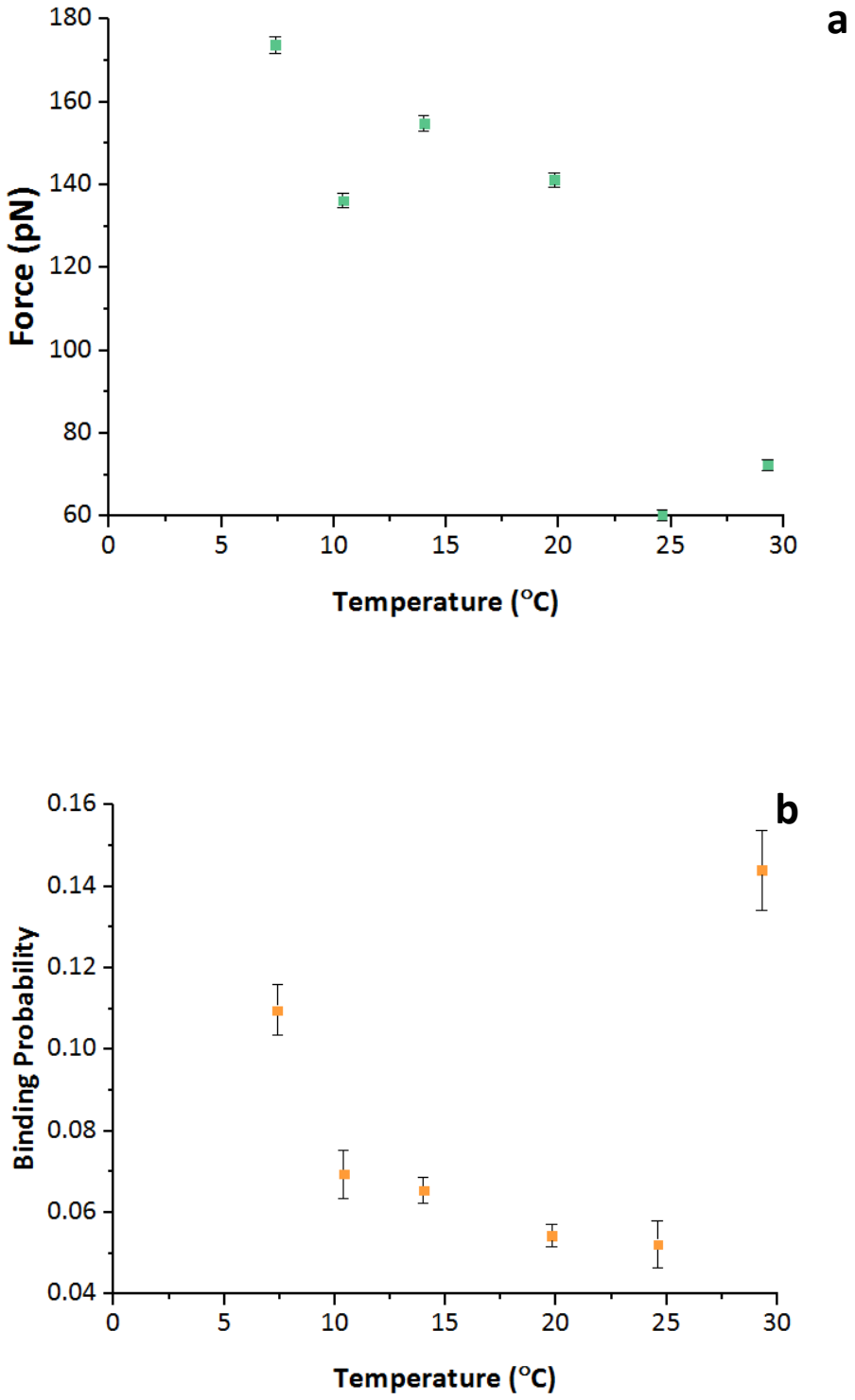

Figure 7.5: Summary of a) unbinding forces and b) binding probabilities for CAL B at different temperatures at a loading rate of 1400 pNs^{-1} and a dwell time of 100 ms.

Most of the results show a small increase in binding probability as the temperatures fall and a sharp increase at 7.4°C. This is encouraging for CAL B in relation to washing detergents as it is an indication that CAL B works much more effectively at the average water temperature of the UK which is 7.3°C. The measured unbinding forces for temperatures below 20°C are consistent with each other and the expected value of 152.3 ± 5.3 pN obtained in Chapter 6.

However there are two surprising results in figure 7.5a. The force measurements for both 29.3°C and 24.6°C are substantially lower. Also the highest temperature shows the largest binding probability of 0.1440 ± 0.0098. There is then a large drop in binding probability at 24.6°C before it starts to increase with reduction in temperature as seen in figure 7.5b.

To find out what may have caused these anomalous results histograms were plotted for 29.3°C, 19.8°C and 7.4°C. For the two lower temperatures the histograms show a normal distribution centred near 150 pN. However the histogram for 29.3°C does not show this. It displays a peak centred on 67 pN and another small peak at 140 pN. The force curves for the two warmest temperatures of 29.3°C and 24.6°C were very noisy potentially due to the extra energy introduced from heating or because of an undiscovered vibration in the heating stage.

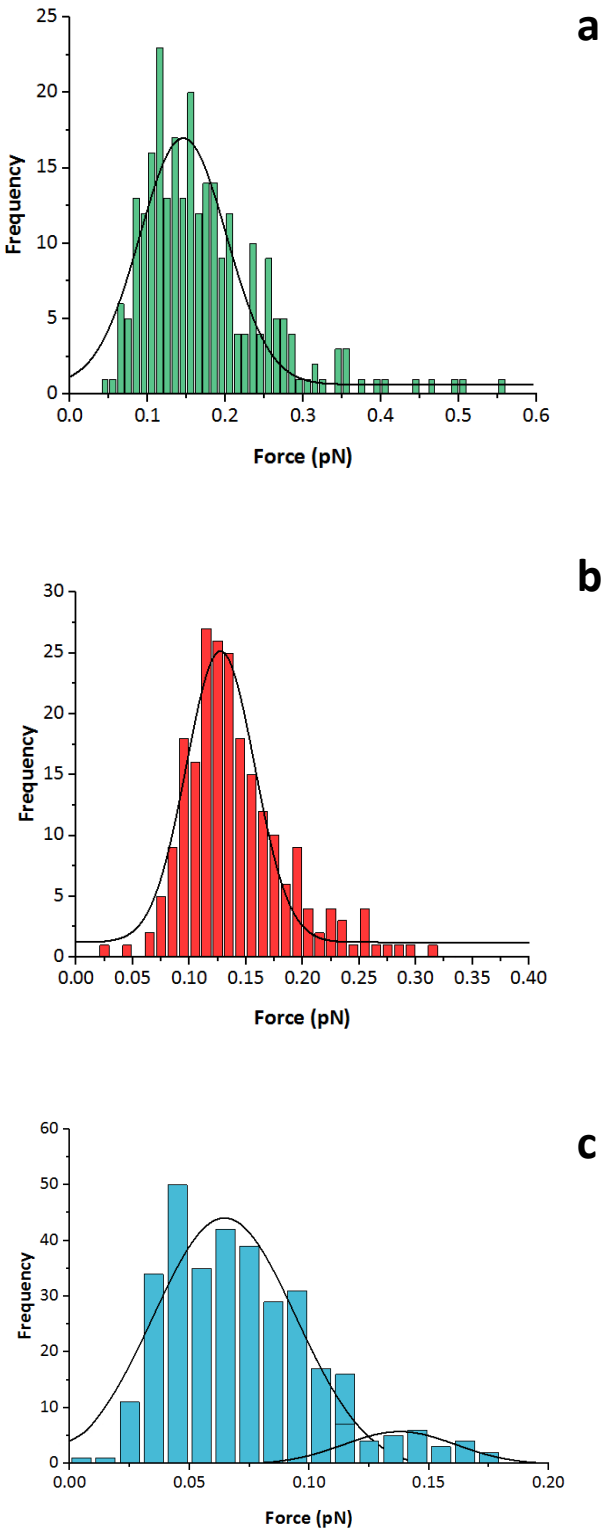

Figure 7.6: Histogram of rupture force values for CAL B at a) 7.4°C, b) 19.8°C and c) 29.3°C at a loading rate of 1400 pNs^{-1} and dwell time 100ms.

It could be that the noisy force curves have been misidentified as specific events causing a large amount of false data to be analysed. This is supported by the small peak at 140 pN in figure 7.6c which could be the real specific events that are being seen along with the fake events. It is expected that the number of specific events would be very low for this temperature which would explain why this peak is so small. 24.6^{o}C also has a small number of force measures around 140 pN but as there are very few events, either correct or false, it is difficult to know for certain if there is a secondary peak. If the data for both 29.3^{o}C and 24.6^{o}C mainly consists of unspecific events this would explain why the measured forces are so different to all other results.

It was hoped that temperatures below 7.4^{o}C would be looked at but it was discovered that imaging for a long time at cool temperatures led to another problem with condensation. Over time condensation would build up on the surface of the TEC. This water would interact with the imaging buffer due to hydrostatic forces and cause the buffer to leak onto the surface of the TEC and alter the laser alignment. The cooler the TEC was the faster the condensation would build up. At temperatures below 7^{o}C the condensation was appearing too fast to complete the force volume image.

To try and remove this problem a stream of nitrogen was set up over the imaging area to remove the water vapour in the air surrounding the TEC. However to keep the air dry enough to remove condensation the pressure of the nitrogen was too high and caused a lot of noise in the AFM images. If this experiment was to be repeated a fluid cell would be highly beneficial as that would keep the condensation on the TEC separate but it would take longer to

thermally equilibrate due to the increase in water volume and so setting the required temperature would be more difficult.

7.5 Conclusion

The purpose of this chapter of work was to vary the environmental temperature for CAL B to see how its activity changes. CAL B is of particular interest due to its potential use in ambient temperature washing detergents so the temperatures chosen to study here ranged from the current lowest washing temperature of 30^{o}C to the average tap water temperatures of the UK of approximately 7^{o}C.

To successfully achieve this both a heating system, which was commercially available, and cooling system were needed for the AFM scanning stage. The cooling system was created using a thermoelectric cooler and a secondary copper cooler. The application of this cooling system showed no differences in contact images taken at a selection of temperatures however force curves showed a lot more noise in cooler conditions but not enough to obscure the unbinding features and therefore were suitable for the CAL B SMRFM experiments.

When these unbinding experiments were carried out an increase in the binding probability of the enzyme to its substrate was witnessed at cooler temperatures, rising from 0.0544 ± 0.0027 to 0.1096 ± 0.0062 which supports the idea that CAL B would be a beneficial addition to a cold water washing detergent as it can work effectively in the cooler temperatures.

Due to the lack of previous studies published on the temperature dependence of CAL B in either bulk solution or at single molecule level it is difficult to say how the results obtained in this chapter compare to external experiments. One investigation suggests that the enzyme should still be active at 0°C which the results found here do not contradict but do not directly support as temperatures below 7°C were not reached.[9].

There was also an increase in binding probability at higher temperatures as well but as discussed this is likely due to non-specific events being measured in noisy force curves. To investigate this in more detail a control image should be taken using an unfunctionalised tip using the heating stage set at different temperatures to see how many 'specific' events are observed. If over 1% (the maximum background found in Section 6.4) of the force curves show apparent events at warmer temperatures then it is highly likely that the majority of events at 29.3°C and 24.6°C are incorrect.

The binding forces for temperature reached using the cooling stage are consistent with each other and give an average of 151.5 ± 3.6 pN which is very similar to the measured values of 152.3 ± 5.3 pN from Chapter 6. From these results it can be concluded that the average rupture force for CAL B at a loading rate of 1400 pNs^{-1} is 151.9 ± 6.4 pN.

It was hoped that the activity of CAL B below 7°C would be able to be studied as the current picture in the literature of CAL B's temperature dependence is fairly incomplete as described in section 2.4 and it would be advantageous to get a more comprehensive description of CAL B's behaviour. However imaging below

7°C proved to be unstable due to condensation present both on the cantilever holder and the TEC. Using a commercial fluid cell would help reduce the condensation problem on the TEC but it is difficult to protect against the condensation on the cantilever holder glass.

The SMRFM system was able to carry out the experiments that this thesis set out to complete but not quite as accurately as expected due to unforeseen noise and issues introduced by imaging at low temperatures. If these could be removed then SMRFM would be a great tool for studying enzymes and other binding molecules in cool environments.

7.6 References

[1] BBC, *Record low for water temperature,* BBC News, 2010.

[2] M. R. Ganjalikhany, B. Ranjbar, A. H. Taghavi and T. T. Moghadam, "Functional Motions of Candida Antarctica Lipase B: A survey through open-close formations," *PloS one,* vol. 7, no. 7, p. e40327, 2012.

[3] J. C. A. Peltier, "Investigation of the heat developed by electric currents in homogeneous materials and at the junction of two different conductors," *Annales de chimie et de physique,* vol. 56, p. 371, 1834.

[4] D. D. Pollock, Thermocouples: Theory and Properties, CRC Press, 1991.

[5] F. J. DiSalvo, "Thermoelectric cooling and power generation," *Science,* vol. 285, no. 5428, pp. 703-706, 1999.

[6] M. R. Ganjalikhany, B. Ranjbar, A. H. Taghavi and T. T. Moghadam, "Functional Motions of Candida antarctica lipase B: A Survey through Open-Close Conformations," *PloS one,* vol. 7, no. 7, p. e40327, 2012.

[7] N. Zhang, W. C. Suen, W. Windsor, L. Xiao, V. Madison and A. Zaks, "Improving tolerance of Candida Antarctica lipase B towards irreversible thermal inactivation through directed evolution," *Protein Engineering,* vol.

16, no. 8, pp. 599-605, 2003.

[8] P. Lozano, T. De Diego, D. Carrié, M. Vaultier and J. L. Iborra, "Over-stabilization of Candida Antarctica Lipase B by ionic liquids in ester synthesis," *Biotechnology Letters,* vol. 23, no. 18, pp. 1529-1533, 2001.

[9] M. R. Ganjalikhany, B. Ranjbar, A. H. Taghavi and T. T. Moghadam, "Functional Motions of Candida Antarctica Lipase B: A Survey Through Open-Close Conformations," *PloS one,* vol. 7, no. 7, p. e40327, 2012.

Chapter 8 - Conclusion

8.1 Comparison to Project Aims

The research carried out in this thesis set out to investigate whether the carboxylic esterase enzyme *Candida Antarctica* Lipase B could potentially be used in cool water washing detergents with the aim of saving energy by removing the need for heating. In Chapter 1 three primary aims were outlined. This section will assess how well these targets were fulfilled and highlight any shortcomings found during the process of obtaining these results.

The first target was to set up a system for single molecule force spectroscopy using known molecules that have successfully been employed in previous studies. This was completed in Chapter 5 with the molecules avidin and biotin. Simultaneously two types of AFM imaging modes QNM and force volume were compared to see if the relatively new and much faster technique of QNM could be used as an alternative to force volume to reduce the time taken to perform the SMRFM experiments.

The results found in this chapter gave very reliable evidence that specific unbinding events were being witness between the two molecules. In the well established force volume imaging, specific events were regularly visible in the force curves and were significantly reduced when free avidin was introduced into the imaging solution indicating that the interactions between the avidin and biotin were being blocked. QNM mode showed strong adhesion events that correlate very well with the avidin aggregates shown on the topography image.

Force volume AFM also measured a quantitative unbinding force value of 217.0 ± 3.6 pN which corresponds very well to previously published results taken at the same loading rate of 236.05 ± 4.31 pN [1]. However QNM's measured quantitative results of a value of 244.5 ± 3.1 pN was less than half the magnitude expected for the avidin-biotin from the literature which stated that the force should be greater than 550 pN. This was possibly due to an overestimate of the loading rate but could have been due to inadequate automatic analysis of the force curves. The extracted QNM force curves were examined to carry out the same analysis as the force volume curves but they were too noisy to see the specific unbinding events that were likely to be occurring. For this reason it was decided that force volume would be the imaging technique used for the remainder of the project.

The second research aim was to apply the system created in Chapter 5 to the enzyme CAL B and to witness unbinding events at room temperature. As the tip functionalisation chemistry was suitable for the avidin-biotin system it was applied to the enzyme system. As well as CAL B another carboxylic esterase 3859 from *Pseudomonas Aeruginosa* was probed as the two enzymes have similar chemistry and enzymic mechanism so PA3859 was a good test system for the substrate choice [2]. The substrate chosen was the carboxylic ester ±-2-acetoxypropionic acid because it could be easily immobilised onto a mica surface for imaging. Both the PA3859 and CAL B enzymes showed specific unbinding events when their force curves were analysed with a greater binding probability than the measured background. They also both showed a significant drop in the number of witnessed events, from 0.0938 ± 0.0276 to 0.0107 ± 0.0012 for PA359

and 0.0684 ± 0.096 to 0.0093 ± 0.0024 for CAL B, when free APA was introduced into the imaging solution to block the interactions. PA3859 came in a deactivated form too which showed significantly less unbinding events than active PA3859 at 0.0095 ± 0.0029.

As well as observing specific unbinding events the tip dwell time was varied to study how the binding probability changed. For PA3859 this was found to be a 1000 ms and for CAL B it was 100 ms. It was expected that for all dwell times that the measured unbinding forces would be consistent as they were all obtained at a loading rate of 1400 pNs^{-1}. This was true for CAL B as the majority of results were found to be approximately 150 pN except for dwell times that produced a low binding probability and therefore had a small sample size.

The results for PA3859 initially appeared to be quite different. The majority of dwell times measured rupture forces of ~80 pN but there were three over 100 pN including the dwell time with the largest sample size. However studying the histogram for the 1000 ms dwell time revealed that the discrepancies arose due to multiple bonds forming which caused larger unbinding forces to be measured and pulled the average force away from the expected 80 pN. The histogram showed a large peak at 78 pN and then progressively smaller peaks at integer values of the 78 pN single bond. This was found to be the case for all dwell times that gave anomalous rupture force measurements.

Finally the temperature that the CAL B measurements were undertaken at was varied to investigate how the activity of the enzyme was affected by the environmental changes. The focus of this work was to look at temperatures close

to the ambient temperature of water which was found to be 7.3°C in the UK. This was carried out in Chapter 7, the final experimental chapter of this report.

The first stage to completing these experiments was to produce a cooling system for the AFM which was done using a TEC and a copper conductor to remove the heat away from the imaging area. Images at 19.6°C, 7.7°C and 4.1°C showed that the cooling system did not affect contact images but did show more noise in force curves in the cooler environments possibly due to the electrical current passing through the TEC.

Once the cooling system had been tested and it was ascertained that unbinding features would still be visible in the force curves the temperature was varied between 29.3°C and 7.4°C and the binding probability and unbinding forces were measured. At 7°C the binding probability was 0.1096 ± 0.0062 which was a 100% increase on the binding probability of 0.0544 ± 0.0027 for room temperature at 19.8°C.

29.3°C showed an unexpected large binding probability with almost 0.15. It was seen that the force curves for both the warmer than room temperature images, which required the use of a heating stage, were very noisy compared to all the other images. The measured unbinding forces for both these images were ~70 pN. It is possible that the heating stage introduced an undetected source of noise which caused a lot of unspecific events that were very similar in shape to rupture events and so many features were measured incorrectly accounting for the discrepancy in unbinding force magnitude and the increased binding probability at 29.3°C.

Discarding these rupture forces the average rupture force was measured to be 151.5 ± 3.6 pN which corresponded well to the value of 152.3 ± 5.3 pN determined by dwell time experiments in Chapter 6. This gives an average binding force of 151.9 ± 6.4 pN for CAL B at a loading rate of 1400 pNs^{-1}.

It was discovered that imaging at temperatures near 7^{o}C and below was particularly difficult due to condensation affects from the cool equipment and the warm air around the AFM. This problem was never overcome in a satisfactory and stable way which limited how low the temperature variation experiments could get.

Overall the experiments carried out in this thesis accomplished the aims set out at the start of the research. SMRFM was achieved with avidin and biotin and two lipases and their APA substrate. The experiments were also undertaken at a variety of temperatures which gives an insight into how CAL B's activity changes due to cooler surroundings. It was found that at cooler temperatures CAL B is more active and therefore it is a good potential enzyme for cool water detergents.

An unexpected outcome of the research was the creation of the analysis program discussed in Chapter 4. Initially commercially software was going to be used to analyse the individual force curves but it became apparent that the software was too slow and not able to handle considerable amounts of data. The program created in Matlab was a huge advantage as it allowed the time taken for analysing the data to be reduced allowing more experiments to be completed in the time available.

8.2 Improvements and Extensions

There are a number of improvements that could be made to the experiments reported in this thesis if they were to be repeated. Making it so the analysis program could be left to analyse the data automatically would be highly beneficial as it would mean experiments could be run simultaneously to data analysis. This would allow for a more methodical and thorough temperature variation for CAL B. It would also mean greater sample sizes could be obtained and analysed in the time available which would improve the accuracy of the measured unbinding forces.

Another improvement would be to investigate exactly why QNM was not able to accurately measure rupture forces for avidin and biotin and see if it was possible to change the system so it did work effectively. This would decrease the time taken for imaging allowing for greater sample sizes and more experiments to be carried out.

Improving the cooling system used so that it can handle temperatures below 7^{o}C effectively would be a major aim for any future work on these experiments as currently the system is limited. By achieving this it would open up a wide variety of further experiments that could be undertaken including seeing at which temperature the activity of CAL B starts to be inhibited by the cold. However to do this a different buffer would be needed that would not freeze below zero and could be used at all temperatures so parameters not being investigated remain constant. A way of lowering the freezing point of the buffer is to increase the salt concentration but this could affect the activity of CAL B. It has been shown that

CAL B is very stable and still active in ionic solutions with low water concentrations so it is possible that increasing the salt concentration would be sufficient to study at sub-zero temperatures [3].

Additional work that could be carried out with the imaging and cooling system created in this project would be to investigate how the pH affects the activity of CAL B. pH is another aspect of washing detergents that it is important to consider and so seeing how CAL B worked at pHs that are less environmentally damaging would be advantageous [4].

It would also be interesting to try a number of different fatty substrates for CAL B including those that are likely to be found in clothes stains such olive oil or butter. If the activity of CAL B was still high on these substrates it would be a good indication that the enzyme would work well as a component of washing detergents.

Another expansion to the SMRFM system for seeing how effective a CAL B washing detergent would be is to replicate a washing machine cycle by creating an imaging buffer in a fluid cell that could be changed, removed, heated and cooled as required to simulate a usual cycle. With this it would be possible to see if aspects of the cycle denature or inhibit the enzyme and therefore show what would need to be addressed to allow CAL B to become a component of everyday detergents.

8.3 References

[1] M. de Odrowąż Piramowicz, P. Czuba, M. Targosz, K. Burda and M. Szymoński, "Dynamic force measurements of avidin-biotin and streptavidin-biotin interactions using AFM," *Acta Biochimica Polonica,* vol. 53, no. 1, pp. 93-100, 2006.

[2] M. Nardini and B. W. Dijkstra, "α/β hydrolase fold enzymes: the family keeps growing," *Current opinion in structual biology,* vol. 9, no. 6, pp. 732-737, 1999.

[3] P. Lozano, T. De Diego, D. Carrié, M. Vaultier and J. L. Iborra, "Over-stabilization of Candida Antarctica Lipase B by ionic liquids in ester synthesis," *Biotechnology Letters,* vol. 23, no. 18, pp. 1529-1533, 2001.

[4] R. Karan, M. D. Capes and S. DasSarma, "Function and biotechnology of extremophilic enzymes in low water activity," *Aquatic Biosystems,* vol. 8, no. 4, 2012.

Appendix

In this section the Matlab algorithm discussed in Chapter 4 is presented. This program was used to analyse all force volume images taken over the course of the work carried out in this thesis.

```
%clear any open windows
clc; close all; clear all;

% ====================================
% Variable Initialisation
% ====================================

%PUT IN PARAMETERS HERE:
SpringConstant = 0.082980; %nN/nm
DeflectionSensitivity = 21.8; %nm/V
GreatestDistance=20; %nm
NumberofFiles=4096;
StartPoint=0;

%Counts how many good curves there are
NumGoodCurves=0;
%Array to store the measured force value
Adhesion=0;

%Loop over all force curves
for FileNum=StartPoint:StartPoint+NumberofFiles-1,

        %Print file number to screen
        FileNum

        % ==================================
        % Load Force Curve
        % ==================================

        %Taken from the Nanoscope Matlab files
        %Opens the force curve of interest
        NSMU=NSMatlabUtilities();
        FileName=strcat('ForceCurves/100ms.001-435B-',num2str(FileNum),'.spm');
        NSMU.Open(FileName);
        [trace,retrace,scale_units,type_desc]=NSMU.GetForceCurveData(1,NSMU.METR
        IC);
        %Get curves in metric units.
        [xTrace,xRetrace,yTrace,yRetrace,xLabel,yLabel]=NSMU.CreateForceZPlot(1,NS
        MU.METRIC,0);
```

```
% ====================================
% Baseline correct
% ====================================

%Sets the origin to the contact point and flattens the baseline of the curve
%Find the line of best fit for the out of contact section by taking last 300 data
points
xAway=xRetrace(length(xRetrace)-300:length(xRetrace));
 yAway=yRetrace(length(yRetrace)-300:length(yRetrace));
%Find the gradient and intercept by doing a polyfit
FitAway=polyfit(xAway,yAway,1);
%    y    =     m         *      x     +        c
FityAway=FitAway(1).*xRetrace+FitAway(2);

%Find the line of best fit for contact section by taking the first few data points
xContact=xRetrace(5:40);
yContact=yRetrace(5:40);
%Find the gradient and intercept by doing a polyfit
FitContact=polyfit(xContact,yContact,1);
%     y      =       m         *      x     +        c
FityContact=FitContact(1).*xRetrace+FitContact(2);

%Calculate the intersect of the two fits - gives the contact point of the tip
Intersect=(FitAway(2)-FitContact(2))/(FitContact(1)-FitAway(1));

%Set y baseline by subtracting the fit line
yRetrace=(yRetrace-FityAway);
%Set contact point as the zero point
xRetrace=Intersect-xRetrace;
%Correct for deflection of cantilever
xRetrace=xRetrace+yRetrace;
%Convert to the correct units
yRetrace=yRetrace*SpringConstant;

%Cut out unwanted data
UpperLimit=find(xRetrace>100);
LowerLimit=find(xRetrace>-20);
xRetrace=xRetrace(LowerLimit:UpperLimit);
yRetrace=yRetrace(LowerLimit:UpperLimit);

% ====================================
% Find potential events
% ====================================

%Find the thermal noise spread by analysing the last 50nm of the cut data
Limit=find(xRetrace>50);
Tempy=yRetrace(Limit:length(yRetrace));
%Find minimum and maximum forces
MinValue=min(Tempy);
MaxValue=max(Tempy);
%Spread given by the difference
ThermalNoiseSpread=MaxValue-MinValue;
```

```
%To find important bits smooth the curve temporarily to reduce noise so it is
easier to find large dips in the data and only look in the area where there can be
specific events
UpperLimit=find(xRetrace>GreatestDistance);
Tempy=smooth(yRetrace(1:UpperLimit));
Tempx=xRetrace(1:UpperLimit);

%Initialise trough counter for each file
DipCounter=0;

%Loop over data in the smoothed data set. Start at 4th element and finish at 8th
element before end
for i=4:length(Tempy)-8,

        %If the data elements 3 either are side are larger than the data 1 either
        side and the data 1 either side are both larger than the chosen data
        point the chosen data point is a potential event. Checking that the data
        element in question is at a dip
        if Tempy(i-3)>Tempy(i-1) && Tempy(i-1)>Tempy(i) &&
        Tempy(i+3)>Tempy(i+1) && Tempy(i+1)>Tempy(i)

                % if the size of the peak compared to its nearby neighbours is
                larger than the thermal noise then it's a peak
                if (Tempy(i+7)-Tempy(i))>(ThermalNoiseSpread) ||
                (Tempy(i+6)-Tempy(i))>(ThermalNoiseSpread) || (Tempy(i+5)-
                Tempy(i))>(ThermalNoiseSpread)

                %Add one to the number of dips
                DipCounter=DipCounter+1;

                end

        end

end

%Variable that is used as a Boolean by the user. Pass = 0 means no. Pass = 1
means yes.
Pass=0;

%If there is between 1-3 peaks found the curve is worth a look at in more detail
if PeakCounter>0 && PeakCounter<4

        %Plot the unsmoothed data
        plot(xRetrace,yRetrace);
        %User input saying if the curve passes or not
        Pass=input('Is it a good curve? ');

        if Pass==1
```

```
                        %If the curve passes the user clicks on the bottom part of the
                        adhesion dip and then the top part of the feature

                        %Display cursors on the file, click on the value to input into
                        the workspace
                        dcm_obj=datacursormode;

        set(dcm_obj,'DisplayStyle','datatip','SnapToDataVertex','off','Enable','on')

                        disp('Bottom Value ')
                        pause(2)
                        c_info=getCursorInfo(dcm_obj);
                        x1=c_info.Position(1);
                        y1=c_info.Position(2);

                        disp('Top Value ')
                        pause(2)
                        c_info=getCursorInfo(dcm_obj);
                        x1=c_info.Position(1);
                        y2=c_info.Position(2);

                        %Add one to the number of good curves, take a note of the
                        file number and measure the adhesion
                        NumGoodCurves=NumGoodCurves+1;
                        FileNumbers(NumGoodCurves)=FileNum;
                        Adhesion(NumGoodCurves)=y2-y1;

                end

        end

end


%After looping over all files print out the desired information
if Adhesion(1)==0
        disp('No files passed')
else
        %Print required values
        NumGoodCurves
        Adhesion'
        FileNumbers'
        FMean=mean(Adhesion)
        SD=std(Adhesion)

end
```